REPUBLIC OF TURKEY YILDIZ TECHNICAL UNIVERSITY GRADUATE SCHOOL OF SCIENCE AND ENGINEERING

UNSTABLE EQUILIBRIA OF SOME DYNAMICAL SYSTEMS

Tahir COŞGUN

DOCTOR OF PHILOSOPHY THESIS

Department of Mathematics

Program of Mathematics

Supervisor Prof. Dr. Murat SARI

REPUBLIC OF TURKEY YILDIZ TECHNICAL UNIVERSITY GRADUATE SCHOOL OF SCIENCE AND ENGINEERING

UNSTABLE EQUILIBRIA OF SOME DYNAMICAL SYSTEMS

A thesis submitted by Tahir COŞGUN in partial fulfillment of the requirements for the degree of **DOCTOR OF PHILOSOPHY** is approved by the committee on 08.03.2022 in Department of Mathematics, Program of Mathematics.

Prof. Dr. Murat SARI Yildiz Technical University Supervisor

Approved By the Examining Committee Prof. Dr. Murat SARI, Supervisor Yildiz Technical University Prof. Dr. Doğan KAYA, Member Istanbul Commerce University Prof. Dr. Beyza A. ÖZKÖK, Member Yildiz Technical University Prof. Dr. Canan Ç. KARAASLANLI, Member Yildiz Technical University Prof. Dr. İdris DAĞ, Member Eskisehir Osmangazi University

I hereby declare that I have obtained the required legal permissions during data collection and exploitation procedures, that I have made the in-text citations and cited the references properly, that I haven't falsified and/or fabricated research data and results of the study and that I have abided by the principles of the scientific research and ethics during my thesis study under the title of *Unstable Equilibria of Some Dynamical Systems* supervised by my supervisor, Prof. Dr. Murat SARI. In the case of a discovery of false statement, I am to acknowledge any legal consequence.

Tahir COŞGUN

Signature

Dedicated to my wife Gamze and my beloved son Emir

ACKNOWLEDGEMENTS

First and foremost I want to thank my extraordinary hard-working advisor Prof. Dr. Murat SARI for supporting me throughout my study, and for his astonishing enthusiasm, dynamism and vision that motivates me.

I would like to express my gratitude and appreciation for Prof. Dr. Doğan Kaya and Prof. Dr. Beyza A. Özkök whose guidance, support and encouragement have been invaluable throughout this study. I also wish to thank our research team who have been a great source of support for me, especially Hande Uslu for her genuine support.

I offer my sincere gratitude to Prof. Dr. İdris Dağ, Prof. Dr. M. Fatih Köksal, Prof. Dr. Mustafa Kandemir, Prof. Dr. Canan Ç. Karaaslanlı, Assoc. Prof. Dr. Ahmet Altürk, and Asst. Prof. Dr. Hilmi Gürleyen for their profound, perpetual, and precious support and guidance in possessing my academic personality.

I would like to thank my mother and father whose love and guidance were with me in whatever I have pursued, and the support and advice they provide are beyond the measures. Especially, I would like to thank my brother, Tayip, for his continuous support throughout my life. My beloved family deserve plenty of thanks, for their endless support and encouragement during not only this thesis but all my endeavours. I wish to thank my wife Gamze and my beloved son, Emir, for their affection and love, they give me unending vitality, passion and never-ending strength. My greatest luck in life is to share it with you.

Tahir COŞGUN

TABLE OF CONTENTS

LI	ST O	F SYMBOLS	vii
LI	ST OI	F ABBREVIATIONS	viii
LI	ST OI	FFIGURES	X
LI	ST OI	F TABLES	xiii
Αŀ	3STR	ACT	xvi
Ö	ZET		xvii
1	INT	RODUCTION	1
	1.1	Literature Review	1
	1.2		2
	1.3		3
	1.4	Outline of the Thesis	4
2	LITE	ERATURE	7
3	MAI	N THEORETICAL RESULTS	12
4	VAI	RIOUS APPLICATIONS	15
	4.1	Roots of Polynomials	15
	4.2	Root Finding in the Complex Field: Julia Sets	20
	4.3	2D Root Finding	22
	4.4	Population Dynamics Model with a Critical Threshold	24
	4.5	3D Root Finding Problem: A Sophisticated but Robust Approach	27
	4.6	Fredholm Integral Equations via a Reverse Approach	29
	4.7	Unstable Equilibria in Control Problems: The Simple Pendulum	31
	4.8	Unstable Equilibria in Chaotic Structures	34
	4.9	Discussions Regarding the Applications	36
	4.10	Use of Relatively Larger Step Sizes	39
5	LIN	EAR ADVECTION DIFFUSION PROCESSES	40

	5.1	A Criterion for Convergence	40
	5.2	Stability Issues	42
	5.3	Numerical Illustrations	48
6	NOI	NLINEAR ADVECTION DIFFUSION PROCESSES	57
	6.1	Solution Procedure	58
	6.2	Numerical Illustrations	58
7	SIN	GULARLY PERTURBED CASES IN NONLINEAR ADVECTION DIFFU-	
	SIO	N REACTION PROCESSES	66
	7.1	Analytical Solution of the Singularly Perturbed Generalized	
		Burgers-Huxley Equation	68
		7.1.1 Solution Procedure of the SPGBHE	68
		7.1.2 Stability Analysis for the SPGBHE	70
		7.1.3 Stability Analysis under Advection Dominant Case	73
	7.2	Analytical Solution of the Singularly Perturbed Generalized Burgers	
		Fisher Equation	75
		7.2.1 Stability Analysis for the SPGBFE	75
	7.3	Numerical Solutions via the RFPIM	77
8	TWO	D DIMENSIONAL ADVECTION DIFFUSION PROCESSES	84
	8.1	Implementation of the RFPIM and Numerical Observations	84
9	RES	ULTS AND DISCUSSION	87
RI	REFERENCES		89
ΡĮ	PUBLICATIONS FROM THE THESIS 9		96

LIST OF SYMBOLS

α	Phase Speed
β	Reaction Coefficient in SPGBFE and SPGBFE
γ	Reaction Coefficient in SPGBHE
δ	Non-linearity Coefficient in SPGBFE and SPGBFE
ϵ	Diffusion Coefficient
Δx	Spatial Increment 1
Δt	Time Increment
Δy	Spatial Increment 2
r_1	$\alpha \Delta t / \Delta x$
r_2	$\epsilon \Delta t/\Delta x^2$
Α	Amplification Factor
\mathbb{C}	Complex Numbers
h	Step-size in 1D problems
\mathbb{R}	Real Numbers
\mathbb{R}^+	Positive Real Numbers
\mathbb{R}^n	Real Number Space of Dimension <i>n</i>
$C^1(a,b)$	Space of Continuously Differentiable Functions over the interval (a, b)
$L^2(a,b)$	Space of Square Integrable Functions over the interval (a, b)
N	Natural Numbers

LIST OF ABBREVIATIONS

1D One Dimensional

2D Two Dimensional

3D Three Dimensional

AE Absolute Error

BC Boundary Condition

BTBS Backward in Time Backward in Space Scheme

BTCS Backward in Time Central in Space Scheme

BTFS Backward in Time Forward in Space Scheme

CFL Courant-Friedrichs-Lewy

CPU Central Process Unit

FPIM Conventional Fixed-Point Iteration Method

FTBS Forward in Time Backward in Space Scheme

FTCS Forward in Time Central in Space Scheme

FTFS Forward in Time Forward in Space Scheme

IBC Initial Boundary Conditions

IC Initial Condition

Im Imaginary Part

ODE Ordinary Differential Equation

PDE Partial Differential Equation

RBTBS Reversed Backward in Time Backward in Space Scheme

RBTCS Reversed Backward in Time Central in Space Scheme

RBTFS Reversed Backward in Time Forward in Space Scheme

Re Real Part

RE Relative Error

RFPIM Reversed Fixed-Point Iteration Method

RFTBS Reversed Forward in Time Backward in Space Scheme

RFTCS Reversed Forward in Time Central in Space Scheme

RFTFS Reversed Forward in Time Forward in Space Scheme

RMSE Root Mean Square Error

SPGBFE Singularly Perturbed and Generalized Burgers Fisher Equation

SPGBHE Singularly Perturbed and Generalized Burgers Huxley Equation

LIST OF FIGURES

Figure 1.1	The numerical flow governed by the conventional fixed point	
	iteration	4
Figure 4.1	Seven equidistant fixed-points	18
Figure 4.2	Fixed-points of $g(x) = 6/11 + 6x^2/11 - x^3/11 \dots$	19
Figure 4.3	The iterations obtained from equation (4.14) after 15 steps via the	
	RFPIM	21
Figure 4.4	The Julia set of function $f(x) = x^2 - 1$	22
Figure 4.5	Combination of Figures 4.3 and 4.4	23
Figure 4.6	Stream plot and locations of the equilibria for system (4.15)	23
Figure 4.7	Geometrical observations regarding model (4.18)	25
Figure 4.8	Equilibrium positions for a simple pendulum	31
Figure 4.9	Chaotic orbit of system (4.43), for the parameters $(a, b, c) =$	
	$(2.1, 0.6, 30)$ and initial condition $(x_0, y_0, z_0) = (0.1, -0.3, 0.2)$	35
Figure 4.10	Chaotic orbit obtained via the RFPIM of system (4.43), for	
	the parameters $(a, b, c) = (-2, -1, 10)$ and initial condition	
	$(x_0, y_0, z_0) = (1, 1, 1). \dots$	36
Figure 5.1	Final condition (blue), initial condition (red), and the recovered	
	initial data (black dashed) via the RFTFS scheme for $T=5$ (left)	
	and $T=10$ (right) with $\alpha=0.5,\ \epsilon=0.001,\ \Delta x=0.01,$ and	
	$\Delta t = 0.01.\dots$	49
Figure 5.2	Final condition (blue), initial condition (red), and the recovered	
	initial data (black dashed) via the RFTCS scheme for $T = 1$ with	
	$\alpha = 10$, $\epsilon = 0.1$, $\Delta x = 0.01$, and $\Delta t = 0.0005$ (left), and for $T = 2$	
	with $\alpha = 0.5$, $\epsilon = 0.01$, $\Delta x = 0.1$, and $\Delta t = 0.1$ (right)	49
Figure 5.3	Final condition (blue), initial condition (red), and the recovered	
	initial data (black dashed) via the RFTBS scheme for $T = 10$ with	
	$\epsilon = 10^{-5}$ (left), and $\epsilon = 0$ (right) where $\alpha = 0.5$, $\Delta x = 0.01$, and	
	$\Delta t = 0.01.\dots$	50
Figure 5.4	Sample noise (left) and noisy final data (right)	50

Figure 5.5	initial condition (red), and the recovered initial data (black dashed)	
	via the RFTCS scheme for $T=10$ with $\epsilon=10^{-3}$ where $\alpha=0.5$,	
	$\Delta x = 0.01$, and $\Delta t = 0.005$ (left) and absolute errors (right)	51
Figure 5.6	Final condition (blue), initial condition (red), and the recovered	
	initial data (black dashed) via the FTCS scheme for $T=1$ with	
	$\epsilon=10^{-3}$, $\alpha=1.0$, $\Delta x=0.01$, and $\Delta t=0.001$ (left), and $\epsilon=0.01$	
	, $\alpha = 1.0$, $\Delta x = 0.01$, and $\Delta t = 0.001$ (right) regarding Example 2.	52
Figure 5.7	Exact solution of the problem in Example 3	53
Figure 5.8	The exact final data (red) and the noisy final data (black) regarding	
	Example 3	53
Figure 5.9	The final data (blue), the initial data (red), and the recovered initial	
	data (dashed) obtained via the RFTCS scheme regarding Example 3.	54
Figure 5.1	0 Propagation of the absolute error obtained via the RFTCS scheme	
	regarding Example 3	54
Figure 5.1	1 The exact final data (red) and sample noisy final data (black)	
	regarding Example 3	55
Figure 5.1	2 The numerical response obtained via the RFTCS scheme by starting	
	with approximately 100% noisy data regarding Example 3	56
Figure 6.1	Shock wave behaviour of the problem in Example 1 for $\epsilon = 0.0001$.	60
Figure 6.2	Behaviours of the problem in Example 2 for various time spans such	
	as $t = 1$, $t = 2$, $t = 10$ seconds (left) and the solution profile at the	
	end-time (right)	62
Figure 6.3	Pressure signature of a supersonic plane [69]	63
Figure 6.4	Pressure signature $u^*(x)$ for the model	64
Figure 6.5	Behaviour of the target function u^* (black), the optimal solution u_0	
	(red) and the recovered final data u_T (green) for $T=50$ seconds	
	with $\Delta x = 0.8$ (first), $\Delta x = 0.4$ (second), $\Delta x = 0.2$ (third), and	
	$\Delta x = 0.1$ (fourth)	65
Figure 7.1	Profile of a kink	67
Figure 7.2	Profile of an anti-kink	67
Figure 7.3	2D graph of the vector field $(p(v, w), q(v, w))$ for c_1 with $\alpha = 1$,	
	$\beta = 1$, $\epsilon = 1$, $\delta = 1$, and $\gamma = 0.4$	73
Figure 7.4	2D graph of the vector field $(p(v, w), q(v, w))$ for c_5 with $\alpha = 1$,	
	$\beta = 1$, $\epsilon = 1$, and $\delta = 1$	76
Figure 7.5	Recovery of the initial condition and the absolute error for the	
	inverse problem in the SPGBHE at $T=1.0$ with $\alpha=1,~\beta=1,$	
	$\delta = 1$, $\epsilon = 10^{-10}$, and $\gamma = 0.01$ with $\Delta t = T$	81

Figure 7.6	Recovery of the initial condition and the absolute error for the	
	inverse problem in the SPGBFE at $T=1.0$ with $\alpha=1.0$, $\beta=-1.0$,	
	$\delta = 1.0$ and $\epsilon = 1.0$ with $\Delta t = T$	8

LIST OF TABLES

Table 4.1	Some values obtained via the RFPIM from the orbits of some points	
	around $x = 2$	19
Table 4.2	Some values obtained via the conventional method from the orbits	
	of some points around $x = 1$ or $x = 3$	20
Table 4.3	Absolute errors after application of the RFPIM for equation (4.15)	
	with different initial choices at different steps	24
Table 4.4	Fifth and tenth iterations after application of the fixed-point iteration	
	method for equation (4.15) with different initial choices	24
Table 4.5	Numerical simulation of model (4.24) via the RFPIM with different	
	initial values (y_0) with $h = 1, \ldots, \ldots$	26
Table 4.6	Absolute errors for model (4.24) after the first step of the RFPIM	
	with various step sizes	27
Table 4.7	Norm of the absolute errors for corresponding unstable fixed-points	
	at the first step of the RFPIM towards the solution of system (4.26)	
	with an initial guess $(x_0, y_0, z_0) = (0, 0, 0)$ and various values of step	
	sizes	28
Table 4.8	Some iterations obtained via the RFPIM with initial guess $\phi_0(x) =$	
	7x/3 for problem (4.35)	30
Table 4.9	Some iterations obtained via the RFPIM with initial guess $\phi_0(x) = 0$	
	for problem (4.35)	31
Table 4.10	Absolute errors towards finding repelling fixed-point $\theta = 5\pi/6 \approx$	
	2.618 with the use of the RFPIM after single iteration with $h = 100$.	33
Table 4.11	Absolute errors towards finding attracting fixed-point $\theta=\pi/6\approx$	
	0.524 with the use of conventional fixed-point iteration method after	
	1000 iterations with $h = 0.01$	34
Table 4.12	Norms of the absolute errors at the first step of the RFPIM towards	
	the solution of system (4.43) with different initial values and various	
	values of step sizes	36
Table 5.1	Stability conditions for the present method	47
Table 5.2	The RMSE, the maximum absolute (AE) and relative (RE) errors for	
	various values of space and time increments regarding Example 1	50

Table 5.3	The RMSE, the maximum absolute (AE) and relative (RE) errors for	
	various values of space and time increments with 5% noise regarding	
	Example 1	51
Table 5.4	The RMSE, the maximum absolute error, the absolute error in	
	the mean, and relative error in the mean for various noise levels	
	regarding Example 1	51
Table 5.5	The RMSE and the maximum absolute errors (AE) for various values	
	of space and time increments with 10% noise in the mean	55
Table 5.6	The RMSE and the maximum absolute errors (AE) for various values	
	of space and time increments with 100% noise in the mean via the	
	RFTCS scheme	55
Table 6.1	Comparison of numerical results with literature for $\epsilon=0.0001$ at	
	t = 1.0 and various grid points for Example 1	60
Table 6.2	$L^2(0,1)$ errors for various values of ϵ regarding the problem	
	represented by Equations 2.2, 6.1, and 6.10	61
Table 6.3	Maximum absolute errors for various values of ϵ regarding the	
	problem represented by Equations 2.2, 6.1, and 6.10	61
Table 6.4	Values of the functional \mathbb{J} for $T=50s$ and various values of spatial	
	and temporal increments	64
Table 7.1	Eigenvalues in the limiting case, $\epsilon \to 0$, for the wave speeds c_1 and c_2 .	74
Table 7.2	Eigenvalues in the limiting case, $\epsilon \rightarrow 0$, for the wave speeds c_3 and c_4 .	74
Table 7.3	$L^{2}(-\infty,\infty)$ errors for Example 1 for various values of δ with $\alpha=1$,	
	$\beta = 1$, $\epsilon = 10^{-5}$, and $\gamma = 0.5$ with $\Delta t = T$	78
Table 7.4	$L^2(-\infty,\infty)$ errors for Example 1 for various values of ϵ with $\alpha=1$,	
	$\beta = 1$, $\gamma = 0.5$, and $\delta = 1$ with $\Delta t = T$	79
Table 7.5	$L^{2}(-\infty,\infty)$ errors for Example 1 for various values of γ with $\alpha=1$,	
	$\beta = 1$, $\delta = 1$, and $\epsilon = 10^{-5}$ with $\Delta t = T \dots \dots \dots \dots$	79
Table 7.6	$L^2(-\infty,\infty)$ errors for Example 1 for various values of β with $\alpha=1$,	
	$\delta = 1$, $\gamma = 0.5$, and $\epsilon = 10^{-5}$ with $\Delta t = T$	80
Table 7.7	$L^{2}(-\infty,\infty)$ errors for Example 1 for various values of α with $\beta=1$,	
	$\delta = 1$, $\gamma = 0.5$, and $\epsilon = 10^{-5}$ with $\Delta t = T$	80
Table 7.8	$L^2(-\infty,\infty)$ errors for Example 2 for various values of δ with $\alpha=1$,	
	$\beta = -1$, and $\epsilon = 1$ with $\Delta t = T$	81
Table 7.9	$L^2(-\infty,\infty)$ errors for Example 2 for various values of ϵ with $\alpha=1$,	
	$\beta = -1$, and $\delta = 1$ with $\Delta t = T$	82
Table 7.10	$L^2(-\infty,\infty)$ errors for Example 2 for various values of β with $\alpha=1$,	
m 11 = -:	$\delta = 1$, and $\epsilon = 1$ with $\Delta t = T$	82
Table 7.11	$L^2(-\infty,\infty)$ errors for Example 2 for various values of α with $\beta =$	0.0
	-1 , $\delta = 1$, and $\epsilon = 0.1$ with $\Delta t = T$	82

Table 8.1	$L^2(0,1)$ errors for various values of Δt with $\epsilon = 0.01$ and $T = 0.5$.	85
Table 8.2	$L^2(0,1)$ errors for various values of Δt with $\epsilon = 0.01$ and $T = 1.0$.	86
Table 8.3	$L^2(0,1)$ errors for various values of Δt with $\epsilon = 0.001$ and $T = 0.1$.	86
Table 8.4	$L^{2}(0,1)$ errors for various values of ϵ and T with $\Delta t = T$	86

Unstable Equilibria of Some Dynamical Systems

Tahir COŞGUN

Department of Mathematics Doctor of Philosophy Thesis

Supervisor: Prof. Dr. Murat SARI

Although there are various numerical techniques to find the stable equilibria of a dynamical system in scientific computing, no widely-used computational approach has been encountered to discover the unstable equilibria of a system in the literature. This thesis aims at presenting a new approach to uncover the equilibrium positions of a dynamical system exhibiting a repelling nature. A newly developed algorithm called the reversed fixed point iteration method (RFPIM) is presented to find the unstable equilibrium positions of a nonlinear system. The current method is able to uncover the behaviour of a nonlinear system near the unstable equilibria by preserving the realistic features of the system without facing any conventional drawbacks. In this respect, it is mathematically proven and numerically observed that the present approach has various superiorities over the conventional approach.

Keywords: Unstable equilibrium, repelling fixed-points, dynamical systems, advection-diffusion processes, inverse problems.

YILDIZ TECHNICAL UNIVERSITY
GRADUATE SCHOOL OF SCIENCE AND ENGINEERING

Bazı Dinamik Sistemlerin Kararsız Dengeleri

Tahir COŞGUN

Matematik Anabilim Dalı Doktora Tezi

Danışman: Prof. Dr. Murat SARI

Bilimsel hesaplamalarda doğrusal olmayan bir sistemin kararlı dengesini bulmak için çeşitli sayısal teknikler olmasına rağmen, literatürde bir sistemin kararsız dengesini keşfetmek için yaygın olarak kullanılan bir hesaplama yaklaşımına rastlanmamıştır. Bu doktora tezi, itici bir davranış sergileyen dinamik bir sistemin denge konumlarını ortaya çıkarmak için yeni bir yaklaşım sunmayı amaçlamaktadır. Doğrusal olmayan bir sistemin kararsız denge konumlarını bulmak için ters sabit nokta yineleme yöntemi (RFPIM) adı verilen yeni geliştirilmiş bir algoritma sunulmuştur. Bir problemin gerçek özelliklerini koruyan mevcut yöntem, herhangi bir geleneksel dezavantajla karşılaşmadan, kararsız denge civarında doğrusal olmayan bir sistemin davranışını ortaya çıkarabilir. Bu açıdan mevcut yaklaşımın geleneksel yaklaşıma göre çeşitli üstünlüklerinin olduğu matematiksel olarak ispatlanmış ve bu durum sayısal olarak da gözlemlenmiştir.

Anahtar Kelimeler: Kararsız denge, itici sabit noktalar, dinamik sistemler, adveksiyon-difüzyon süreçleri, ters problemler.

YILDIZ TEKNİK ÜNİVERSİTESİ FEN BİLİMLERİ ENSTİTÜSÜ

1 INTRODUCTION

Solving a linear and/or nonlinear problem at the heart of science has been of great importance for ages. Where possible, the solution of such systems has directly and explicitly been derived. The solutions, acquired in such a manner, are so-called exact or analytical solutions of the system. Under suitable assumptions, the existence of solutions, and if it exists, the uniqueness of the solution to the problem could be investigated further. Usually, linear problems possess a unique solution if the problem is accompanied by acceptable initial and boundary conditions. It is not the case for the nonlinear side of the coin in most cases. The number of solutions which a nonlinear problem is still quite ambiguous for the scientific society. Moreover, there does not exist in the literature a general way or method to handle the solution processes.

1.1 Literature Review

The literature includes a diversity of approaches and techniques depending on the studied problem. In any case, numerical methods are needed to reach the desired solutions due to the difficulties and impossibilities in the analytical solution procedures, especially for more realistic problems. Moreover, the abundance of techniques and approaches have been in question regarding the numerical methods. However, most of the nonlinear systems still have not possessed an exact solution procedure. Therefore, it is essential to study some numerical solution procedures for nonlinear systems. In this context, Picard's invention of the method of successive approximations, in the pursuit of Liouville and Poincare, deserves a special care. Brouwer [1] proved the fixed point theorem for continuous mappings in finite dimensional spaces, and later on, Schauder [2] generalized the results of Brouwer to infinite dimensional spaces. It is important to note that this was the first fixed-point theorem for infinite dimensional spaces. Despite their extraordinary contributions, both of them focused only on some existence results. Further generalizations of Schauder's fixed-point theorem was given by Tychonoff [3] and Ky Fan [4] by extending the properties of the space of interest.

Banach, among his contemporaries, can be regarded in a leading position because of his great contribution to the fixed-point theory for contractive mappings. His famous theorem [5] can be stated as follows:

Theorem 1.1 (Contraction Mapping Principle). Let $(X, \|.\|)$ be a Banach space, and U be a subset of X, and let $N: U \to U$ be a contraction with Lipschitz constant λ . Then N has a unique fixed-point ξ in U. Precisely, if $x_0 \in U$ then the sequence $\{x_n\}_{n=0}^{\infty}$ with

$$x_{n+1} = N(x_n), \quad n \ge 0$$

converges to ξ .

The reputation of Banach contraction mapping principle comes from that it provides rigorous information about the existence, uniqueness and determination procedure of the solution of the nonlinear system

$$Nx = x. (1.1)$$

The Banach fixed-point theorem was generalized for non-expansive mappings independently by Kirk [6] and Browder [7]. Many further generalizations of these fundamental fixed-point theorems were studied in the literature such as in the references [7–13].

In this context, it is considerable to note that the evolution and generalizations of the fixed-point theory thrive upon two motivations: one is to change the nature of the mapping, and the other is to expand the related structures or topological properties of the space. Therefore, it is of great importance to study the nature or the characteristics of a fixed-point locally by taking into account the global properties of the space.

To preserve the fluency of the subject, we are closing the discussion about the literature for now. The literature will be discussed in more detail in the next chapter.

1.2 Objective of the Thesis

The numerical methods that have been discussed in the literature for centuries could be categorized in a number of diversified ways. But, the current thesis focuses mainly on a local numerical method, the fixed-point iteration method. So far, the researches concentrate on the attracting equilibrium solutions of a system, and therefore, the main objective of this study is to develop an approach, namely the reversed fixed point iteration method (RFPIM), to uncover the equilibrium positions behaving a repelling

nature.

Fixed-points of system (1.1), could be categorized as stable and unstable equilibrium solutions. Although there exist further sub-classifications of these equilibria, in this thesis, attracting fixed-points stand for asymptotically stable equilibria and repelling fixed-points represent unstable equilibria. Hereby, the main objective of this thesis emerges as finding the unstable equilibrium positions or fixed-points of repelling nature. To achieve this goal a novel approach, the RFPIM, has been developed in this thesis.

1.3 Original Contribution

The essence of this thesis could be clarified via an example problem in fluid dynamics consisting of a sink and a source as in Figure 1.1. Assume a particle with negligible mass suspended at the starting point, x_0 , in a pool with a source u_i and a sink s_i . The release of the particle x_0 will lead to its slide into the sink s_3 with the flow. If the positions of the particle are recorded step by step, each of the steps can then be considered as a step of the conventional fixed-point iteration method (FPIM). It is possible to accelerate the iteration by improving the FPIM, and of course, there are plenty of such improvements in the literature succeeded so far. In the end, the particle is going to meet inevitably with the sink, and hence, the position of the sink will be located. On the other hand, source localization or identification is a harder issue to handle. It requires more complicated observations via more advanced equipment. At least, it is relatively tedious and exhausting to convey the particle against the stream. This difficulty could be eliminated via the use of higher-order numerical methods. Moreover, due to the inner structure of the fluid flow in the pool, it will be difficult to decide the domain of dependence of the particle for a particular position. Precisely, there could be several possible previous positions for any intermediate location. Exactly, this is the case for most realistic problems.

Now at erst, some logical, reasonable and admissible restrictions should be imposed on the current problem. First of all, the mathematical space of interest to be studied should be determined. Although the ideas constructed in the thesis can be performed in metric spaces, Banach spaces have been preferred to scrutinize since they are more relevant for application purposes. In most realistic scientific problems, Banach spaces include necessary and sufficient technical tools such as a distance function or norm, sufficiently well-experienced and well-established concepts of derivative and integral. Moreover, in some particular cases, Banach spaces could be equipped with an inner product and turn into a Hilbert space as in the space of signals with finite energy,

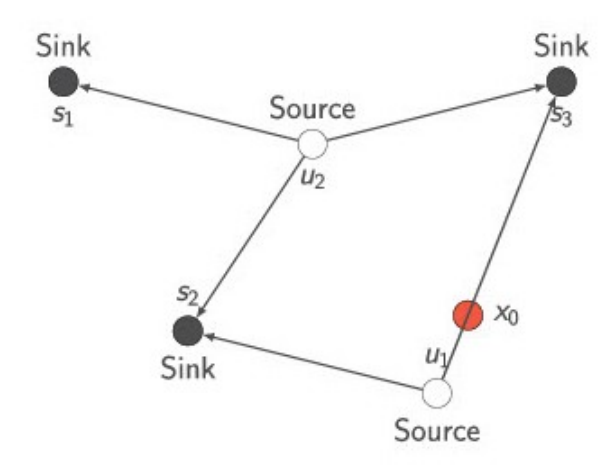


Figure 1.1 The numerical flow governed by the conventional fixed point iteration.

 $L^2(a, b)$. Secondly, the problems of interest have been restricted to dynamic systems in which time dependence is crucial. The reason why this limitation has been set is the desire to examine more realistic problems.

1.4 Outline of the Thesis

Being equipped with enough technology, the current thesis reveals its findings as follows: Chapter 3 provides main theoretical results including the construction of the RFPIM and rigorous error bounds. Chapter 4 consists of implementations of the RFPIM regarding various applications. The structure of the thesis has been prepared in a harmony with the advance of the examined applications throughout the forthcoming chapters so that the investigated applications have been getting more and more sophisticated and realistic through the chapters. In this respect, the polynomial root finding problem has been investigated, and it has been deduced that if the roots of the polynomial are positive and distinct then necessarily the Picard iteration converges to the least root, and if the roots are enumerated with respect to their magnitudes then the roots of even indices are needed to be of repelling nature, i.e. they must be unstable equilibria. The quantitative results indicate that the RFPIM is able to catch these unstable roots while the conventional FPIM cannot.

In the next application, the repelling property of the boundary of the filled in the Julia sets has been observed. Hence, the RFPIM has been implemented in complex number field, \mathbb{C} . Then, the applicability of the RFPIM has been shown for 2D and 3D root-finding problems. For a population dynamics model with a critical threshold, it has been justified that the critical threshold is an unstable equilibrium position for

admissible spatial increments, Δx . Both the qualitative and quantitative indications exhibit the effectiveness of the RFPIM towards to localization of this threshold.

In the same chapter, a nonlinear Fredholm integral equation of the second kind has been debated. As expected, the mentioned problem possesses more than one solution, and it has been seen that some of these solutions are unstable equilibria of the corresponding integral operator. The RFPIM is viewed as highly capable of finding these unstable equilibria.

The pendulum problem representing a nonlinear and highly oscillatory behaviour has been discussed as well. In this respect, the RFPIM has been verified to succeed in finding the unstable equilibrium position of the concerned fundamental control problem. When closing this chapter, a 3D chaotic system has been examined. The origin of \mathbb{R}^3 exhibits a resonating behaviour in this example. Accordingly, the origin is shown to be an unstable equilibrium position, and as a result, the RFPIM seems excellent to figure out this source-like behaviour. Thus far, the RFPIM has been implemented on problems from various application areas including a system of ordinary differential equations (ODEs).

In Chapter 5, the RFPIM has been implemented for a linear and unsteady advection-diffusion process. The main aim of this chapter is to demonstrate the applicability of the present method to solve a partial differential equation (PDE). In this context, the RFPIM has been utilized via a hybrid approach that combines the current method and the conventional finite difference schemes. The reversed nature of the method has forced us to consider an inverse problem in advection-diffusion processes, specifically the source identification or the initial data identification problem. During the observations, whenever it is possible, the advection dominant cases have been particularly focused on. This is exactly a challenge condition for any advection-diffusion mechanisms. Although it is not encountered in everyday life frequently, the movement of the atoms become too stagnant under extremely low temperatures. Since the temperature of the space, 2.7 Kelvins, is just above the absolute zero, -273.15 centigrade degrees or 0 Kelvin, the advection dominant cases become severely important in space studies, and aeronautics as well.

When the inverse problems are concerned, the dependence on the initial data should be taken into account inevitably. This consideration is crucial, particularly regarding the numerical methods since it is important to know how any wrong measurement in the initial data will affect the overall mechanism and the final time data.

Chapter 6, has been devoted to applying the mentioned ideas to a nonlinear PDE. In this respect, Chapter 7 examines a more complicated class of partial differential

equations, namely the singularly perturbed and generalized Burgers-Huxley and Burgers-Fisher equations. In this chapter, a bunch of solitary wave solutions of the mentioned equations have been derived for comparison purposes to test the current method. In accordance with this generalization purpose, Chapter 8 illustrates the way of handling the initial data identification problems in 2D coupled advection-diffusion processes via the RFPIM.

When closing this section it is vitally important to note that not only the numerical schemes or stencils have been reversed, but also physical processes are reversed whenever it is needed during the implementation of the RFPIM. Thereby, throughout this thesis, more than a numerical method, in fact an approach, based on the exploit of inherent power or dynamics of the investigated problem, has been constructed.

2 LITERATURE

A nonlinear system of the form (1.1) has usually more than one equilibrium solution from the application viewpoint. These equilibria may be either stable or unstable. Once the obtained equilibrium is stable, the Banach contraction mapping principle provides a rigorous analysis about this equilibrium. Moreover, the mentioned equilibrium solution can be found via the fixed-point iteration method. In the meantime, there has not been a commonly adopted algorithm even though unstable equilibrium solutions are encountered frequently in scientific problems.

In this respect, the reason and motivation of this thesis is to locate the unstable fixed-points of an operator defined on Banach spaces, and the aim of this thesis is to construct an approach regarding unstable equilibria of a mapping. It may be a challenging task to find out an unstable equilibrium solution. Even for the fixed point iteration in the space of real numbers, in the presence of more than one fixed-point, the local convergence of the iteration was shown by Stepleman [14]. The following theorem gives a test to decide whether the fixed-point iteration converges or diverges around a fixed-point, that is to say, whether a fixed-point is stable or unstable.

Theorem 2.1. Let $(X, \|.\|)$ be a Banach space, and U be a subset of X. Suppose $N: U \to U$ has a fixed-point at ξ . Then ξ is attracting if $\|N'(\xi)\| < 1$, repelling if $\|N'(\xi)\| > 1$. If $\|N'(\xi)\| = 1$, the test is inconclusive, and the fixed-point at ξ is said to be neutral. ξ may be attracting, repelling or neither.

Theorem 2.1 was proved partially by Ostrowski [15], and a discussion about the remaining part can be found in reference [16].

In Chapter 4, various fundamental problems such as root finding problems[17–19], Julia sets [20, 21], population dynamical models [22], nonlinear Fredholm integral equations [23–25], the simple pendulum, and chaos [26] have been discussed via the RFPIM. The literature on these problems is quite extensive as well as there could be found detailed information on these problems in many different primary sources.

Therefore, the literature regarding more realistic problems like PDEs will be discussed more extensively in the remaining part of this section.

The linear unsteady advection-diffusion equation

$$u_t + \alpha u_r - \epsilon u_{rr} = 0 \tag{2.1}$$

having non-dissipative and dissipative components has been attracting researchers from various disciplines for many years. To begin with, the advection-diffusion equation has been exploited as a model equation in many scientific problems such as flow in porous media [27], thermal pollution in river systems [28], long-range transport of pollutants in the atmosphere [29], contaminant dispersion in shallow lakes [30], the dispersion of dissolved material in estuaries and coastal seas [31, 32], pollutant transport in rivers and streams [33], and dispersion of tracers in porous media [34]. Recently, a cellular automaton model based on the movements of pedestrians that are affected by a hazardous gas leakage represented by an advection-diffusion problem is presented [35]. Besides, advection-diffusion phenomena are studied on a two-dimensional lattice network to maximize the efficient use of energy; and the transfer of the surplus energy to an appropriate direction in the lattice is proposed as one way of utilizing renewable energy in maximum capacity [36].

The advection-diffusion process describes the conservation of momentum in the case of non-uniform fluid flows. In addition to the underlying physical dynamics, the reputation of the advection-diffusion equation originates from its stiff behaviour for relatively small values of the kinematic viscosity, $\epsilon \ll 1$. If the equation is diffusion dominated, then Equation 2.1 performs a parabolic behaviour. In such cases, the diffusion equation could be solved instead of Equation 2.1 by neglecting the advection term. However, if the viscosity is relatively small, the equation is advection dominant, then Equation 2.1 behaves in a hyperbolic nature. In this situation, if the diffusive term is neglected, an undesirable numerical fluctuation is observed in the solution especially due to central differencing of convective terms. In addition to that, the upwind schemes usually cause an artificial numerical diffusion [37].

In the light of precious and praiseworthy contributions of antecedents, solution procedures of the advection-diffusion equation still captivate scientists endeavoring in a wide range of disciplines. Some of the studies carried out in this context can be summarized as follows: The method of characteristics was combined with the finite difference or finite element methods to treat advection-dominated diffusion problems [38]. The authors showed the optimal error estimates for various schemes

in $L^2(\mathbb{R})$ or $W^{1,2}(\mathbb{R})$ with the corresponding norms. Their findings, allowing the use of larger time steps, are persuasive about the efficacy of the proposed method since the derived error estimates depend on the rate of change of the solution with respect to the characteristic direction instead of time; and the solution of the model equation changes much more slowly in the direction of the characteristics than in the time direction. Superconvergence of local discontinuous Galerkin scheme, being a class of finite element methods and formerly developed to analyze the hyperbolic conservation laws, was enhanced for the advection-diffusion equation [39]. Orders of superconvergence were seen to be k + 3/2 for piecewise P^k polynomials with $k \geq 1$. Also, a second-order nearly analytic discrete method was offered for the one-dimensional unsteady advection dominated diffusion equations such as singularly-perturbed advection-diffusion equation and viscous Burgers equation with slightly better stability results [40]. An unconditionally stable fourth order semi-discrete method was derived by exploiting the Padé approximation method [41]. A binding Fourier stability analysis of the flux reconstruction method was implemented for the linear advection-diffusion equation [42], and findings confirm that the maximum acceptable time step for the advection-diffusion equation is greater than that of pure advection or pure diffusion. A total variation diminishing and L-stable difference scheme, based upon a second or third order Lax-Wendroff type difference scheme, was studied [43]. The proposed method was seen to be as accurate as of the Holly-Preissmann backward characteristic method. A fully-discrete finite difference method consisting of a third-order total variation diminishing Runge-Kutta method for time and a local discontinuous Galerkin method for space with piecewise polynomials was suggested [44]. Also, the energy technique was utilized to derive the optimal error estimate in the energy norm. An error estimating method involving an upwind scheme and Lax-Wendroff scheme was proposed for the model equation by employing a sensitivity analysis on the parameters Δt , Δx , and ϵ [45]. To treat the advection-diffusion equation, a polynomial based differential quadrature method for space and a third-order Runge-Kutta scheme for the time, because of its strong stability preserving property, were coupled; and the results indicated that the proposed technique yields high accuracy and maximal gain of computational effort [46]. A sixth-order compact finite difference method and RK4, for space and time, respectively, were combined to model the concentration of a contaminant in a water reservoir [47]. An inclusive research about Taylor polynomial based difference schemes up to tenth order was proposed [48].

In addition to the numerical methods mentioned above, some analytical or semi-analytical methods are also encountered in the literature. Two different techniques were offered to achieve solutions of the advection-diffusion equation having a polynomial flow field [49]. The first approach is an iterative method thriving upon the idea of converting the model equation to a singular integro-differential equation, and the second one is relying on the use of the associated heat polynomial expansion directly in the model equation. The responses were seen to be effective for short time spans, and especially, the iterative method was seen to be more suitable for the two-dimensional advection-diffusion problems as opposed to the expansion methods. Another analytical solution procedure of the advection-diffusion equation with time-varying boundary conditions was obtained based on the eigenfunction expansion method for modeling the contaminant transport in the groundwater reservoir [50].

As far as numerical methods are concerned, in the literature, they are inevitably accompanied by debates regarding the convergence and stability issues. this respect, L^2 -stability analysis was carried out for a mixed strategy such as implicit-explicit Runge-Kutta schemes in time and discontinuous Galerkin methods based on the (σ, μ) -family of diffusion schemes in space [51]. The findings are located on a rigorous ground by providing necessary and sufficient conditions on the parameters σ and μ which guarantee the L^2 stability for the time steps $\Delta t = O(\epsilon/\alpha^2)$. Spectral analysis of various difference schemes for the advection-diffusion equation was investigated, and qualitatively presented through figures depicting the stability regions in the CFL number- $\Delta x \Delta t$ plane [52]. Alternating-direction explicit finite difference methods, formerly developed to solve linear partial differential equations such as heat distribution, were analyzed [53], and in the direction of advection from left to right, the scheme was seen to be unconditionally stable. Moreover, another significant finding of the authors was that the stability of the scheme is limited mainly by the advection term. The enthusiastic readers should consult the work of Chan [54] for a comprehensive paper as to the stability analysis of various difference schemes concerning the advection-diffusion equation. In the mentioned paper, Chan provides a rigorous stability analysis for different schemes such as Crank-Nicolson, DuFort-Frankel, leap-frog, Pade approximation schemes, and so on by taking advantage of the Schur-Cohn theory. Regarding the stability analysis for the advection-diffusion equation, the concepts of the von Neumann analysis, the CFL condition, and the matrix method were reviewed in a historical manner [55].

Particularly, describing the nonlinear advection-diffusion mechanisms, systems of the type

$$u_t + \alpha u u_x - \epsilon u_{xx} = 0, \quad x \in (a, b), t > 0.$$
 (2.2)

have been widely discussed in the literature [46–48, 56–73] with testing purposes for the newly developed algorithms. Besides, there are many books and research

articles published in the literature to discover the behaviour of the nonlinear advection-diffusion-reaction mechanisms using continuous or discrete methods [27, 48, 74–87]. In this respect, the aim of the later chapters of this thesis focused on developing a novel method and approach to derive numerical responses of the mentioned class of PDEs. In particular, the method introduced by Wang et al. [44] and Abdelkader [88] is followed to infer some solitary wave solutions of the singularly perturbed nonlinear advection-diffusion-reaction mechanisms.

For many researchers, in addition to its physical importance, the advection-diffusion-reaction equations are test problems towards the solution procedures of more complicated problems such as the Navier-Stokes equation. In this respect, a newly produced method called the reversed fixed point iteration method has been implemented in this thesis to find out numerical solutions of the advection-diffusion-reaction equations by hybridizing it with various difference schemes [56].

MAIN THEORETICAL RESULTS

Fixed-points of system (1.1), with the notions of Lyapunov stability, have been categorized as stable and unstable equilibrium solutions. Although there exist further sub-classifications of these equilibria, in this study, an attracting fixed-point stands for an asymptotically stable equilibrium and a repelling fixed-point represents an unstable equilibrium.

Theorem 3.1 (Reversed Fixed Point Iteration Method). Let $(X, \|.\|)$ be a Banach space, and $N: X \to X$ be a continuously differentiable nonlinear mapping in the Fréchet sense. Let ξ be an unstable equilibrium solution for Nx = x. Then the sequence $\{x_n\}_{n \in \mathbb{N}}$ constructed implicitly by the reversed fixed-point iteration

$$x_n = N(x_{n+1}) \tag{3.1}$$

converges to ξ for every initial guess x_0 , which is sufficiently close to ξ .

Proof. Let $V \subset X$ be the region of repulsion for the unstable fixed-point ξ . Since N is a continuously differentiable mapping around ξ , the inverse function theorem guarantees that N^{-1} exists in a sufficiently small neighbourhood, say U, of ξ . For the sake of notational clarity, we can choose $U \subset V$, and we can safely restrict N to U. Since ξ is an unstable fixed-point, $N:U \to X$ is an expansive mapping, and for any $x,y \in U$ we have

$$\lambda \|N^{-1}(N(x)) - N^{-1}(N(y))\| = \lambda \|x - y\| \le \|N(x) - N(y)\|$$

where λ is a scalar with $\lambda > 1$. The last inequality implies that

$$||N^{-1}(N(x))-N^{-1}(N(y))|| \le \frac{1}{\lambda}||N(x)-N(y)||.$$

Hence, $N^{-1}: N(U) \to U$ is a contraction with the Lipschitz constant $1/\lambda$. Then, Banach contraction mapping principle necessitates that for any initial guess $x_0 \in$

N(U), the sequence $\{x_n\}_{n\geq 0}$ defined by the iteration

$$x_{n+1} = N^{-1}(x_n), \quad n \ge 0$$

converges to unstable fixed-point ξ of N. In addition, the inverse function theorem guarantees also that $N^{-1}:N(U)\to U$ is of class C^1 . Now, using the contractivity of N^{-1} in N(U), the followings can be observed:

$$||(N^{-1})'(\xi)h|| = \left| \left| \lim_{t \to 0} \frac{N^{-1}(\xi + th) - N^{-1}(\xi)}{t} \right| \right|$$

$$= \lim_{t \to 0} \left| \left| \frac{N^{-1}(\xi + th) - N^{-1}(\xi)}{t} \right| \right|$$

$$\leq \lim_{t \to 0} \frac{1}{\lambda} \left| \left| \frac{th}{t} \right| \right| = \frac{1}{\lambda} ||h||.$$

In the second step of the above calculations, uniform continuity of the norm and existence of the Gâteaux derivative, by assumption, allow us to commute the norm and the limit. Since the existence of continuous Gâteaux derivative implies the existence of Fréchet derivative, we can use derivatives in the Fréchet sense. Thereby, it can be concluded directly from definition of the operator norm that ξ is an attractive fixed point of N^{-1} i.e.

$$\|(N^{-1})'(\xi)\| = \sup_{h} \frac{\|(N^{-1})'(\xi)h\|}{\|h\|} \le \frac{1}{\lambda} < 1.$$
 (3.2)

This completes the proof.

Remark 3.1. Notice that finding the inverse mapping N^{-1} is as hard as finding the fixed-point ξ . Therefore, instead of using the iteration $x_{n+1} = N^{-1}(x_n)$, we can use the iteration $x_n = N(x_{n+1})$. This is the main motivation of this thesis. However, in this case we must carry the burden of solving an ill-posed problem in some cases.

The following corollary can be stated as a conclusion of Theorems 1.1 and 3.1.

Corollary 3.1. Let $(X, \|.\|)$ be a Banach space, and N be an expansive mapping near the fixed-point ξ with expansion coefficient $\lambda > 1$. If the sequence x_n is defined by iteration (3.1), then for any initial guess x_0 sufficiently close to the fixed-point ξ of N, the errors in the application of the reversed fixed-point iteration method is estimated by

$$||x_n - \xi|| \le \frac{1}{(\lambda - 1)\lambda^{n-1}} ||x_1 - x_0|| \tag{3.3}$$

and

$$||x_n - \xi|| \le \frac{1}{\lambda^n} ||x_0 - \xi|| \tag{3.4}$$

for n = 1, 2, 3, ...

Proof. Since N is an expansive mapping with expansion constant λ , N^{-1} is a contraction with a contraction coefficient $1/\lambda$, in other words

$$||N^{-1}(x) - N^{-1}(y)|| \le \frac{1}{\lambda} ||x - y||$$
(3.5)

for any x, y in a sufficiently small neighbourhood of ξ . Now, by taking $x_{n+1} = N^{-1}(x_n)$ into account, the followings can be deduced:

$$\begin{aligned} \|x_{n+p} - x_n\| &\leq \sum_{k=1}^p \|x_{n+k} - x_{n+k-1}\| \\ &\leq \sum_{k=1}^p \frac{1}{\lambda^{n+k-1}} \|x_1 - x_0\| \\ &\leq \frac{1}{\lambda^n} \|x_1 - x_0\| \sum_{k=1}^\infty \frac{1}{\lambda^{k-1}} \\ &\leq \frac{1}{(\lambda - 1)\lambda^{n-1}} \|x_1 - x_0\|. \end{aligned}$$

Hence, taking limit as $p \to \infty$ in the last inequality, it can be deduced that

$$\lim_{p \to \infty} \|x_{n+p} - x_n\| = \|x_n - \xi\| \le \frac{1}{(\lambda - 1)\lambda^{n-1}} \|x_1 - x_0\|. \tag{3.6}$$

This completes the proof of the first inequality. The proof of the second inequality comes from the application of (3.5) repetitively:

$$||x_n - \xi|| = ||N^{-1}(x_{n-1}) - N^{-1}(\xi)|| \le \frac{1}{\lambda} ||x_{n-1} - \xi|| \le \dots \le \frac{1}{\lambda^n} ||x_0 - \xi||.$$
 (3.7)

4 VARIOUS APPLICATIONS

In the previous chapter, since unstable equilibria are frequently encountered in scientific problems, a numerical procedure that reveals unstable fixed-points in Banach spaces has been established. From the viewpoint of fixed-point theory, it is inevitable that an unstable equilibrium solution is of repelling nature. To find out repelling fixed-points, Theorem 3.1 gives a sufficient theoretical basis while Corollary 3.1 supplies a tool of accuracy for the current method.

In this chapter, different illustrative examples originated from a wide range of applied areas are considered. For this purpose, examples regarding root finding problems in \mathbb{R} , \mathbb{R}^2 , and \mathbb{R}^3 are considered, the repelling property of the Julia sets are observed, a population dynamics model with an unstable critical threshold is analyzed, unstable solutions of nonlinear Fredholm integral equations of the second kind are studied, the pendulum is one of the basic examples of nonlinear control problems is analyzed, and lastly, a 3D system of ODEs that exhibits a chaotic behaviour is examined.

4.1 Roots of Polynomials

First of all, the root finding problem

$$f(x) = 0 \tag{4.1}$$

where $x \in \mathbb{R}$ is considered. To begin with, f(x) is taken as a polynomial.

Theorem 4.1. Assume that f(x) is a monic nth degree polynomial with real coefficients and it has n positive distinct real roots i.e.

$$f(x) = \prod_{k=1}^{n} (x - x_k)$$

where $x_1, x_2, ..., x_n$ are the roots of f, and suppose that $0 < x_1 < x_2 < \cdots < x_{n-1} < x_n$. If m is an even number, then x_m is an unstable equilibrium solution of problem (4.1).

Proof. The linear term of f(x) is $(-1)^{n-1}S_{n-1}x$, where S_{n-1} is the (n-1)st elementary symmetric function of $\{x_1, x_2, \dots, x_n\}$ defined by

$$S_{n-1}(x_1, x_2, \dots, x_n) := \sum_{k=1}^n \prod_{\substack{i=1 \ i \neq k}}^n x_i.$$

Now, root finding problem (4.1) can be reconsidered as a fixed-point problem as in the following

$$g(x) := x + \frac{(-1)^n}{S_{n-1}} \prod_{k=1}^n (x - x_k) = x.$$
 (4.2)

The roots of f are just the fixed-points of g. Derivative of g can be computed as

$$\frac{dg(x)}{dx} = 1 + \frac{(-1)^n}{S_{n-1}} \sum_{i=1}^n \prod_{\substack{k=1\\k \neq i}}^n (x - x_k).$$
 (4.3)

For a particular root, say x_m , the following computations can be carried out

$$g'(x_m) = 1 + \frac{(-1)^n}{S_{n-1}} \prod_{\substack{k=1\\k \neq m}}^n (x_m - x_k)$$
(4.4)

$$=1+\frac{(-1)^n}{S_{n-1}}\prod_{k=1}^{m-1}(x_m-x_k)\prod_{k=m+1}^n(x_m-x_k)$$
(4.5)

$$=1+\frac{(-1)^{n}(-1)^{n-m}}{S_{n-1}}\prod_{k=1}^{m-1}(x_{m}-x_{k})\prod_{k=m+1}^{n}(x_{k}-x_{m})$$
(4.6)

$$=1+\frac{(-1)^m}{S_{n-1}}\prod_{k=1}^{m-1}(x_m-x_k)\prod_{k=m+1}^n(x_k-x_m). \tag{4.7}$$

According to Theorem 2.1, if m is an even number then the corresponding fixed-point x_m of g is necessarily an unstable fixed-point since $|g'(x_{2k})| > 1$ for k = 1, 2, ...

Although Theorem 4.1 suffices for our observations on unstable equilibria, some corollaries have been provided regarding the stable equilibrium solutions of problem (4.1).

Corollary 4.1. x_1 is an asymptotically stable equilibrium solution of nonlinear system (4.1).

Proof. In the proof of previous theorem, if x_1 is plugged in g'(x), then the followings

can be observed

$$g'(x_1) = 1 - \frac{1}{S_{n-1}} \prod_{k=2}^{n} (x_k - x_1)$$

$$= 1 - \frac{\prod_{k=2}^{n} (x_k - x_1) / S_n}{S_{n-1} / S_n}$$

$$= 1 - \frac{\prod_{k=2}^{n} (1 - \frac{x_1}{x_k})}{\sum_{k=1}^{n} \frac{x_1}{x_k}}.$$

Since the inequalities $\prod_{k=2}^n (1 - \frac{x_1}{x_k}) < 1$ and $\sum_{k=1}^n \frac{x_1}{x_k} > 1$ both hold, so does the inequality $|g'(x_1)| < 1$. In other words, the smallest root of f(x), namely x_1 , is always an asymptotically stable equilibrium solution to equation (4.1).

Application of the Picard iteration to problem (4.1) produces the solution x_1 . The reason of this consequence is that the orbit of 0 converges to x_1 , that is to say, 0 lies in the basin of x_1 , and of course, the constant term of g lies in the attraction region of x_1 .

Corollary 4.2. Let the roots of nonlinear system (4.1) satisfy the inequality

$$M^{n-1} < 2S_{n-1} (4.8)$$

where M is defined as

$$M := \max\{(x_{2j-1} - x_1), (x_n - x_{2j-1})\}.$$

Then the root x_{2j-1} is an asymptotically stable equilibrium solution of system (4.1) for $j = 2, 3, \ldots$

Proof. In the proof of Theorem 4.1, let m = 2j - 1 to obtain

$$g'(x_{2j-1}) = 1 - \frac{1}{S_{n-1}} \prod_{k=1}^{2j-2} (x_{2j-1} - x_k) \prod_{k=2j}^{n} (x_k - x_{2j-1})$$
 (4.9)

where $j = 2, 3, \ldots$ Now, considering the following observations

$$0 < \frac{1}{S_{n-1}} \prod_{k=1}^{2j-2} (x_{2j-1} - x_k) \prod_{k=2j}^{n} (x_k - x_{2j-1}) < \frac{M^{2j-2} M^{n-2j+1}}{S_{n-1}}$$

$$= \frac{M^{n-1}}{S_{n-1}}$$

$$< \frac{2S_{n-1}}{S_{n-1}}$$

$$= 2$$

it can be deduced for j = 2, 3, ... that

$$|g'(x_{2j-1})| < 1.$$

Remark 4.1. Since $M < (x_n - x_1)$, the assumption in the corollary can be replaced by $(x_n - x_1)^{n-1} < 2S_{n-1}$ instead of $M^{n-1} < 2S_{n-1}$. Moreover, from Maclaurin's inequality for symmetric polynomials, instead of inequality in (4.8) the following inequality can be checked

$$M < \sqrt[n]{S_n}. (4.10)$$

Remark 4.2. A steady state equilibrium solution, that can be found via the fixed-point iteration method, depends on basin where the initial guess lies in. Similarly, a steady state unstable equilibrium solution, that can be found via the RFPIM, depends on which region of repulsion the initial guess lies in.

Notice that Corollary 4.2, Remarks 4.1 and 4.2 impose some conditions on the distribution of the roots $x_1, x_2, ..., x_n$ in \mathbb{R}^+ for characterization purposes. Attracting and repelling characteristics of these roots alternate between two consecutive roots if there does not exist any relatively high or small root in comparison to the other roots. Particularly, when a 7th degree polynomial with fixed-points 1, 2, ..., 6, 7 is considered, the attracting fixed-points are shown by black dots while the repelling fixed-points are shown by open dots in Figure 4.1.

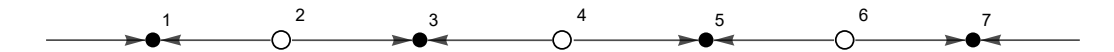


Figure 4.1 Seven equidistant fixed-points.

Now, being equipped with sufficient tools, consider the following algebraic equation

$$x^3 - 6x^2 + 11x - 6 = 0 (4.11)$$

Table 4.1 Some values obtained via the RFPIM from the orbits of some points around x = 2.

Doints			1	1		
Points	5	10	15	20	25	30
1.1	1.40938	1.77559	1.93860	1.98490	1.99638	1.99914
1.5	1.82776	1.95453	1.98892	1.99735	1.99937	1.99985
1.9	1.97481	1.99393	1.99856	1.99966	1.99992	1.99998
2.3	2.06108	2.01401	2.00330	2.00078	2.00019	2.00004
2.7	2.12110	2.02690	2.00629	2.00149	2.00035	2.00008

with roots x = 1, x = 2, and x = 3 [17].

Equation (4.11) can be rewritten in the form of (4.2) as

$$x = \frac{6}{11} + \frac{6x^2}{11} - \frac{x^3}{11}. (4.12)$$

Thus, the problem of finding the roots of f(x) is reduced to the determination of the fixed-points of $g(x) := 6/11 + 6x^2/11 - x^3/11$. By solving equation |g'(x)| = 1, it can be observed that x = 1 is an attracting fixed-point with basin (-0.768..., 1.422...), x = 2 is a repelling fixed-point with the region of repulsion (1.422..., 2.577...) and x = 3 is an attracting fixed-point with region of attraction (2.577..., 4.768...) (see Figure 4.2). Particularly, 6/11 = 0.545... is in the basin of x = 1. Therefore, both the Picard method and Adomian decomposition method yield the solution x = 1 for initial guess $x_0 = 6/11$.

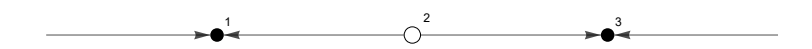


Figure 4.2 Fixed-points of $g(x) = 6/11 + 6x^2/11 - x^3/11$.

The unstable solution x = 2 can be obtained by applying the fixed-point iteration method in the reverse direction. Some starting points and nth iterations obtained from the reversed fixed-point iteration are shown in Table 4.2. Since the RFPIM is an implicit method for this problem, the Newton-Raphson method has been utilized in every intermediate step.

The results of the usual fixed-point iteration method have been presented in Table 4.2 for some starting points and the corresponding nth iterations. Even though randomly distributed starting points are used, the conventional algorithm fails to capture the unstable fixed-point.

Table 4.2 Some values obtained via the conventional method from the orbits of some points around x = 1 or x = 3.

Points			1	ı		
Politis	3	5	10	15	20	30
-0.7	0.90536	0.94028	0.97956	0.99268	0.99734	0.99964
-0.2	0.78456	0.87449	0.96016	0.98605	0.99497	0.99933
0.3	0.79288	0.87865	0.96129	0.98643	0.99510	0.99935
0.8	0.90759	0.94160	0.97999	0.99283	0.99739	0.99965
1.3	1.20772	1.15640	1.06888	1.02737	1.01036	1.00142
1.8	1.74343	1.69830	1.55807	1.38828	1.22415	1.04442
2.3	2.37922	2.43969	2.60925	2.77379	2.89184	2.98261
2.8	2.87146	2.90728	2.96211	2.98548	2.99459	2.99927
3.3	3.12700	3.07849	3.02629	3.00935	3.00339	3.00045
3.8	3.21593	3.12575	3.03991	3.01397	3.00504	3.00067
4.3	3.20538	3.12047	3.03846	3.01349	3.00487	3.00065

4.2 Root Finding in the Complex Field: Julia Sets

In this example, the reversed fixed-point iteration is applied in the complex plane \mathbb{C} , and the obtained iterations are observed in the complex plane. Backward iteration was proposed firstly by Devaney [20] to find out the Julia set of a function. Repelling property of the Julia set is hereby observed one more time by using the RFPIM. In this context, the following root finding problem has been examined:

$$x^2 - 1 = x. (4.13)$$

Solutions of equation (4.13) can be found exactly as $x_1 = \frac{1-\sqrt{5}}{2}$ and $x_2 = \frac{1+\sqrt{5}}{2}$. Since $|f'(x_1)| = |1-\sqrt{5}| \approx 0.618 < 1$ and $|f'(x_2)| = |1+\sqrt{5}| \approx 1.618 > 1$, according to Theorem 2.1, x_1 is an attracting fixed-point while x_2 is a repelling fixed-point. Using the backward iteration

$$x_{n+1}^2 - 1 = x_n, (4.14)$$

system (4.13) can be solved in \mathbb{R} to find out unstable equilibrium solution $x_2 = \frac{1+\sqrt{5}}{2}$. However, if the system is solved in the complex field and if all of the obtained iterations in the final step are plotted in \mathbb{C} , an interesting image has been encountered. For instance, if the reversed fixed-point iteration is started to be applied with initial choice $x_0 = 1$, then iterations obtained from relation $x_{n+1}^2 - 1 = x_n$ after 15 steps can be seen in the complex plane as in Figure 4.3.

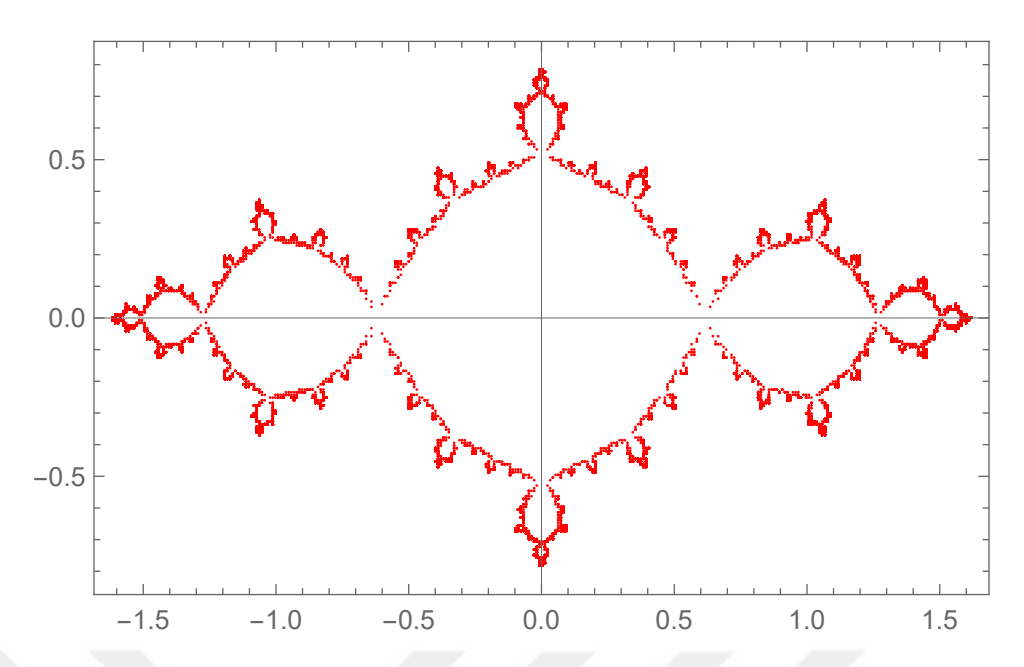


Figure 4.3 The iterations obtained from equation (4.14) after 15 steps via the RFPIM.

In the figure, the iterations depicted in the complex plane are obtained through the RFPIM after 15 steps. If the obtained set of numbers are restricted to the real line \mathbb{R} , then it could be seen that the points in the intersection accumulate near the unstable equilibrium solution $x_2 = (1 + \sqrt{5})/2$.

Now, let us consider the Julia set of function $f(x) = x^2 - 1$. The Julia set is the boundary of the filled Julia set which consists of $x_0 \in \mathbb{C}$ such that the sequence $f^n(x_0) = f(f(f(...f(x_0))))$ remains bounded as $n \to \infty$. As is the case in the literature, infinity is assumed to be an attracting fixed point for any polynomial of degree greater than or equal to 2. Hence, another characterization about the Julia set can be given as the boundary of the region of attraction of ∞ . The Julia set of function $f(x) = x^2 - 1$ is depicted in Figure 4.4. Notice that, there is a similarity between Figures 4.3 and 4.4. If we put them together in the same picture, Figure 4.5 is obtained. It can be observed in Figure 4.5 that the obtained points in Figure 4.3 accumulates near the boundary of the shape in Figure 4.4. The reason behind this situation is that the Julia set is a dynamical repeller.

Boundary of the Julia set is a fractal except some cases. Further information about the Julia sets can be found in references [20, 21].

Remark 4.3. The sequence defined through the RFPIM converges to the Julia set of the function. Here, we do not mean a point-wise convergence, we mean that the obtained set after each iteration converges to the boundary of the filled Julia set as $n \to \infty$, in other words, we mean a set-wise convergence.

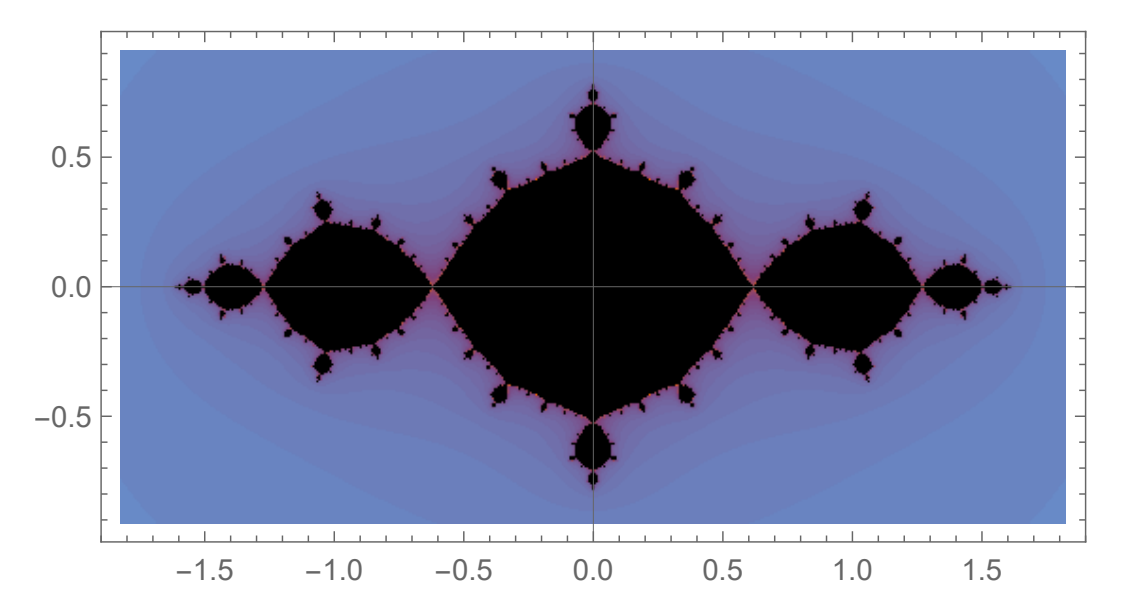


Figure 4.4 The Julia set of function $f(x) = x^2 - 1$.

4.3 2D Root Finding

In this example, following 2D root finding problem [18] is considered

$$x^{2}-2x-y+0.5=0$$
$$x^{2}+4y^{2}-4=0.$$

When we have tried to solve this system using the conventional or the RFPIM, we need to rewrite it as a fixed-point problem as follows:

$$\begin{bmatrix} x \\ y \end{bmatrix} = \begin{bmatrix} 0.5x^2 - 0.5y + 0.25 \\ x^2 + 4y^2 + y - 4 \end{bmatrix}.$$
 (4.15)

Solutions of the system are $\xi_1 = (-0.222..., 0.993...)$ and $\xi_2 = (1.900..., 0.311...)$. If we denote system (4.15) as $N(\mathbf{x}) = \mathbf{x}$, where \mathbf{x} stands for the column vector $(x, y)^T$, then the eigenvalues of the Jacobian matrix of N can be computed approximately as

$$\lambda_1 \approx 8.97$$
 and $\lambda_2 \approx -0.25$ (4.16)

for the fixed-point ξ_1 and as

$$\lambda_{3.4} \approx 2.70 \pm 1.13i$$
 (4.17)

for the fixed-point ξ_2 . Since magnitude of both eigenvalues are strictly greater than 1, the fixed-point ξ_2 is an unstable equilibrium of the system. A stream plot and locations

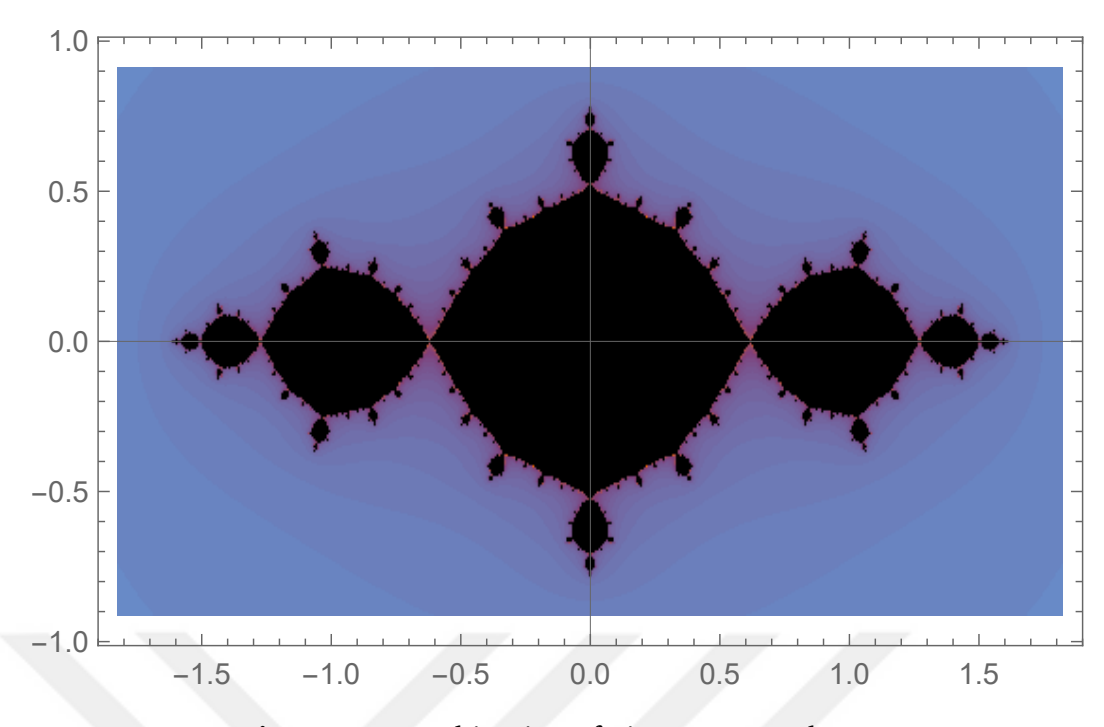


Figure 4.5 Combination of Figures 4.3 and 4.4.

of the fixed points, which are depicted by red dots, can be seen in Figure 4.6.

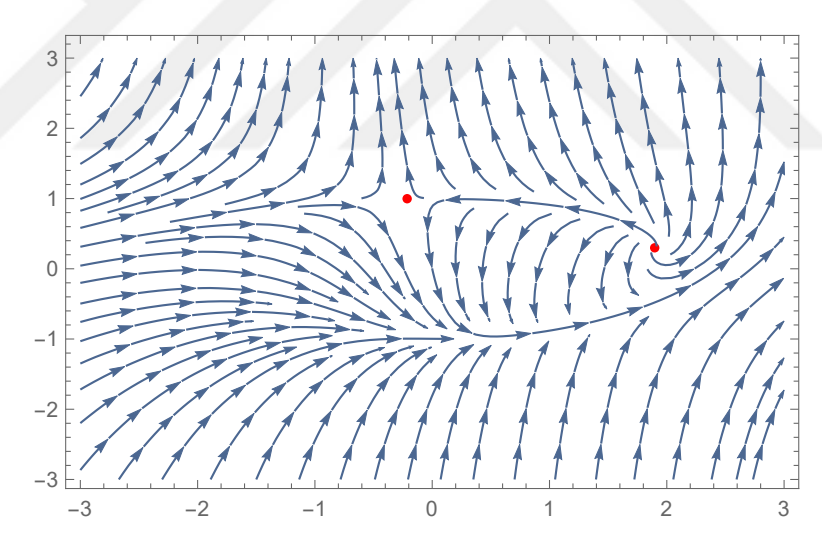


Figure 4.6 Stream plot and locations of the equilibria for system (4.15)

Soundness and accuracy of the proposed method can be observed in Table 4.3. In the intermediate steps of the RFPIM, the Newton method has been utilized to solve implicit equations.

When the conventional fixed-point iteration method is applied to solve system (4.15), even by starting with fairly close initial guesses to desired solutions, the obtained sequence of iterations is seen to diverge as presented in Table 4.4. Notice also that the fixed-point ξ_1 is a saddle point. Hence, the usual fixed-point iteration method fails to find out both of the equilibria ξ_1 and ξ_2 . This situation has been investigated

Table 4.3 Absolute errors after application of the RFPIM for equation (4.15) with different initial choices at different steps.

Points	n				
FOIIItS	5	10	15	20	
			2.31×10^{-10}	1.64×10^{-12}	
(1.90, 0.32)	3.68×10^{-5}	8.27×10^{-8}	1.01×10^{-9}	2.75×10^{-12}	
(1.91, 0.31)	1.29×10^{-4}	5.66×10^{-7}	1.16×10^{-9}	1.50×10^{-11}	
(1.91, 0.32)	1.80×10^{-4}	5.69×10^{-7}	2.22×10^{-9}	1.92×10^{-11}	

numerically in Table 4.4. Although the initial guesses are chosen fairly close to the equilibrium solutions, the sequence obtained through the traditional fixed-point iteration method diverges suddenly.

Table 4.4 Fifth and tenth iterations after application of the fixed-point iteration method for equation (4.15) with different initial choices.

Doints	n				
Points	5	10			
(-0.22,0.99)	$(-0.51, 2.28 \times 10^{1})$	NW^1			
(-0.23,0.99)	(0.54, -3.18)	NW			
(-0.22,1.00)	NW	NW			
(-0.23,1.00)	NW	NW			
(1.90, 0.31)	$(2.14,7.58\times10^{-2})$	NW			
(1.90, 0.32)	(1.12, 2.91)	NW			
(1.91, 0.31)	$(-1.78, 1.45 \times 10^2)$	NW			
(1.91, 0.32)	$(-5.42,6.01\times10^2)$	NW			

4.4 Population Dynamics Model with a Critical Threshold

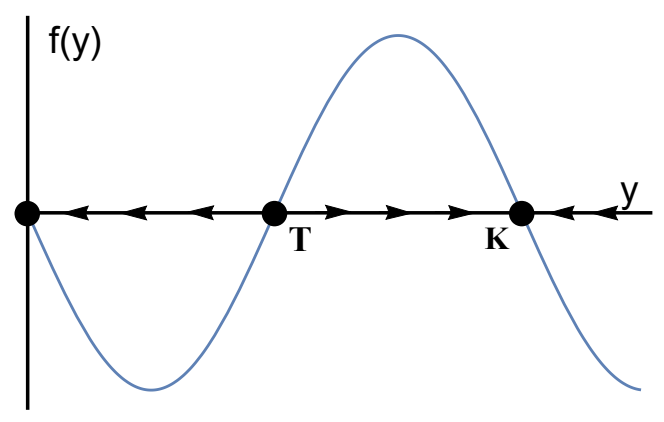
Growth of a population with a critical threshold can be modeled by the autonomous equation

$$\frac{dy}{dt} = -r\left(1 - \frac{y}{T}\right)\left(1 - \frac{y}{K}\right)y\tag{4.18}$$

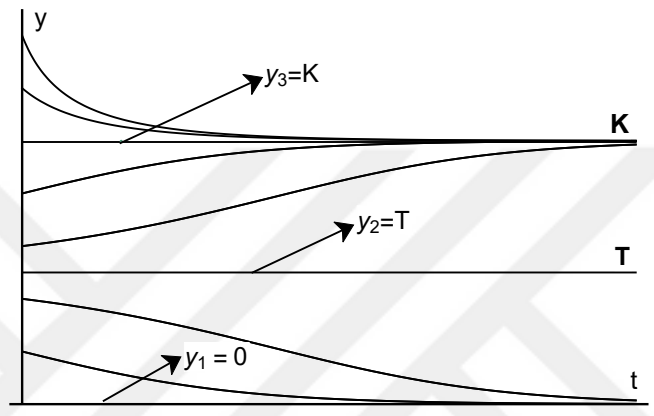
where r is a positive constant depending on the population and environment, T is the critical threshold, and K is the environmental carrying capacity or saturation level. The phase line and sample plots with different initial conditions can be seen in Figure 4.7.

It can be perceived geometrically from Figure 4.7 that y = 0, y = T, and y = K are equilibrium solutions of model (4.18). Critical threshold y = T is an unstable

¹NW=Not Working



(a) Phase line for model (4.18).



(b) Sample solutions for model (4.18) with various initial conditions.

Figure 4.7 Geometrical observations regarding model (4.18).

equilibrium solution while zero population y = 0 and environmental carrying capacity y = K are stable equilibria [22]. These conclusions can be drawn in a more theoretical way in accordance with Theorem 3.1. For this purpose, let us discretize problem (4.18) with the use of a forward finite difference scheme for dy/dt as

$$\frac{y_{n+1} - y_n}{h} = -r \left(1 - \frac{y_n}{T} \right) \left(1 - \frac{y_n}{K} \right) y_n, \tag{4.19}$$

and define an operator N(.) as

$$N(y_n) = y_n + h \left[-r \left(1 - \frac{y_n}{T} \right) \left(1 - \frac{y_n}{K} \right) y_n \right]. \tag{4.20}$$

Thus, equation (4.18) has been converted to be a fixed-point problem as N(y) = y. Notice also that N(.) has become a real-valued third-degree polynomial after discretization. Consequently, it can be differentiated near the fixed-points and the

obtained derivative can be evaluated at the fixed-points as

$$N'(0) = 1 - hr (4.21)$$

$$N'(T) = 1 + hr\left(1 - \frac{T}{K}\right) \tag{4.22}$$

$$N'(K) = 1 + hr\left(1 - \frac{K}{T}\right). {(4.23)}$$

Since 0 < T < K and r is positive, it can be deduced from Equations (4.21)-(4.23) that N'(0) < 1, N'(T) > 1 and N'(K) < 1 for conventionally used small step sizes. Same results can be observed by defining N(.) on C^1 , the space of continuously differentiable functions, instead of \mathbb{R} . Ultimately, threshold level is going to be an unstable equilibrium while zero population level and environmental carrying capacity are going to be asymptotically stable equilibria. From a theoretical viewpoint, the RFPIM is more suitable to find out unstable equilibrium, while the conventional fixed-point iteration method is far more suitable to find out stable equilibria.

For a numerical observation, consider the following problem:

$$\frac{dy}{dt} = -0.5\left(1 - \frac{y}{3}\right)\left(1 - \frac{y}{10}\right)y, \qquad y(0) = y_0. \tag{4.24}$$

For model (4.24), the zero population level y=0 and the environmental carrying capacity y=10 are stable equilibria while the critical threshold level y=3 is an unstable equilibrium. The computed results of the reversed fixed-point algorithm have been presented in Table 4.5. In the solution procedure, the step size is taken to be h=1. To solve inverse problems encountered in the intermediate steps, the Newton-Raphson method has been utilized.

Table 4.5 Numerical simulation of model (4.24) via the RFPIM with different initial values (y_0) with h = 1.

1/			1	1		
y_0	5	10	15	20	25	30
0.5	1.96891	2.73448	2.93893	2.98629	2.99694	2.99932
1	2.34687	2.84176	2.96407	2.99196	2.99820	2.99960
2	2.74389	2.94117	2.98679	2.99705	2.99934	2.99985
4	3.20384	3.04450	3.00988	3.00220	3.00049	3.00011
6	3.55614	3.11745	3.02587	3.00575	3.00128	3.00029
8	3.92696	3.18997	3.04153	3.00922	3.00205	3.00046

Table 4.6 Absolute errors for model (4.24) after the first step of the RFPIM with various step sizes.

	F	S	
\mathcal{Y}_0	h=10	h=100	h=1000
0.5	2.07×10^{-1}	2.35×10^{-2}	2.37×10^{-3}
1.0	1.61×10^{-1}	1.87×10^{-2}	1.90×10^{-3}
2.0	7.69×10^{-2}	9.31×10^{-3}	9.50×10^{-4}
4.0	7.19×10^{-2}	9.21×10^{-3}	9.49×10^{-4}
6.0	2.06×10^{-1}	2.74×10^{-2}	2.84×10^{-3}
8.0	3.33×10^{-1}	4.52×10^{-2}	4.74×10^{-3}

Since the main goal is to find an unstable equilibrium solution, it makes sense to work with relatively larger step sizes at a relatively low cost as usual. When differential equation solving is concerned, it could be observed that the use of larger step sizes increases the speed of the current method. Hence, the desired unstable solution can be obtained after a few steps instead of tedious calculations in each separate single iteration. Notice that the error could be diminished as much as required by increasing the coefficient of expansion of N because of Corollary 3.1. Moreover, the desired accuracy could be captured in the first step by increasing the step size h further.

Remark 4.4. One of the critically important results of using relatively larger step sizes is that the spectral radius of the Jacobian matrix of an operator N is getting larger by increasing h. Thus, in the application process of the Newton method, the possibility to encounter with a too small Jacobian becomes almost impossible.

4.5 3D Root Finding Problem: A Sophisticated but Robust Approach

In this example, the 3D root finding problem

$$x + y + z = 0$$

$$x^{2} + y^{2} + z^{2} - 2 = 0$$

$$xy + xz + 1 = 0$$
(4.25)

is considered [19]. In the previous example, the use of relatively larger step sizes has been observed to be a significant advantage of the RFPIM through the solutions of differential equations. To take advantage of the presented method, the following ODE

Table 4.7 Norm of the absolute errors for corresponding unstable fixed-points at the first step of the RFPIM towards the solution of system (4.26) with an initial guess $(x_0, y_0, z_0) = (0, 0, 0)$ and various values of step sizes.

Fixed Doints			Absolute E	rrors	
Fixed Points	h=10	h=100	h=1000	$h = 10^6$	$h = 10^{10}$
(-1,0,1)	0.11	1.01×10^{-2}	1.00×10^{-3}	1.00×10^{-6}	4.00 ×10 ⁻¹⁵
(1,0,-1)	2.44	1.72×10^{-2}	1.73×10^{-3}	1.73×10^{-6}	1.41×10^{-10}
(-1,1,0)	2.86	7.10×10^{-3}	7.07×10^{-4}	7.07×10^{-7}	5.00×10^{-11}
(1,-1,0)	1.54	1.21×10^{-2}	1.22×10^{-3}	1.22×10^{-6}	1.12×10^{-10}

system could be considered instead of considering system (4.25)

$$\dot{x} = x + y + z
\dot{y} = x^2 + y^2 + z^2 - 2
\dot{z} = xy + xz + 1.$$
(4.26)

System (4.25) has four exact solutions: $(\pm 1, 0, \mp 1)$, $(\pm 1, \mp 1, 0)$. Notice that the fixed-points of system (4.25) are equilibrium solutions of system (4.26). Now, a nonlinear operator can be defined by discretizing system (4.26) as follows

$$N\begin{pmatrix} x_n \\ y_n \\ z_n \end{pmatrix} := \begin{pmatrix} x_n + h_1(x_n + y_n + z_n) \\ y_n + h_2(x_n^2 + y_n^2 + z_n^2 - 2) \\ z_n + h_3(x_n y_n + x_n z_n + 1) \end{pmatrix}.$$
 (4.27)

All of the four exact solutions of system (4.25) can be determined by applying the RFPIM with an initial guess $(x_0, y_0, z_0) = (0, 0, 0)$. For the sake of clarity, the step sizes are taken to be $h_1 = h_2 = h_3 = h$. Note that for any positive values of the step size h, the spectral radius of the Jacobian matrix of N is greater than 1 for any fixed-point of N. Hence, every fixed-point of N must be unstable.

The produced results reveal that the proposed technique may be utilized to obtain fixed-points of a function even in higher dimensions. Notice that the errors in Table 4.7 have been produced by applying the RFPIM only one step. When the step size is getting larger, the tendency of decrease in the norm of absolute errors can be observed as another remarkable point in the example. A significant output of this example is that when the Newton method is considered to be used, the current method can be utilized to avoid too small Jacobians.

4.6 Fredholm Integral Equations via a Reverse Approach

Consider the nonlinear Fredholm integral equation

$$u(x) = f(x) + \lambda \int_{a}^{b} K(x, t)F(u(t))dt$$
(4.28)

where f(x) is a known source function, K(x,t) is a known kernel, a and b are known end points and F(.) is a nonlinear function with one variable. Also, λ is a parameter. A thorough discussion about this topic can be found in references [23, 25]. Let us define an integral operator N(.) as

$$N: L^2(a,b) \longrightarrow L^2(a,b) \tag{4.29}$$

$$u \longmapsto f(x) + \lambda \int_{a}^{b} K(x, t) F(u(t)) dt. \tag{4.30}$$

Here, notice that the Fréchet derivative of *N* can be computed as

$$N'(u) = \lambda \int_a^b K(x, t)F'(u(t))dt. \tag{4.31}$$

Thereby, the requirements of Theorem 3.1 can be checked, and after this step, the procedure in the RFPIM could be followed by solving a Fredholm integral equation of the first kind at each intermediate step. In the first step,

$$u_0(x) - f(x) = \lambda \int_a^b K(x, t) F(u_1(t)) dt.$$
 (4.32)

is needed to be solved for $u_1(x)$. Particularly, in the nth step

$$u_n(x) - f(x) = \lambda \int_a^b K(x, t) F(u_{n+1}(t)) dt.$$
 (4.33)

must be solved for $u_{n+1}(x)$. However, since it is a backward problem and an ill-posed problem, equation (4.33) is not easy to handle. Lavrentiev's regularization method should be utilized to seek solution(s) to such kind of equations. Instead of solving equation (4.33) it is proposed to solve

$$\alpha u_{n+1,\alpha}(x) = f(x) - u_{n,\alpha}(x) + \lambda \int_{a}^{b} K(x,t) F(u_{n+1,\alpha}(t)) dt$$
 (4.34)

where α is a parameter. Notice that when $\alpha \to 0$, the solution obtained from equation (4.34) reduces to solution of equation (4.33).

Particularly, let us consider the following example [23]

$$u(x) = \frac{5x}{6} + x \int_0^1 t^2 u^3(t) dt$$
 (4.35)

with three exact solutions: $u_1(x) = x$, $u_2(x) = \frac{\sqrt{21}-1}{2}x \approx 1.79129x$ and $u_3(x) = \frac{-\sqrt{21}-1}{2}x \approx -2.79129x$. Here, the Fréchet derivative of N can be computed as

$$N'(u) = 3x \int_0^1 t^2 u^2(t) dt.$$

Notice that $||N'(u_1)||_{L^2(0,1)}=0.34641<1$, $||N'(u_2)||_{L^2(0,1)}=1.11153>1$ and $||N'(u_3)||_{L^2(0,1)}=2.69898>1$. Therefore, only $u_1(x)=x$ is an asymptotically stable solution to Equation (4.35). Hence, if the conventional fixed-point iteration method is started to be applied with an initial guess ϕ_0 , lying in a sufficiently small neighbourhood of $u_1(x)$, the solution $u_1(x)=x$ is reached.

To find out unstable solutions, let us use the reversed fixed-point algorithm. At each intermediate step, an equation of the following type has to be solved

$$cx = x \int_0^1 t^2 u^3(t) dt$$
 (4.36)

where c is a scalar. After application of the regularization method, it can be deduced that Equation (4.36) has solutions of the form $(\sqrt[3]{6c})x$ (for the solution procedure please see [24]). Some iterations and the errors in L^2 sense can be seen in Tables 4.8 and 4.9.

Table 4.8 Some iterations obtained via the RFPIM with initial guess $\phi_0(x) = 7x/3$ for problem (4.35).

Number of Iterations	Approximate solutions	L ² Errors
1	2.41014x	3.57×10^{-1}
2	2.11500x	1.87×10^{-1}
3	1.97382x	1.05×10^{-1}
4	1.89852x	6.19×10^{-2}
5	1.85577x	3.72×10^{-2}
6	1.83061x	2.27×10^{-2}
7	1.81547x	1.40×10^{-2}
8	1.80624x	8.63×10^{-3}
9	1.80056x	5.35×10^{-3}
10	1.79705x	3.32×10^{-3}

Table 4.9 Some iterations obtained via the RFPIM with initial guess $\phi_0(x) = 0$ for problem (4.35).

Number of Iterations	Approximate Solutions	L^2 Errors
1	-0.8333x	1.13
2	-2.4804x	1.80×10^{-1}
3	-2.70908x	4.75×10^{-2}
4	-2.77002x	1.23×10^{-2}
5	-2.78582x	3.16×10^{-3}
6	-2.78988x	8.12×10^{-4}
7	-2.79093x	2.09×10^{-4}
8	-2.79120x	5.47×10^{-5}
9	-2.79126x	1.50×10^{-5}
10	-2.79128x	4.77×10^{-6}

4.7 Unstable Equilibria in Control Problems: The Simple Pendulum

Let us now consider the motion of a pendulum exposed to a control torque. Consider a solid rod whose mass is neglected. A particle is attached to the endpoint of the rod as seen in Figure 4.8.

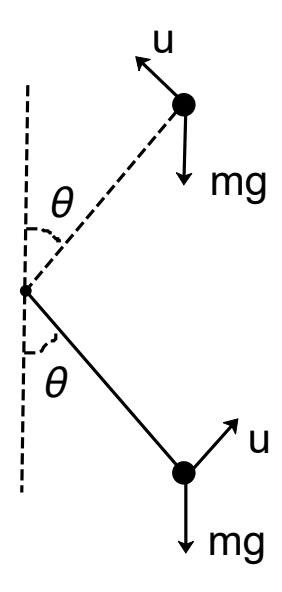


Figure 4.8 Equilibrium positions for a simple pendulum.

Suppose also that there is a resisting force due to friction. If the mass is exposed to a control torque u in the counterclockwise direction, the motion of the pendulum could be represented by

$$\frac{d^2\theta}{dt^2} = -\frac{g}{l}\sin(\theta) - \frac{k}{m}\frac{d\theta}{dt} + \frac{1}{ml^2}u\tag{4.37}$$

where g is the gravitational acceleration, m is the mass, l is the length of the rod, k is the coefficient of friction and θ is the positive angle between the vertical line and the ray pointing towards the position of the mass. Looking at the free body diagrams, existence of two different equilibrium angles can be observed. The first one is between 0 and $\pi/2$ is a stable equilibrium, while the second one is between $\pi/2$ and π is an unstable equilibrium.

Equation (4.37) can be converted to a system of first order ODEs by taking $x = \theta$, and $y = d\theta/dt$:

$$\frac{\frac{dx}{dt} = y}{\frac{dy}{dt} = -\frac{g}{l}\sin(x) - \frac{k}{m}y + \frac{1}{ml^2}u.$$
(4.38)

To analyze the stability of the system, consider the Jacobian of system (4.38):

$$J = \begin{pmatrix} 0 & 1 \\ -\frac{g\cos(x)}{L} & -\frac{k}{m} \end{pmatrix}. \tag{4.39}$$

The spectrum σ of the Jacobian matrix J can be obtained as:

$$\sigma(J) = \left\{ -\frac{k}{2m} - \sqrt{\frac{k^2}{4m^2} - \frac{g}{l}\cos(x)}, -\frac{k}{2m} + \sqrt{\frac{k^2}{4m^2} - \frac{g}{l}\cos(x)} \right\}. \tag{4.40}$$

Therefore, if $\cos(x) \ge \frac{k^2 l}{4m^2 g}$ then both eigenvalues have negative real parts and the system is asymptotically stable. However, if $\cos(x) < \frac{k^2 l}{4m^2 g}$ then, since one of the eigenvalues lies in the right half complex plane, and hence, the system is unstable. Note that the physical nature of the problem reveals that if $\cos(x) < 0$ then the mass m rests on an unstable equilibrium position. Furthermore, a nonlinear operator N(.) could be defined as follows to check the requirements of Theorem 3.1

$$N\begin{pmatrix} x_n \\ y_n \end{pmatrix} := \begin{pmatrix} x_n + hy_n \\ y_n - h\left(\frac{g}{l}\sin(x_n) + \frac{k}{m}y_n - \frac{u}{ml^2}\right) \end{pmatrix}. \tag{4.41}$$

Spectrum of the Jacobian matrix J of N can be computed as

$$\sigma(J) = \left\{ 1 - \frac{hk}{2m} \pm h\sqrt{\left(\frac{k}{2m}\right)^2 - \frac{g\cos(x)}{l}} \right\}. \tag{4.42}$$

If cos(x) > 0, then spectral radius of J is less than 1 for conventionally used small step sizes. Hence, the equilibrium position is necessarily attracting and asymptotically stable. However, if cos(x) < 0 then the spectral radius of J is greater than 1, and the corresponding equilibrium position is of repelling nature, and hence it is unstable.

Particularly, if the parameters of the system are taken to be u = 25 Newton, m = 5 kg, g = 10 m/s², k = 1 and l = 1 m, then the equilibrium solutions are found to be $\theta = \pi/6$ and $\theta = 5\pi/6$. Since $\cos(5\pi/6) < 0$, $\theta = 5\pi/6$ is an unstable equilibrium solution for model (4.37) while $\theta = \pi/6$ is an asymptotically stable equilibrium.

To obtain the unstable equilibrium, system (4.38) should be discretized through a finite difference scheme as in (4.41). Then the results obtained after only one step by applying the RFPIM have been shown in Table 4.10 where the step size h is taken to be 100.

Table 4.10 Absolute errors towards finding repelling fixed-point $\theta = 5\pi/6 \approx 2.618$ with the use of the RFPIM after single iteration with h = 100.

Initial Guess for θ	Absolute Errors	Relative Errors
0.0	5.74×10^{-4}	2.19×10^{-4}
0.5	4.65×10^{-4}	1.78×10^{-4}
1.0	3.55×10^{-4}	1.36×10^{-4}
1.5	2.45×10^{-4}	9.37×10^{-5}
2.0	1.36×10^{-4}	5.18×10^{-5}
2.5	2.59×10^{-5}	9.89×10^{-6}
3.0	8.38×10^{-5}	3.87×10^{-5}
3.5	1.94×10^{-4}	7.39×10^{-5}

Note that the conventional fixed-point iteration method is not suitable to apply in the solution procedure of this kind of problems due to the oscillatory nature of the stable equilibrium position. The results have been obtained after 1000 steps by applying the fixed point iteration to system (4.38) for various initial guesses with h=0.01 (see Table 4.11). A decrease in errors in the vicinity of the fixed-points can be observed in the results due to the locality of the fixed-point iteration. Nevertheless, the conventional fixed-point iteration method suffers from the oscillatory nature of the problem.

Table 4.11 Absolute errors towards finding attracting fixed-point $\theta = \pi/6 \approx 0.524$ with the use of conventional fixed-point iteration method after 1000 iterations with h = 0.01.

Initial Guess for θ	Absolute Errors	Relative Errors
0.0	2.65×10^{-1}	5.06×10^{-1}
0.5	5.84×10^{-3}	1.11×10^{-2}
1.0	1.76×10^{-1}	3.36×10^{-1}
1.5	4.37×10^{-1}	8.34×10^{-1}
2.0	1.71×10^{-1}	3.27×10^{-1}
2.5	6.25×10^{-1}	1.19
3.0	$1.55\times10^{+2}$	$2.96 \times 10^{+2}$
3.5	$1.60\times10^{+2}$	$3.05 \times 10^{+2}$

4.8 Unstable Equilibria in Chaotic Structures

Chaos is one of the most challenging areas of interest in contemporary science. Unstable equilibria are encountered in chaotic processes as an isolated unstable equilibrium or a strange repeller. A chaotic problem studied in reference [26] is considered here:

$$\dot{x} = a(y-z)$$

$$\dot{y} = (c-a)x - axz$$

$$\dot{z} = xy - bz$$
(4.43)

where $a,b,c \in \mathbb{R}$, and $a \neq 0$. When the parameters of system (4.43) are taken to be (a,b,c)=(2.1,0.6,30) and initial condition is taken to be $(x_0,y_0,z_0)=(0.1,-0.3,0.2)$ then the chaotic behaviour of the system reveals a strange attractor as in Figure 4.9. Besides, if the parameters a,b,c are taken to be (a,b,c)=(-2,-1,10) then the origin becomes an isolated unstable equilibrium, as is the case in reference [26]. Therefore, the conventional fixed-point iteration method diverges even under the consideration of fairly close initial guesses to O(0,0,0). The chaotic orbit of the system corresponding to the mentioned set of parameters can be seen in Figure 4.10.

It can be observed that O(0,0,0) is the only isolated equilibrium of system (4.43). The origin behaves as a source since it is an unstable equilibrium. Therefore, the reversed fixed-point algorithm is efficient to find out this unstable and chaotic equilibrium.

To observe the instability of the origin and to check the requirements of Theorem 3.1,

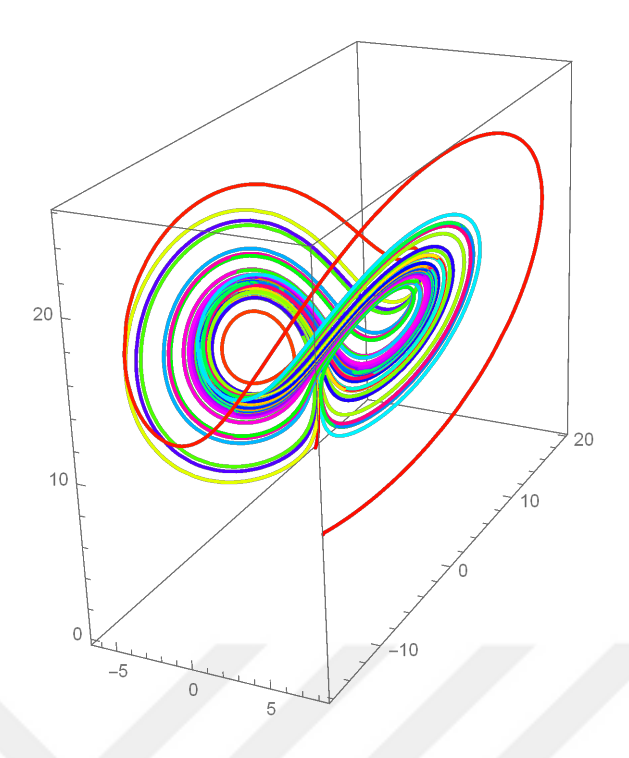


Figure 4.9 Chaotic orbit of system (4.43), for the parameters (a, b, c) = (2.1, 0.6, 30) and initial condition $(x_0, y_0, z_0) = (0.1, -0.3, 0.2)$.

let us define an operator N as

$$N \begin{pmatrix} x_n \\ y_n \\ z_n \end{pmatrix} := \begin{pmatrix} x_n + h_1 a(y_n - z_n) \\ y_n + h_2 ((c - a)x_n - ax_n z_n) \\ z_n + h_3 (x_n y_n - bz_n) \end{pmatrix}.$$
(4.44)

Spectrum of the Jacobian matrix J of N at the origin can be found as

$$\sigma(J)|_{(0,0,0)} = \left\{1 - \sqrt{h_1 h_2 a(1-a)}, 1 + \sqrt{h_1 h_2 a(1-a)}, 1 - h_3 b\right\}. \tag{4.45}$$

Hence, whenever $a \neq 0$ or $a \neq 1$, the origin becomes an unstable equilibrium since the spectral radius $\rho(\sigma) > 1$. Regarding the solution of system (4.43) with different initial guesses, absolute errors can be found in Table 4.12. A forward difference scheme is utilized to discretize the problem with step sizes $h_1 = h_2 = h_3 = h$. More efficient results could be observed using larger step sizes.

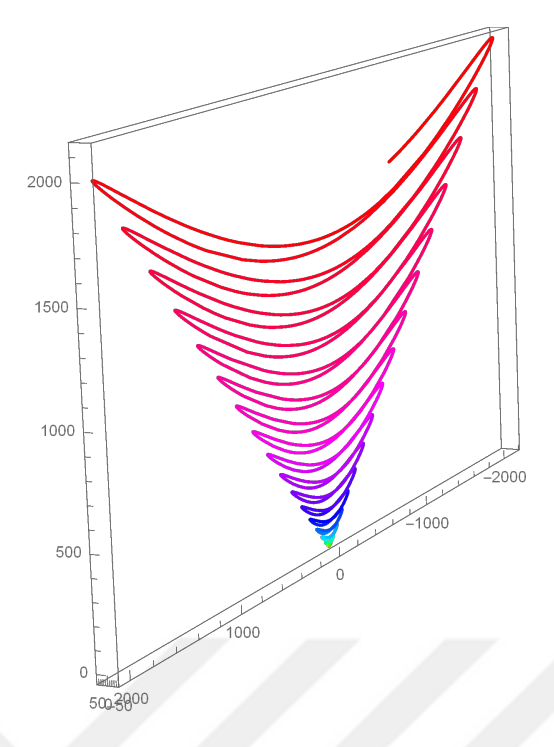


Figure 4.10 Chaotic orbit obtained via the RFPIM of system (4.43), for the parameters (a, b, c) = (-2, -1, 10) and initial condition $(x_0, y_0, z_0) = (1, 1, 1)$.

Table 4.12 Norms of the absolute errors at the first step of the RFPIM towards the solution of system (4.43) with different initial values and various values of step sizes.

Points	Absolute Errors				
FOIIIIS	h=10	h=100	h=1000		
(1,1,1)	1.00×10^{-1}	1.08×10^{-2}	1.09×10^{-3}		
(-1,1,1)	1.08×10^{-1}	1.15×10^{-2}	1.16×10^{-3}		
(1,-1,1)	1.08×10^{-1}	1.15×10^{-2}	1.16×10^{-3}		
(1,1,-1)	9.97×10^{-2}	1.08×10^{-2}	1.09×10^{-3}		
(-1,-1,1)	1.00×10^{-1}	1.08×10^{-2}	1.09×10^{-3}		
(-1,1,-1)	1.09×10^{-1}	1.15×10^{-2}	1.16×10^{-3}		
(1,-1,-1)	1.09×10^{-1}	1.15×10^{-2}	1.16×10^{-3}		
(-1,-1,-1)	9.97×10^{-2}	1.08×10^{-2}	1.09×10^{-3}		

4.9 Discussions Regarding the Applications

In the previous sections of this chapter, it is investigated that the behaviour of an unstable equilibrium solution, without facing any conventional drawbacks or without any linearization, and thus by preserving the nonlinear features of nature, could be understood by using the RFPIM. Moreover, the conventional fixed-point iteration method has been seen to fail for capturing the behaviour near unstable equilibria in

the examples demonstrated in the previous sections.

Since the characterization of all fixed points for a randomly determined function is almost impossible, at least for now, the characterization of the fixed-points of an nth degree polynomial which has n different positive real roots has been illustrated in the first example. A numerical example regarding the subject has been examined by using the arguments of Theorem 4.1, Corollaries 4.1 and 4.2. In this respect, the produced results have revealed that the present approach is able to locate the unstable fixed-points. However, the conventional fixed-point iteration method has been seen to fail to find out such equilibrium points (see Tables 4.1 and 4.2).

Repelling property of the Julia sets has been observed one more time in a different way in Example 2. An important result of the example is that the ill-posedness in the intermediate steps produces multiple solutions in each step even if this situation leads to a beauty like a fractal. Particularly, 2¹⁵ points have been used to produce Figure 4.3 by applying the RFPIM 15 times. Therefore, the present method is seen to be slightly complicated to apply repetitively.

It has been observed that the method can also be used to solve 2-dimensional root finding problems. Effectiveness and efficiency of the current method versus the conventional fixed-point iteration method could have been understood by comparing the results in Tables 4.3 and 4.4. The current method has been seen to be far better than the conventional approach.

An application regarding population dynamics has been investigated as an illustrative example in the previous section. It is observed, as seen in Table 4.5, that the present method is able to find out the threshold level which is an unstable equilibrium solution for population dynamical models while the usual fixed-point iteration method fails to explore such unstable thresholds.

In Example 5, a 3-dimensional root-finding problem has been studied in an unorthodox way by equipping with the efficacy of the current method for capturing the mathematical behaviour of a differential operator near unstable equilibria. For this purpose, the given system of equations has been converted to a system of differential equations to take advantage of the current method for solving differential equations, then the derivatives are approximated by a forward finite difference scheme, and hereby, a new 3-dimensional root-finding problem has been constructed. Thus, the obtained system has been solved by applying the RFPIM only one step and by using the Newton method. It can be concluded from the results in Table 4.7 that the errors are in a tendency to decrease which is proportional to h^{-1} . Hence, to understand the mathematical behaviour of a differential operator near an unstable equilibrium, the

RFPIM supplies also a tool of accuracy.

Generally, integral operators are difficult to handle when they are compared with differential operators. For instance, the Newton method has been used for solving root-finding problems in intermediate steps in this thesis. However, it is a tedious job to apply the Newton method in the solution procedure of an integral equation, because, it is a slightly difficult task to obtain the inverse of an integral operator. Therefore, in the application procedure of the RFPIM regarding the solution of the Fredholm integral equation of the second kind in Example 6, Lavrentiev's regularization method has been utilized to solve the Fredholm integral equations of the first kind encountered in the intermediate steps. In this context, the produced results show that the present method is able to discover unstable equilibria with some admissible initial guesses (see Tables 4.8 and 4.9).

Control of an unstable equilibrium has been an ongoing problem for many researchers. The pendulum is one of the fundamental examples studied in nonlinear control theory. In this study, once more, the existence of two different equilibria of the pendulum system has been observed, and one of these equilibrium positions has been seen to be unstable. Effective results in Table 4.10 show how much the current method is accurate to find out this unstable equilibrium. On the other hand, when the system is solved by using the conventional fixed-point iteration method, the oscillatory nature of the problem has caused fluctuations in the errors as shown in Table 4.11. Moreover, the conventional fixed-point iteration method has been seen to discover the attracting fixed-point of the system only if the iteration has been started by admissible initial guesses.

In the previous parts of this chapter, although examples up to the last one are of different characteristics, the last example, related to the unpredictable systems, is of great importance. The notions of unpredictability and chaos frequently have been mentioned together in the literature. A chaotic system that has an unstable fixed point has been considered in Example 8. The repelling fixed-point situated at the origin of \mathbb{R}^3 can be viewed as an isolated source performing a resonance behaviour. By discretizing the given set of ordinary differential equations with the use of a forward finite difference scheme as is the case in the previous differential equations, the given system can be converted to a 3D root finding problem. Hence, by choosing relatively larger step sizes, the errors in Table 4.12 can be produced after the application of the present method in only one step. Increasing the step size h, the error can be diminished as much as required. Thus, the storage drawback has been greatly overcome.

4.10 Use of Relatively Larger Step Sizes

One of the most outstanding aspects of the current method is that the use of relatively larger step sizes produces more accurate results when the solution procedures of ordinary differential equations are concerned. Application of the RFPIM just one step by using relatively larger step sizes has been seen to be quite effective according to the results in Table 4.6. Therefore, solving only one implicit equation is seen to be more reasonable as compared to iterating an explicit relation many times. Besides, since an increase in the step size h yields a Jacobian matrix with a high spectral radius, the Newton method could be safely used to solve the implicit equations come out in the intermediate steps.

It has been observed in this chapter that the RFPIM is great to capture the behaviour of unstable equilibrium solutions, it is not the case for stable equilibrium solutions in general. On the other hand, the conventional fixed-point iteration method fails to find out unstable equilibrium solutions. Usually, an ill-posed problem having more than one solution must be solved at each intermediate step to run the reversed fixed-point algorithm. After this first step in the application areas, in the following chapters, the more realistic problems represented by PDEs are going to be dealt with.

5 LINEAR ADVECTION DIFFUSION PROCESSES

Even the RFPIM is employed originally to find out unstable equilibria of nonlinear mappings defined on Banach spaces, it has been applied to obtain the responses of various advection diffusion reaction processes represented by fundamental partial differential equations (PDEs) such as advection-diffusion equation, Burgers equation and singularly perturbed generalized Burgers Huxley equation in the forthcoming chapters of this thesis. The von-Neumann stability analysis has been employed for the linear problems as one dimensional linear advection diffusion equation. Concordantly, the stability of the method is examined for different schemes, and the findings reveal that the method usually has a slightly different but significant stability region as compared to the conventional approach.

In the previous chapters, the RFPIM has been constructed and has been implemented to observe its effectiveness through various problems. Starting from this chapter the direction of this thesis is going to focus on more realistic problems represented by PDEs, hereby, the opportunity to uncover the validity, strength, and persuasiveness of the present method. In this chapter, being a linear, unsteady, and one-dimensional PDE, Equation 2.1 is studied.

5.1 A Criterion for Convergence

The linear advection-diffusion equation possesses a unique solution under suitable assumptions, and since the equation is linear, the attracting or repelling property of the solution should be a global feature due to its uniqueness. In the existing study, this characteristic is of top priority even before the crucial stability issues. Therefore, an approach to check the requirements of Theorem 2.1 will be developed in this section. To achieve this, the left hand side of Equation 2.1 will be integrated once with respect to time variable (t) and twice with respect to the space variable (x) aiming at getting an operator N as in Equation 1.1. To begin with, let us note that Equation 2.1, the initial condition u(x,0) = f(x), and the boundary conditions u(a,t) = g(t),

and u(b,t) = h(t) together form an initial-boundary value problem over the domain $(x,t) \in [a,b] \times [0,T]$ where a and b are the spatial endpoints and T is the final time. Now, let us construct the corresponding integral operator for Equation 2.1 as follows

$$0 = \int_{a}^{x} \int_{a}^{x} u(\xi, t) - u(\xi, 0) d\xi d\xi$$

$$+ \alpha \int_{0}^{t} \int_{a}^{x} u(\xi, \tau) - u(a, \tau) d\xi d\tau$$

$$- \epsilon \int_{0}^{t} u(x, \tau) - u(a, t) - x u_{x}(a, \tau) d\tau.$$

$$(5.1)$$

To eliminate the term $u_x(a, \tau)$, it will be a useful trick to write x = b in one of the intermediate steps of the integration processes. Hence the following integral relation is derived

$$\int_0^t u_x(a,\tau) d\tau = -\frac{1}{\epsilon b} \int_a^b (b-\xi) (u(\xi,t) - u(\xi,0)) d\xi$$

$$-\frac{\alpha}{\epsilon b} \int_a^b \int_0^t u(\xi,\tau) - u(a,\tau) d\tau d\xi$$

$$+\frac{1}{b} \int_0^t u(b,\tau) - u(a,\tau) d\tau. \tag{5.2}$$

Now, the corresponding integral operator could be defined as

$$N(u(x,t)) := u(x,t) + \int_{a}^{x} \int_{a}^{x} u(\xi,t) - u(\xi,0) d\xi d\xi$$

$$+ \alpha \int_{0}^{t} \int_{a}^{x} u(\xi,\tau) - u(\alpha,\tau) d\xi d\tau$$

$$- \epsilon \int_{0}^{t} u(x,\tau) - u(\alpha,\tau) d\tau$$

$$- \frac{x}{b} \int_{a}^{b} (b - \xi) (u(\xi,t) - u(\xi,0)) d\xi$$

$$- \frac{\alpha x}{b} \int_{a}^{b} \int_{0}^{t} u(\xi,\tau) - u(\alpha,\tau) d\tau d\xi$$

$$+ \frac{\epsilon x}{b} \int_{0}^{t} u(b,\tau) - u(\alpha,\tau) d\tau.$$
 (5.3)

Hence, being a fixed-point problem, N(u) = u is obtained. By applying the Cauchy integral reduction formula and by using the initial-boundary conditions, N(u) could be simplified further. In the end, the derivative of N with respect to u could be derived

as follows:

$$N'(u) := 1 + (x - a)^{2} - \int_{a}^{x} (x - \xi)f(\xi) d\xi + \alpha(x - a)t$$

$$-\alpha(x - a) \int_{0}^{t} g(\tau) d\tau - \epsilon t + \epsilon \int_{0}^{t} g(\tau) d\tau$$

$$-\frac{(b - a)^{2}x + 2\alpha(b - a)xt}{2b}$$
(5.4)

for the integral form of the debated advection diffusion problem. In accordance with Theorems 3.1 and 2.1, $||N'(u)||_{L^2([a,b]\times[0,T])}$ must be greater than 1. Therefore, this criterion should be checked before the stability criteria and numerical implementations in the following sections.

5.2 Stability Issues

The mentioned initial-boundary value problem could be discretized via various difference schemes by constructing a two-dimensional uniform lattice on the rectangle $[a,b] \times [0,T]$. Throughout the computations and observations carried out in this chapter, the initial values are represented by the nodal values $u_{j,1}$ for $j=1,2,3,\ldots M+1$, and the boundary conditions are represented by the nodal values $u_{1,n}$ and $u_{M+1,n}$ for $n=2,3,\ldots,L+1$ where $M,L\in\mathbb{N}$. Also, two constants, namely r_1 and r_2 , are defined as follows

$$r_1 := \alpha \Delta t / \Delta x$$
$$r_2 := \epsilon \Delta t / \Delta x^2$$

for the use in stability analysis.

Theorem 5.1. The RFTFS scheme is stable whenever one of the conditions

$$r_1 \le 1$$
 and $r_2 \le r_1/2$ OR
$$1 < r_1 < 2$$
 and $(r_1^2 - r_1)/2 \le r_2 \le r_1/2$ (5.5)

is satisfied.

Proof. Let us discretize Equation 2.1 by using the FTFS scheme:

$$\frac{u_{j,n+1} - u_{j,n}}{\Delta t} + \alpha \frac{u_{j+1,n} - u_{j,n}}{\Delta x} - \epsilon \frac{u_{j+2,n} - 2u_{j+1,n} + u_{j,n}}{\Delta x^2} = 0.$$
 (5.6)

By reversing the iteration, the following scheme is obtained

$$\frac{u_{j,n} - u_{j,n+1}}{\Delta t} + \alpha \frac{u_{j,n+1} - u_{j+1,n+1}}{\Delta x} - \epsilon \frac{u_{j,n+1} - 2u_{j+1,n+1} + u_{j+2,n+1}}{\Delta x^2} = 0.$$
 (5.7)

Now, by employing the von Neumann stability analysis the following equation is derived

$$\frac{A^{n}e^{ijk\Delta x} - A^{n+1}e^{ijk\Delta x}}{\Delta t} + \alpha \frac{A^{n+1}e^{ijk\Delta x} - A^{n+1}e^{i(j+1)k\Delta x}}{\Delta x} - \epsilon \frac{A^{n+1}e^{ijk\Delta x} - 2A^{n+1}e^{i(j+1)k\Delta x} + A^{n+1}e^{i(j+2)k\Delta x}}{\Delta x^{2}} = 0.$$
(5.8)

$$-\epsilon \frac{A^{n+1}e^{ijk\Delta x} - 2A^{n+1}e^{i(j+1)k\Delta x} + A^{n+1}e^{i(j+2)k\Delta x}}{\Delta x^2} = 0.$$
 (5.9)

By solving this equation for *A*,

$$A = \frac{1}{1 - r_1 + r_2 + (r_1 - 2r_2)e^{ik\Delta x} + r_2e^{i2k\Delta x}}$$
 (5.10)

is acquired. If the exponentials are expanded by using the Euler identity and the result is simplified, then |A| could be computed as

$$|A| = \left[1 + 4\sin^2\left(\frac{k\Delta x}{2}\right)\left[r_1^2 - 2r_2r_1 - r_1 + 2r_2^2 + \left(-2r_2^2 + 2r_1r_2 - 2r_2\right)\cos(k\Delta x)\right]\right]^{-1/2}$$

Here, necessarily, the inequality

$$-\left(r_1^2 - 2r_2r_1 - r_1 + 2r_2^2\right) \ge |-2r_2^2 + 2r_1r_2 - 2r_2| \tag{5.11}$$

must hold. There are two possible cases

•
$$-(r_1^2 - 2r_2r_1 - r_1 + 2r_2^2) \ge (-2r_2^2 + 2r_1r_2 - 2r_2)$$
 or

•
$$-(r_1^2 - 2r_2r_1 - r_1 + 2r_2^2) \ge -(-2r_2^2 + 2r_1r_2 - 2r_2).$$

Further simplifications yield

•
$$(r_1^2 - r_1)/2 \le r_2$$
 or

•
$$(r_1-1)/2 \le r_2 \le r_1/2$$
.

respectively. Here, if $r_1 < 1$ then $(r_1 - 1)/2 \le (r_1^2 - r_1)/2 \le 0 \le r_2$. Hence the only required condition is $r_2 \le r_1/2$. Besides, if $1 < r_1 < 2$ then $(r_1 - 1)/2 \le (r_1^2 - r_1)/2 \le r_1/2$ $r_2 \le r_1/2$ must hold. Therefore, |A| is always greater than 1 whenever condition 5.5 is satisfied.

It is important to note that the reversion process is applied for each term in Equation 2.1 separately. Another significant issue regarding the stability analysis is the need for the criterion |A| > 1 instead of |A| < 1. The reverse nature of the RFPIM forces us to prefer such a condition.

Theorem 5.2. The RFTCS scheme is stable whenever the conditions

$$r_1 < 1$$
 and $\frac{r_1^2}{2} \le r_2 \le \frac{1}{2}$ (5.12)

are fulfilled.

Proof. By applying the present method using the FTCS scheme, the equation

$$\frac{u_{j,n} - u_{j,n+1}}{\Delta t} + \alpha \frac{u_{j-1,n+1} - u_{j+1,n+1}}{2\Delta x} - \epsilon \frac{u_{j-1,n+1} - 2u_{j,n+1} + u_{j+1,n+1}}{\Delta x^2} = 0$$
 (5.13)

is obtained. If the von Neumann stability analysis is performed to observe the numerical stability,

$$\begin{split} \frac{A^n e^{ijk\Delta x} - A^{n+1} e^{ijk\Delta x}}{\Delta t} + \alpha \frac{A^{n+1} e^{i(j-1)k\Delta x} - A^{n+1} e^{i(j+1)k\Delta x}}{2\Delta x} \\ - \epsilon \frac{A^{n+1} e^{i(j+1)k\Delta x} - 2A^{n+1} e^{ijk\Delta x} + A^{n+1} e^{i(j-1)k\Delta x}}{\Delta x^2} = 0 \end{split}$$

is achieved. By solving the last equation for A, it is obtained that

$$A = \frac{1}{1 - 2r_2(1 - \cos(k\Delta x)) - ir_1\sin(k\Delta x)}.$$
 (5.14)

Consequently, the magnitude of the amplification factor is to be found as

$$|A| = \left[(1 - 2r_2(1 - \cos(k\Delta x)))^2 + (r_1\sin(k\Delta x))^2 \right]^{-1/2}$$
(5.15)

$$= \left[1 + (1 - \cos(k\Delta x))\left[r_1^2 - 4r_2 + 4r_2^2 + \cos(k\Delta x)\left(r_1^2 - 4r_2^2\right)\right]\right]^{-1/2}.$$
 (5.16)

Since $1-\cos(k\Delta x) \ge 0$, |A| is greater than 1 if $-(r_1^2-4r_2+4r_2^2) \ge |r_1^2-4r_2^2|$ is satisfied. In the present circumstance, there are two possibilities:

•
$$-r_1^2 + 4r_2 - 4r_2^2 \ge r_1^2 - 4r_2^2$$
,

•
$$-r_1^2 + 4r_2 - 4r_2^2 \ge -(r_1^2 - 4r_2^2)$$
.

The first possibility necessitates $\frac{1}{2} \ge r_2$, and the second one necessitates $r_2 \ge \frac{r_1^2}{2}$. Here,

 $r_1 < 1$ immediately comes from the relation $r_1^2/2 < r_2 \le 1/2$. Hence, the magnitude of *A* remains greater than 1 with the assumptions $r_1 < 1$ and $r_1^2/2 \le r_2 \le 1/2$.

Theorem 5.3. The RFPIM is unstable for the FTBS scheme.

Proof. If the RFPIM is implemented by combining it with the FTBS scheme, then the amplification factor is obtained as

$$A = \frac{1}{1 + r_1 + r_2 - (r_1 + 2r_2)e^{-ik\Delta x} + r_2 e^{-i2k\Delta x}}.$$
 (5.17)

By using the Euler identity and by rearranging the trigonometric terms, |A| is computed as

$$|A| = \left[1 + 4\sin^2\left(\frac{k\Delta x}{2}\right) \times \left[\left(r_1^2 + 2r_2r_1 + r_1 + 2r_2^2\right) + \left(-2r_2^2 - 2r_1r_2 - 2r_2\right)\cos(k\Delta x)\right]\right]^{-1/2}.$$
 (5.18)

If $-(r_1^2 + 2r_2r_1 + r_1 + 2r_2^2) \ge |-2r_2^2 - 2r_1r_2 - 2r_2|$, then |A| could be greater than 1, and hence, |A| > 1 holds. Since $2r_2^2 + 2r_1r_2 + 2r_2 > 0$, there is only one case

$$-\left(r_1^2 + 2r_2r_1 + r_1 + 2r_2^2\right) \ge 2r_2^2 + 2r_1r_2 + 2r_2. \tag{5.19}$$

By arranging the inequality, $(r_1 + 2r_2) + (r_1 + 2r_2)^2 \le 0$ is obtained. However, this holds only for $r_1 = r_2 = 0$.

Theorem 5.4. The RBTFS scheme is stable whenever one of the following conditions

$$r_2 \le r_1/2$$
 OR $(1+r_1)/2 \le r_2$ (5.20)

is satisfied.

Proof. By combining the conventional FPIM and the BTFS scheme for Equation 2.1

$$\frac{u_{j,n} - u_{j,n-1}}{\Delta t} + \alpha \frac{u_{j+1,n} - u_{j,n}}{\Delta x} - \epsilon \frac{u_{j+2,n} - 2u_{j+1,n} + u_{j,n}}{\Delta x^2} = 0$$
 (5.21)

is obtained. Then, by reversing the iteration

$$\frac{u_{j,n-1} - u_{j,n}}{\Delta t} + \alpha \frac{u_{j,n-1} - u_{j+1,n-1}}{\Delta x} - \epsilon \frac{u_{j,n-1} - 2u_{j+1,n-1} + u_{j+2,n-1}}{\Delta x^2} = 0$$
 (5.22)

is obtained. Now, if the von Neumann stability analysis is performed to observe the

numerical stability, the amplification factor A is obtained as

$$A = 1 + r_1 - r_2 + (-r_1 + 2r_2)e^{ik\Delta x} - r_2 e^{i2k\Delta x}.$$
 (5.23)

By expanding the exponentials into trigonometric form by using the Euler identity and simplifying the result, |A| is computed as

$$\begin{split} |A| = & \left[1 + 4 \sin^2 \left(\frac{k \Delta x}{2} \right) \times \right. \\ & \left. \left[r_1^2 - 2 r_2 r_1 + r_1 + 2 r_2^2 + \left(-2 r_2^2 + 2 r_1 r_2 + 2 r_2 \right) \cos(k \Delta x) \right] \right]^{1/2} \end{split}$$

The only case to be considered for stability is $\left[r_1^2-2r_2r_1+r_1+2r_2^2+\left(-2r_2^2+2r_1r_2+2r_2\right)\cos(k\Delta x)\right]>0$. There are two cases to consider here

•
$$r_1^2 - 2r_2r_1 + r_1 + 2r_2^2 > (-2r_2^2 + 2r_1r_2 + 2r_2)$$

•
$$r_1^2 - 2r_2r_1 + r_1 + 2r_2^2 > -(-2r_2^2 + 2r_1r_2 + 2r_2)$$

The second condition always holds. The inequality $(r_1 - 2r_2)(r_1 - 2r_2 + 1) > 0$ can be deduced from the first case. Hence, the conditions in Equation 5.20 have been concluded by reducing the last inequality. This completes the proof.

Theorem 5.5. *The RFPIM is unconditionally stable for the BTCS scheme.*

Proof. After the implementation of the RBTCS scheme, by performing the von Neumann stability analysis, the amplification factor *A* is obtained as

$$A = 1 + 2r_2(1 - \cos(k\Delta x)) - ir_1 \sin(k\Delta x). \tag{5.24}$$

Hence, |A| is attained as

$$|A| = \left[(1 - \cos^2(k\Delta x))r_1^2 + (1 + 2r_2(1 - \cos(k\Delta x)))^2 \right]^{1/2}.$$
 (5.25)

Since each term is positive in the square-root, and particularly the second term is greater than 1 the norm of the amplification factor A is always greater than 1. Therefore, the numerical scheme RBTCS is unconditionally stable.

Theorem 5.6. The RBTBS scheme is stable whenever one of the following conditions

•
$$r_1 \le 1$$
 and $(1-r_1)/2 \le r_2$

• 1 < *r*₁

is satisfied.

Proof. For the RBTBS scheme, the amplification factor A is obtained as

$$A = 1 - r_1 - r_2 + (r_1 + 2r_2)e^{-ik\Delta x} - r_2e^{-i2k\Delta x}.$$
 (5.26)

Here, |A| can be computed as

$$|A| = \left[1 + 4\sin^2\left(\frac{k\Delta x}{2}\right) \times \left(\left(r_1^2 + 2r_2r_1 - r_1 + 2r_2^2\right) + \left(-2r_2^2 - 2r_1r_2 + 2r_2\right)\cos(k\Delta x)\right)\right]^{1/2}.$$
 (5.27)

Here, $\left(r_1^2+2r_2r_1-r_1+2r_2^2\right)\geq |-2r_2^2-2r_1r_2+2r_2|$ must hold. Again, there are two cases

•
$$(r_1^2 + 2r_2r_1 - r_1 + 2r_2^2) \ge (-2r_2^2 - 2r_1r_2 + 2r_2)$$

$$\bullet \ \left(r_1^2+2r_2r_1-r_1+2r_2^2\right) \geq -\left(-2r_2^2-2r_1r_2+2r_2\right).$$

From the first case, it can be deduced that $r_2>(r_1-r_1^2)/2$. From the second case, $(r_1+2r_2)(r_1+2r_2-1)>0$ could be derived. Hence, $r_2>(1-r_1)/2$, and thereby, $r_1\leq 1$. Notice also that if $r_1\leq 1$ then $(1-r_1)/2>(r_1-r_1^2)/2$. Therefore, the strict condition $r_2>(1-r_1)/2$ should be adopted for $r_1\leq 1$. If $r_1\geq 1$ then $(r_1-r_1^2)/2<0$, and $r_2>(r_1-r_1^2)/2$ is always true.

Table 5.1 Stability conditions for the present method.

	FT	BT
FS	$r_1 \le 1 \text{ and } r_2 \le r_1/2 \text{ OR}$ $1 < r_1 < 2 \text{ and } (r_1^2 - r_1)/2 \le r_2 \le r_1/2$	$r_2 \le r_1/2 \text{ OR}$ $(1+r_1)/2 \le r_2$
CS	$r_1 < 1 \text{ and } \frac{r_1^2}{2} \le r_2 \le \frac{1}{2}$	Unconditionally Stable
BS	Unstable	$r_1 < 1 \text{ and } (1 - r_1)/2 \le r_2 \text{ OR} $ $1 < r_1$

Stability behaviours of the current method for the standard schemes are summarized in Table 5.1. Although the conventional method is unstable for the FTFS scheme, the

current method is conditionally stable for the same scheme. Moreover, if the inequality $r_2 \leq \frac{1}{2}(r_1 + r_1^2)$ is solved for the diffusivity constant ϵ then the criterion $\epsilon \leq \frac{\alpha}{2}(\Delta x + \alpha \Delta t)$ is obtained. Hence, if the current method is applied together with the FTFS scheme, then the method is seen to be still effective when the problem is getting stiffer, $\epsilon \ll 1$. In other words, the RFTFS scheme appears to be conditionally stable for challenging advection-dominant diffusion problems even in the case $\epsilon \to 0$.

The change in the explicit or implicit nature of a numerical scheme after hybridizing with the RFPIM is another crucial result of the present study. In this respect, notice that the RBT schemes uncover an explicit relationship between the nodes of the computational molecule, and the RFT schemes reveal an implicit relationship between the nodes.

5.3 Numerical Illustrations

The numerical efficiency of the current method has been tested in this section to recover the initial condition from the final time data. Apparently, this is an inverse problem, being suitable for the spirit of the reversed algorithm, and is designed in such a way that the final time data u(x, T) is obtained via the solution of the accompanying forward problem. Then, the initial condition u(x, 0) is tried to be recovered from the final condition.

Example 1. Consider the inverse problem represented by the one-dimensional, linear, and unsteady advection diffusion equation as stated in Equation 2.1. Here, the initial condition or the data to be recovered is given by

$$u(x,0) = 10e^{-\frac{1}{2}x^2} + 6e^{-\frac{1}{2}(x-6)^2} + 4e^{-\frac{1}{2}(x+8)^2}$$
(5.28)

which represents a sum of three Gaussian functions, as in Figures 5.1, 5.2 and 5.3. The boundary conditions are taken to be the Dirichlet boundary conditions as

$$u(-15, t) = u(15, t) = 0.$$
 (5.29)

Since the current study does not depend upon an experimental basis, the final time data, u(x,T), could be derived by using the corresponding forward problem, either analytically or numerically. Then, the obtained final data u(x,T) could be utilized to recover the initial data via the RFPIM.

The present method is seen to be critically effective for handling such inverse problems. Figure 5.1 illustrates a very accurate response for relatively great final times

such as T=5 or T=10 seconds even under a challenge condition $\epsilon=0.001$. It is known that the advection-diffusion problems under advection dominance are quite challenging and stiff. Similarly, Figure 5.2 exhibits the power of the present approach in the reconstruction process of the initial data when the phase speed is high, in other words, α is getting higher. The strength of the method emerges in Figure 5.3 even under critical advection dominance levels as $\epsilon=0.00001$.

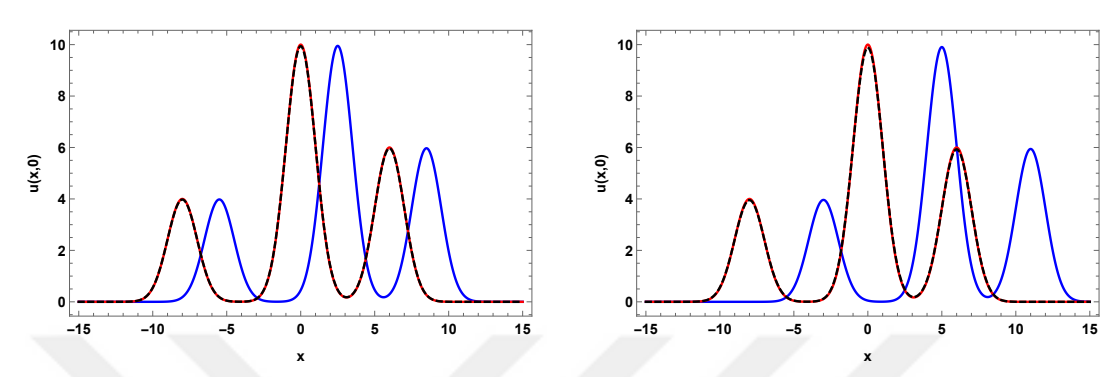


Figure 5.1 Final condition (blue), initial condition (red), and the recovered initial data (black dashed) via the RFTFS scheme for T=5 (left) and T=10 (right) with $\alpha=0.5, \epsilon=0.001, \Delta x=0.01, \text{ and } \Delta t=0.01.$

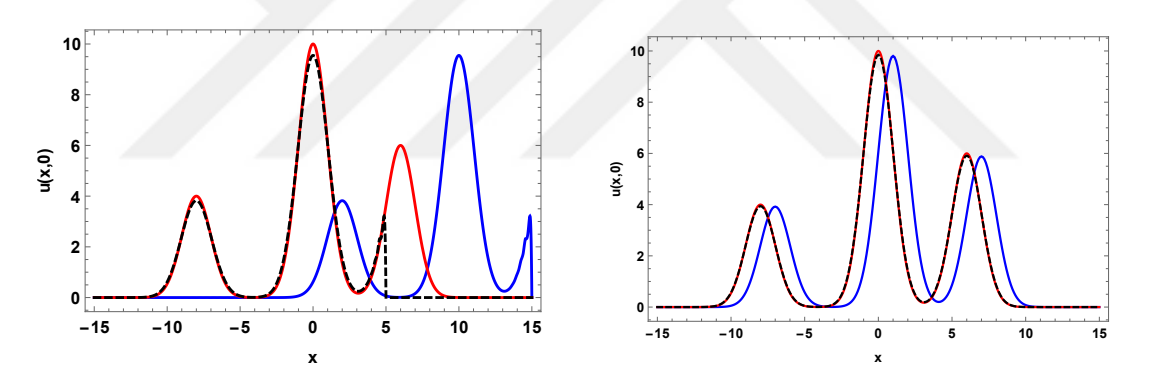


Figure 5.2 Final condition (blue), initial condition (red), and the recovered initial data (black dashed) via the RFTCS scheme for T=1 with $\alpha=10$, $\epsilon=0.1$, $\Delta x=0.01$, and $\Delta t=0.0005$ (left), and for T=2 with $\alpha=0.5$, $\epsilon=0.01$, $\Delta x=0.1$, and $\Delta t=0.1$ (right).

Although the current study is theoretical, an admissible level of error or noise may be expected during the experimental studies in the measurement process of the final time data. To observe the effectiveness of the RFPIM in such cases a noise data is added to the final time data as in Figure 5.4. The sample noise has been produced via **RandomReal** command of the utilized software [57]. The results in Tables 5.2-5.4 reveal that even there are some numerical fluctuations in the errors, the current method is still effective to capture the initial behaviour of the problem under admissible noise levels.

The obtained results via the RFTCS scheme could be observed in Figure 5.5 for T = 10

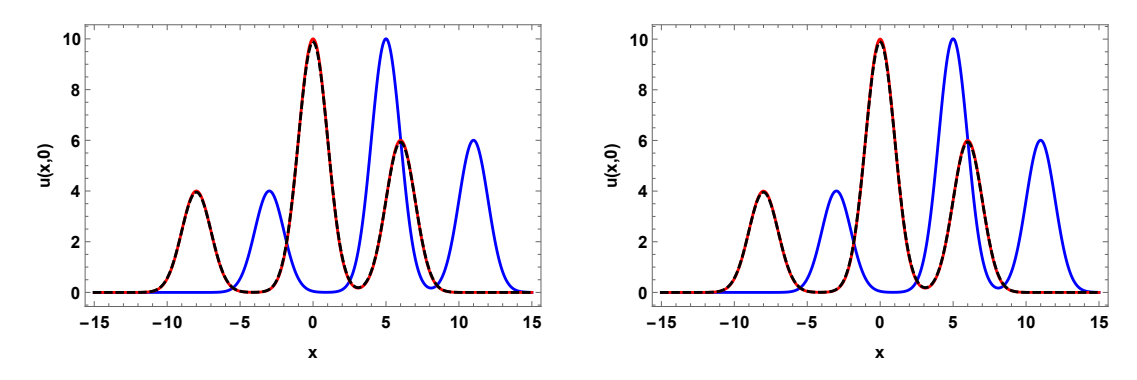


Figure 5.3 Final condition (blue), initial condition (red), and the recovered initial data (black dashed) via the RFTBS scheme for T=10 with $\epsilon=10^{-5}$ (left), and $\epsilon=0$ (right) where $\alpha=0.5$, $\Delta x=0.01$, and $\Delta t=0.01$.

seconds, $\alpha=0.5$ m/s, and $\epsilon=10^{-5}$ m²/s. In this case, the RMSE is computed to be 0.066, the relative error in the mean values is found to be 0.029. Obviously, the present method is able to recover original initial data with a negligible effect of the noise.

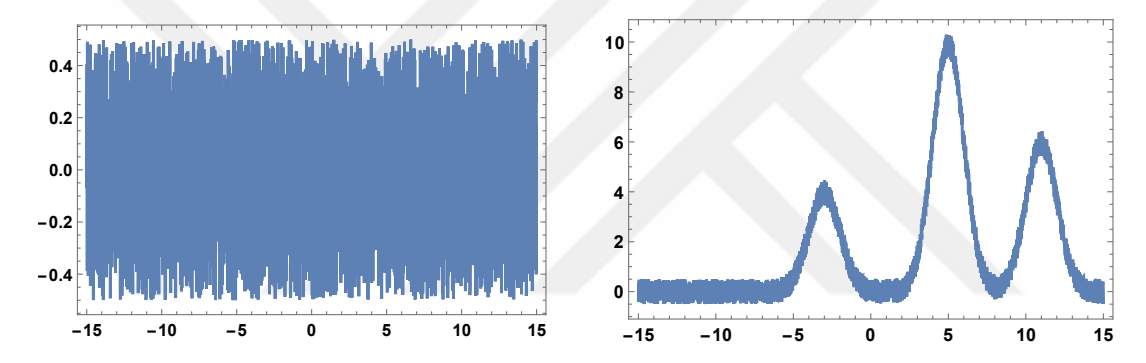
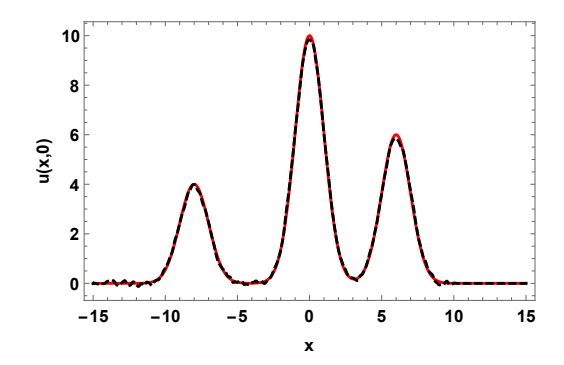


Figure 5.4 Sample noise (left) and noisy final data (right).

Table 5.2 The RMSE, the maximum absolute (AE) and relative (RE) errors for various values of space and time increments regarding Example 1.

Δt	Δx	RMSE	Max AE	Max RE
0.1	0.1	0.1737	0.6557	0.0659
0.01	0.01	0.0418	0.1591	0.0159
0.001	0.1	0.3013	1.1213	0.1127
0.001	0.01	0.0558	0.2123	0.0212



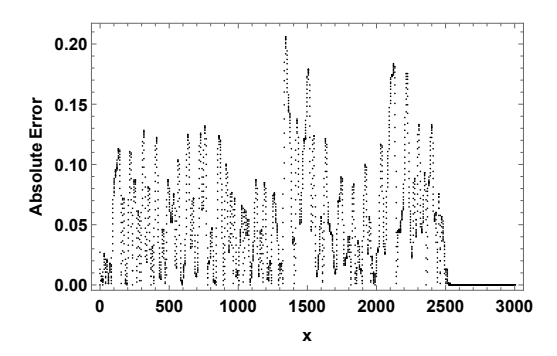


Figure 5.5 initial condition (red), and the recovered initial data (black dashed) via the RFTCS scheme for T=10 with $\epsilon=10^{-3}$ where $\alpha=0.5$, $\Delta x=0.01$, and $\Delta t=0.005$ (left) and absolute errors (right).

Table 5.3 The RMSE, the maximum absolute (AE) and relative (RE) errors for various values of space and time increments with 5% noise regarding Example 1.

$\Delta x \qquad \Delta t$		RMSE	Max AE	Max RE
0.1	0.1	0.2819	0.6500	0.0653
0.01	0.01	0.2637	0.4665	0.0467
0.001	0.1	0.3855	1.2599	0.1266
0.001	0.01	0.2714	0.5500	0.0550

Table 5.4 The RMSE, the maximum absolute error, the absolute error in the mean, and relative error in the mean for various noise levels regarding Example 1.

Noise levels:	100%	50%	30%	10%	5%	0%
RMSE	0.342	0.201	0.135	0.042	0.037	0.035
AE(max)	2.529	1.481	0.763	0.204	0.165	0.132
AE(mean)	0.154	0.083	0.062	0.025	0.022	0.022
RE(mean)	0.092	0.050	0.037	0.015	0.013	0.013

Example 2. In this example, inspired by reference [89], consider Equation 2.1 together with the Dirichlet boundary conditions, u(-15, t) = u(15, t) = 0, and the following initial condition

$$u(x,0) = \begin{cases} 0 & x < -10.5 \\ 8x + 84 & -10.5 \le x < -10. \\ -8x - 76 & -10.0 \le x < -9.5 \\ 0 & -9.5 \le x < -0.5 \\ 20x + 10 & -0.5 \le x < 0 \\ 10 - 20x & 0 \le x < 0.5 \\ 0 & 0.5 \le x < 7.5 \\ 12x - 90 & 7.5 \le x < 8. \\ 102 - 12x & 8.0 \le x < 8.5 \\ 0 & 8.5 \le x \end{cases}$$
(5.30)

Notice that the imposed initial condition is not continuously differentiable for this example. The initial condition is compactly supported through three non-intersecting intervals. Thus, the problem can be regarded also as a sparse source identification problem. As it can be seen in Figure 5.6, the present method is excellent to locate the sparse initial sources. On the other hand, if the effect of diffusion is getting relatively prevalent then the RFPIM suffers to identify the source intensities since the second derivative of the initial condition is almost zero.

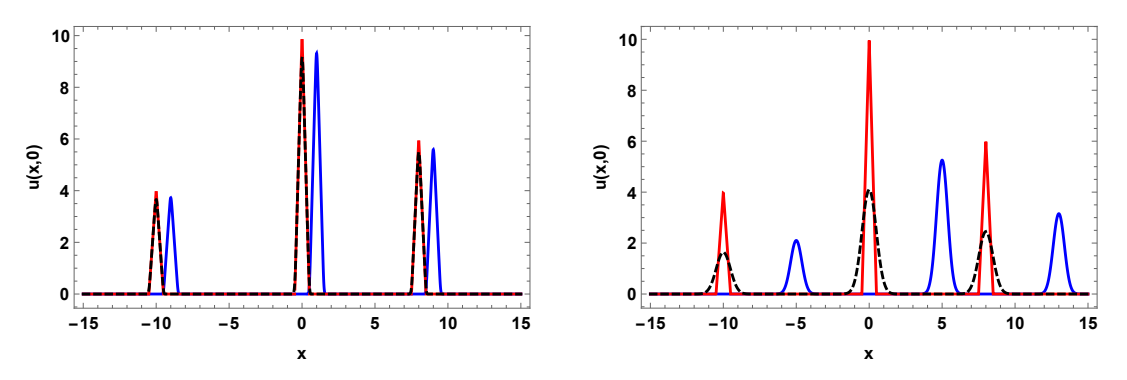


Figure 5.6 Final condition (blue), initial condition (red), and the recovered initial data (black dashed) via the FTCS scheme for T=1 with $\epsilon=10^{-3}$, $\alpha=1.0$, $\Delta x=0.01$, and $\Delta t=0.001$ (left), and $\epsilon=0.01$, $\alpha=1.0$, $\Delta x=0.01$, and $\Delta t=0.001$ (right) regarding Example 2.

Example 3. In this example [90], an advection diffusion equation is considered for $\alpha=1.0$ and $\epsilon=0.01$. For this case, the analytical solution to Equation 2.1 is as follows

$$u(x,t) = \frac{0.025}{\sqrt{0.000625 + 0.02t}} \exp{-\frac{(x+0.5-t)^2}{(0.00125 + 0.04t)}}$$
(5.31)

where $0 \le x \le 1$ and $0 \le t \le 1$. The corresponding initial and boundary conditions

could be derived from the exact solution. Since the exact solution is known as in Figure 5.7, the effectiveness of the RFPIM could be observed in a more convenient and persuasive way in this example.

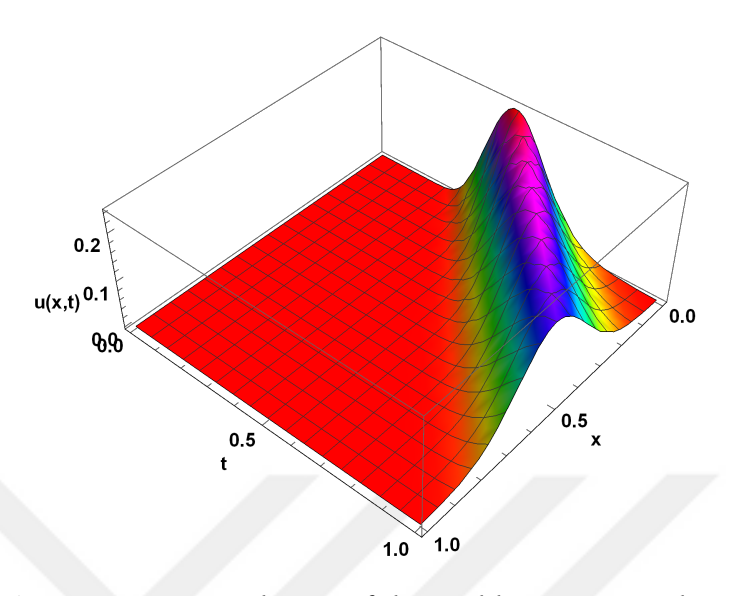


Figure 5.7 Exact solution of the problem in Example 3.

To obtain noisy final time data, a noise signal has been added to the exact final data. Notice that the noise level is approximately 10% of the mean of the final data as it is seen in Figure 5.8. Figure 5.9 reveals the accuracy of the current method even under 10% noisy measurement of the final data. The propagation of the corresponding absolute errors between the initial condition and the recovered initial data could be observed in Figure 5.10.

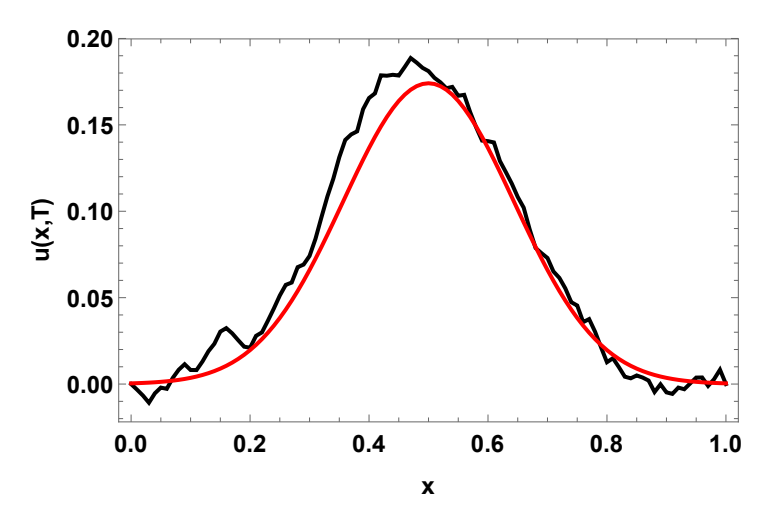


Figure 5.8 The exact final data (red) and the noisy final data (black) regarding Example 3.

As can be concluded from the results in Table 5.5, the current method is able to recapture the initial data even under the circumstances of 10% noisy measurements.

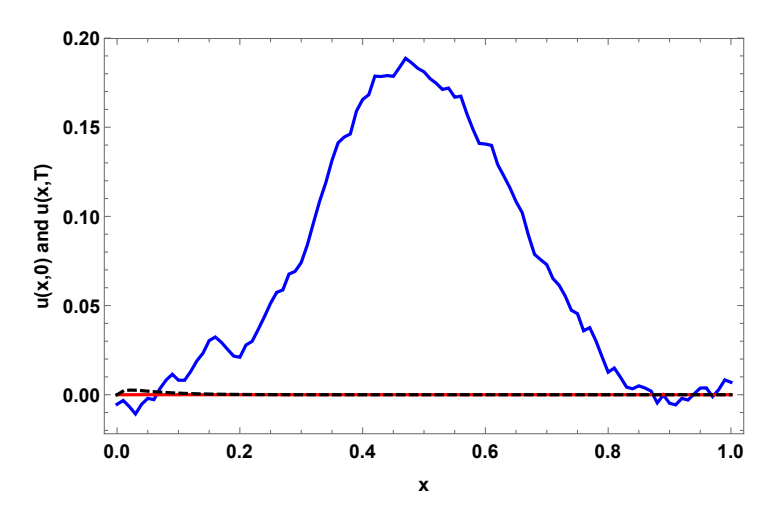


Figure 5.9 The final data (blue), the initial data (red), and the recovered initial data (dashed) obtained via the RFTCS scheme regarding Example 3.

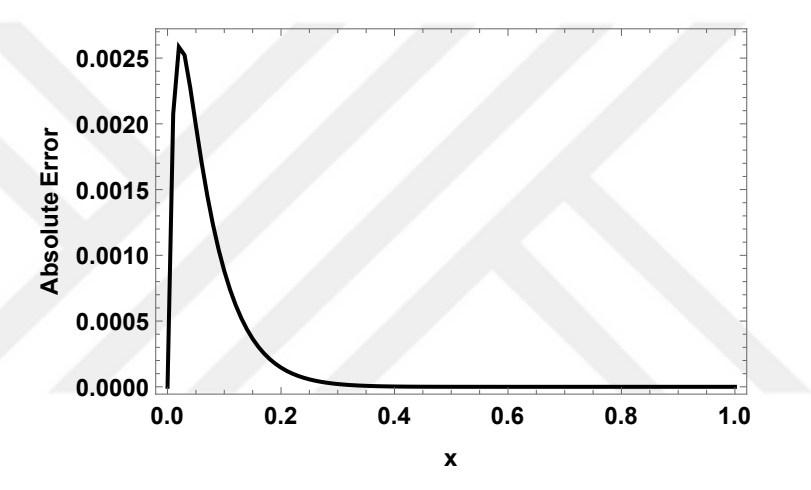


Figure 5.10 Propagation of the absolute error obtained via the RFTCS scheme regarding Example 3.

When we are closing this section, we ardently want to reveal a thought-provoking case. In this respect, a final time data covering a high level of noise up to 100% is considered. In other words, the measured final time data is assumed to include a relative error of up to 100%. As could be seen in Figure 5.11, the seed of the iteration, the noisy final time data, includes undesirable fluctuations. However, the RFPIM is seen to be able to eliminate the unwanted fluctuations rapidly, and strikingly, recover the initial data (see Figure 5.12). The quantitative results regarding the situation has been presented in Table 5.6. The RMSE is found to be **4.08**‰, and the maximum absolute error is computed to be **1.46**%.

Table 5.5 The RMSE and the maximum absolute errors (AE) for various values of space and time increments with 10% noise in the mean.

Δx	Δt	RMSE	Max AE
0.1	0.01	0.0198214	0.0419892
0.1	0.001	0.0168792	0.0168792
0.01	0.001	0.0005695	0.0017127
0.01	0.0001	0.0021366	0.0079092
0.005	0.0001	0.0032523	0.0118425

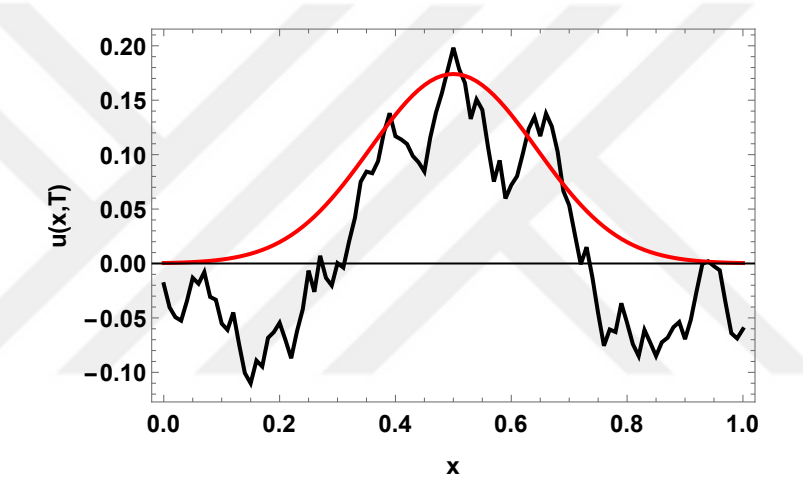


Figure 5.11 The exact final data (red) and sample noisy final data (black) regarding Example 3.

Table 5.6 The RMSE and the maximum absolute errors (AE) for various values of space and time increments with 100% noise in the mean via the RFTCS scheme.

Δx	Δt	RMSE	Max AE
0.1	0.01	0.018618	0.041324
0.1	0.001	0.019349	0.037195
0.01	0.001	0.004080	0.014551

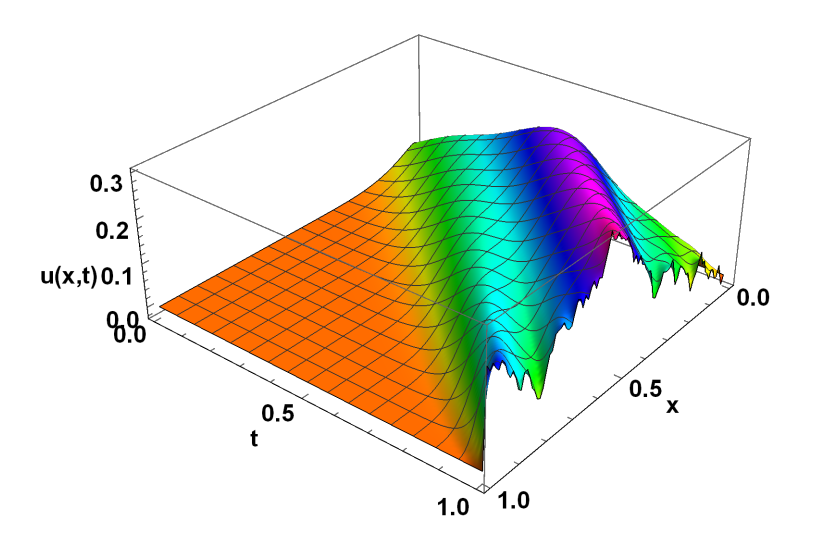


Figure 5.12 The numerical response obtained via the RFTCS scheme by starting with approximately 100% noisy data regarding Example 3.

6 NONLINEAR ADVECTION DIFFUSION PROCESSES

In the previous chapter, the RFPIM has been successfully implemented to identify the initial condition from end-time data in linear advection-diffusion processes. In this chapter and in the following chapters, the main motivation of this thesis is to apply the current method to solve more realistic problems represented by nonlinear PDEs. In this respect, the RFPIM has been utilized to solve a class of fundamental partial differential equations, namely viscous and inviscid Burgers equations, and singularly perturbed and generalized Burgers Huxley equation. Especially, inverse problems in these equations have been investigated by considering the reversed nature of the current method. The results produced confirm that the current method has the potential to effectively solve problems governed by PDEs representing the phenomena of advection, diffusion, and reaction. Derivations reveal that even in challenging situations such as advection dominance, the RFPIM is highly capable of capturing the natural behaviour of the problems under study. Another important finding, regarding the Burgers equation, is that the RFPIM can allow the use of relatively larger time steps. This feature is of great importance, to the best knowledge of the author, in reducing the need of storage space and CPU time for the whole computational community. Therefore, this chapter is devoted to showing how the RFPIM could be utilized through the solution procedures of nonlinear PDEs. In this context, we discuss the RFPIM towards the solution procedure of a fundamental class of PDEs including the inviscid Burgers equation, and the viscous Burgers equation. The mentioned equations can be summarized as in Equation 2.2. Besides, the following initial and boundary conditions are imposed on Equation 2.2

$$u(x,0) = f(x), \quad u(x,a) = g_1(t), \quad u(x,b) = g_2(t).$$
 (6.1)

The Burgers equation, being a reduction of the Navier-Stokes equation to one dimension, is of great importance. It is a test problem for numerical methods since it is well studied in the literature. Moreover, it still attracts a lot of researchers from various disciplines because of its potential applications. Therefore, in the following

sections, the Burgers equation has been utilized to observe the numerical performance of the RFPIM on the numerical treatment of PDEs.

6.1 Solution Procedure

In the solution process, the model equation is discretized by using a basic finite difference scheme, and then the RFPIM is applied. For example, to obtain a fully discretized scheme, for example, the BTCS scheme would be considered as follows

$$\frac{u_{j,n} - u_{j,n-1}}{\Delta t} + \alpha u_{j,n} \frac{u_{j+1,n} - u_{j-1,n}}{2\Delta x} - \epsilon \frac{u_{j+1,n} - 2u_{j,n} + u_{j-1,n}}{\Delta x^2} = 0.$$
 (6.2)

By reversing the numerical scheme and the advective effect, the fully discretized scheme

$$\frac{u_{j,n-1} - u_{j,n}}{\Delta t} + \alpha u_{j,n-1} \frac{u_{j-1,n-1} - u_{j+1,n-1}}{2\Delta x} - \epsilon \frac{u_{j-1,n-1} - 2u_{j,n-1} + u_{j+1,n-1}}{\Delta x^2} = 0.$$
 (6.3)

is reached. Besides, a semi-discrete FT scheme could be written as follows

$$\frac{u_{n+1}(x) - u_n(x)}{\Delta t} + \alpha u_n(x) \frac{d}{dx} u_n(x) - \epsilon \frac{d^2}{dx^2} u_n(x) = 0$$
 (6.4)

where Δt represents the time step size. Now, by applying the RFPIM, the following scheme could be reached

$$\frac{u_n - u_{n+1}}{\Delta t} - \alpha u_{n+1} u'_{n+1} - \epsilon u''_{n+1} = 0.$$
 (6.5)

We can solve the final equation for $u_n(x)$ to obtain an explicit numerical scheme in backward direction. Therefore, the numerical implementations will not require any further root finding problems.

In the next section, some illustrative problems are discussed to show the effectiveness of the use of Equations 6.5 and 6.3.

6.2 Numerical Illustrations

In this section, some numerical examples are implemented to show the effectiveness of the present method to capture the physical nature governed by a class of partial differential equations. In this respect, in the following examples, the inviscid Burgers equation and viscous Burgers equation are considered.

Example 1. [Viscous Burgers Equation: Forward Problem] The model problem could be posed together with an associated sinusoidal initial condition and two accompanying boundary conditions as follows

$$\frac{\partial u}{\partial t} + \alpha u \frac{\partial u}{\partial x} - \epsilon \frac{\partial^2 u}{\partial x^2} = 0, \quad \forall x \in (0, 1), \ t > 0, \tag{6.6}$$

$$u(x,0) = \sin(\pi x),\tag{6.7}$$

$$u(0,t) = u(1,t) = 0.$$
 (6.8)

Under these circumstances, the exact solution of the problem was given by Cole [72] in the following form

$$u(x,t) = 2\pi\epsilon \frac{\sum_{n=1}^{\infty} a_n e^{-n^2 \pi^2 \epsilon t} n \sin n\pi x}{a_0 + \sum_{n=1}^{\infty} a_n e^{-n^2 \pi^2 \epsilon t} \cos n\pi x}$$
(6.9)

where the coefficients a_n could be computed as

$$a_0 = \int_0^1 e^{-(1 - \cos \pi x)/(2\pi\epsilon)} dx,$$

$$a_n = 2 \int_0^1 e^{-(1 - \cos \pi x)/(2\pi\epsilon)} \cos(n\pi x) dx$$

for $n=0,1,2,\ldots$ In the solution procedure of the problem, parameters α and ϵ are taken to be 1 and 0.0001, respectively. The space interval (0,1) is divided into 300 equidistant sub-intervals and the time step is taken as 0.0005 for comparison purposes. The findings in Table 6.1 indicate that the obtained results are in good agreement with the results in the literature. The qualitative results in Figure 6.1 reveal that the current method is able to capture the sharp behaviour near the right boundary, x=1. In this regard, let us note that a relatively small value of ϵ like 0.0001 is especially a challenge condition here.

Example 2. [Initial Data Identification] The exact solution of the Burgers equation together with special initial and boundary conditions may be known in the literature as in the problem of this example. Here, we consider the problem stated in Equations 2.2 and 6.1 together with

$$f(x) = \frac{2\pi\epsilon \sin(\pi x)}{B + \cos(\pi x)}, B > 0, \quad g_1(t) = g_2(t) = 0.$$
 (6.10)

The exact solution of the problem represented by Equations 2.2, 6.1, and 6.10 is given

Table 6.1 Comparison of numerical results with literature for $\epsilon = 0.0001$ at t = 1.0 and various grid points for Example 1.

X	[63]	[64]	[65]	[66]	[67]	[62]	RFPIM
0.05	0.0422	0.0424	0.0419	0.0379	0.0379	0.0379	0.0379
0.16	0.1266	0.1263	0.1253	0.1213	0.1213	0.1212	0.1212
0.27	0.2108	0.2103	0.2034	0.2044	0.2044	0.2044	0.2043
0.38	0.2946	0.2939	0.2527	0.2872	0.2872	0.2871	0.2870
0.50	0.3778	0.3769	0.2350	0.3769	0.3769	0.3768	0.3767
0.61	0.4601	0.4592	0.2578	0.4584	0.4584	0.4583	0.4580
0.72	0.5414	0.5404	0.6014	0.5388	0.5388	0.5387	0.5383
0.83	0.6213	0.6201	0.7011	0.6179	0.6179	0.6178	0.6173
0.88	0.6605	0.6600	0.6717	0.6533	0.6533	0.6530	0.6526
0.94	0.6992	0.6957	0.7261	0.6952	0.6952	0.6890	0.6944

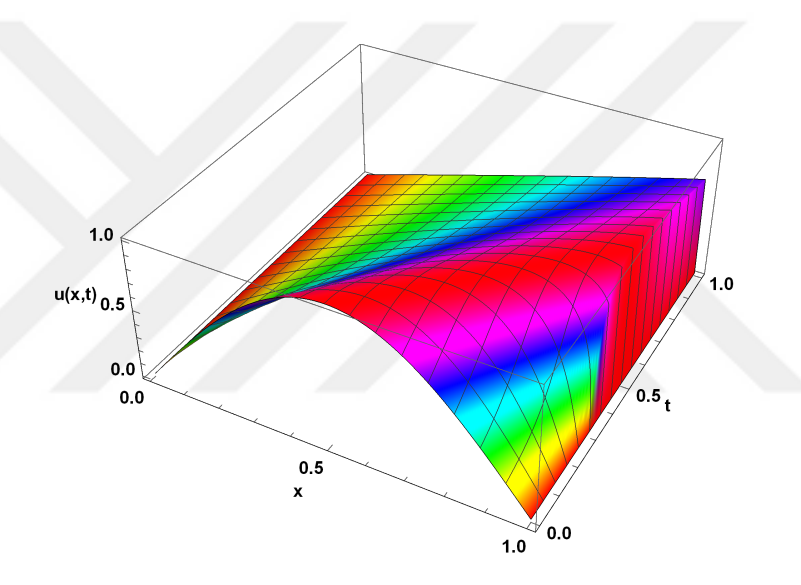


Figure 6.1 Shock wave behaviour of the problem in Example 1 for $\epsilon = 0.0001$.

in reference [61] as follows

$$u(x,t) = \frac{2\pi\epsilon e^{-\pi^2\epsilon t}\sin(\pi x)}{B + e^{-\pi^2\epsilon t}\cos(\pi x)}, \quad B > 0.$$
 (6.11)

In the solution procedure the constant *B* is taken as 1.50. The reversed nature of the current method pushes us to consider the inverse problem in the Burgers equation. In this respect, final time condition is taken from the exact solution in Equation 6.11. Then, the exact initial condition is tried to be recovered from the final time data via the RFPIM.

For extremely challenging conditions, the quantitative results could be seen in Tables 6.2 and 6.3. To the best knowledge of the author, for such small values of diffusivity coefficient, most numerical methods tend to fail to capture the natural behavior of the

problem being analyzed.

Table 6.2 $L^2(0,1)$ errors for various values of ϵ regarding the problem represented by Equations 2.2, 6.1, and 6.10.

\overline{T}	$\epsilon = 10^{-20}$	$\epsilon = 10^{-15}$	$\epsilon = 10^{-10}$		$\epsilon = 10^{-3}$
0.1	8.81×10^{-36}	1.53×10^{-29}	1.67×10^{-19}	1.67×10^{-9}	1.67×10^{-5}
0.2	8.81×10^{-36}	3.58×10^{-29}	3.35×10^{-19}	3.35×10^{-9}	3.33×10^{-5}
0.3	8.81×10^{-36}	5.34×10^{-29}	5.02×10^{-19}	5.02×10^{-9}	4.98×10^{-5}
0.4	8.81×10^{-36}	6.70×10^{-29}	6.70×10^{-19}	6.70×10^{-9}	6.62×10^{-5}
0.5	8.81×10^{-36}	7.96×10^{-29}	8.37×10^{-19}	8.37×10^{-9}	8.25×10^{-5}
0.6	8.81×10^{-36}	9.88×10^{-29}	1.00×10^{-18}	1.00×10^{-8}	9.88×10^{-5}
0.7	8.81×10^{-36}	1.17×10^{-28}	1.17×10^{-18}	1.17×10^{-8}	1.14×10^{-4}
0.8	8.81×10^{-36}	1.33×10^{-28}	1.34×10^{-18}	1.33×10^{-8}	1.31×10^{-4}
0.9	8.81×10^{-36}	1.51×10^{-28}	1.50×10^{-18}	1.50×10^{-8}	1.46×10^{-4}
1.0	8.81×10^{-36}	1.64×10^{-28}	1.67×10^{-18}	1.67×10^{-8}	1.62×10^{-4}

Table 6.3 Maximum absolute errors for various values of ϵ regarding the problem represented by Equations 2.2, 6.1, and 6.10.

\overline{T}	$\epsilon = 10^{-20}$	$\epsilon = 10^{-15}$	$\epsilon = 10^{-10}$	$\epsilon = 10^{-5}$	$\epsilon = 10^{-3}$
0.1	$LDMP^1$	LDMP	9.18×10^{-21}	9.22×10^{-11}	4.04×10^{-5}
0.2	LDMP	1.57×10^{-30}	1.83×10^{-20}	1.85×10^{-10}	8.06×10^{-5}
0.3	LDMP	1.57×10^{-30}	2.75×10^{-20}	2.79×10^{-10}	1.20×10^{-4}
0.4	LDMP	1.57×10^{-30}	3.67×10^{-20}	3.73×10^{-10}	1.60×10^{-4}
0.5	LDMP	2.36×10^{-30}	4.59×10^{-20}	4.69×10^{-10}	1.99×10^{-4}
0.6	LDMP	3.94×10^{-30}	5.51×10^{-20}	5.65×10^{-10}	2.38×10^{-4}
0.7	LDMP	5.52×10^{-30}	6.43×10^{-20}	6.62×10^{-10}	2.77×10^{-4}
0.8	LDMP	5.52×10^{-30}	7.34×10^{-20}	7.59×10^{-10}	3.15×10^{-4}
0.9	LDMP	7.88×10^{-30}	8.26×10^{-20}	8.58×10^{-10}	3.54×10^{-4}
1.0	LDMP	7.88×10^{-30}	9.18×10^{-20}	9.57×10^{-10}	3.92×10^{-4}

Example 3. [Inviscid Burgers Equation] In this example, the current method is utilized to reach a numerical solution of the inviscid Burgers equation. The associated initial boundary value problem is taken from [60] and stated as

$$\frac{\partial u}{\partial t} + \alpha u \frac{\partial u}{\partial x} = 0, \quad \forall x \in (0, 2\pi), \ t > 0, \tag{6.12}$$

$$u(x,0) = 1 + \sin(x), \tag{6.13}$$

$$u(0,t) = u(2\pi,t).$$
 (6.14)

Note that the initial condition is posed as a sinusoidal wave, and periodic boundary conditions are imposed on the model equation. Besides, α is taken to be 1 through

¹LDMP means the maximum absolute error is less than double machine working precision.

the computations. Firstly, the governing equation is discretized by using a backward in time and forward in space scheme (BTFS). Afterwards, the numerical scheme is combined with the RFPIM.

Problem represented by Equations 6.12-6.14 exhibits an N-wave behaviour, and the wave is getting steeper as time increases. The obtained results are depicted in Figure 6.2. Note that one of the most outstanding indication of this example is that the time step Δt is taken to be 0.1 and the spatial increment Δx is taken to be 0.21 throughout the computations.

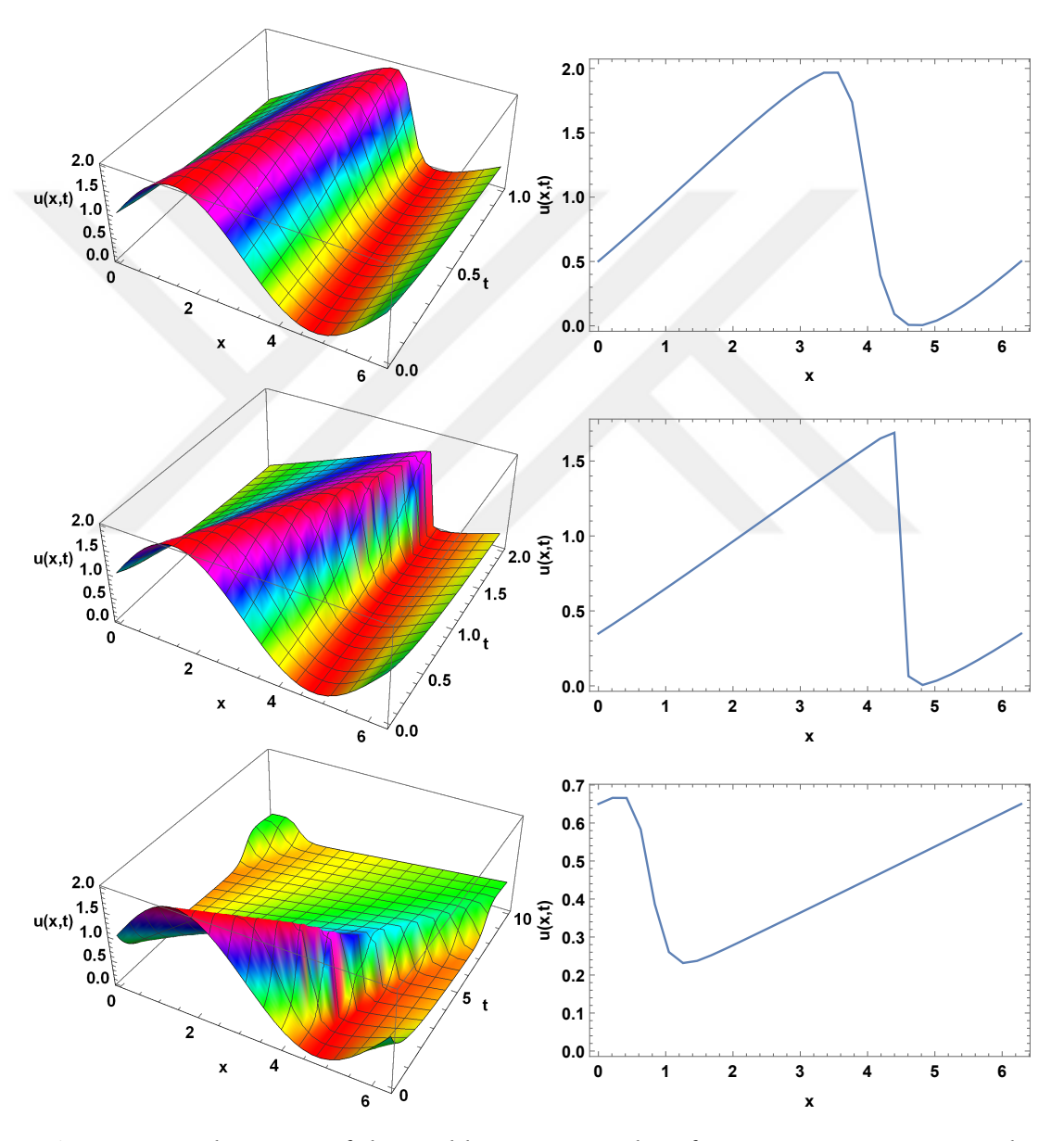


Figure 6.2 Behaviours of the problem in Example 2 for various time spans such as t = 1, t = 2, t = 10 seconds (left) and the solution profile at the end-time (right).

Now, being capable of obtaining the numerical solutions of various types of the Burgers equation via the RFPIM, we intend to carry these results on o more realistic basis. In

this respect, an optimization problem regarding the minimization of the sonic boom of supersonic aircraft is taken into consideration in the next example. This application is of great importance for us since it reveals how the RFPIM is applied to gain responses to a PDE-constrained minimization problem.

Example 4. [An Inverse Problem: Sonic Boom Modelling]

In this example an optimal control problem that represents the sonic boom produced by a supersonic aircraft has been debated. When an air vehicle breaks the sound barrier, in other words, its speed exceeds the speed of sound in the air, a shock wave is propagated through the air. In the literature, this phenomenon is called as sonic boom, and the shape of the shock wave through the propagation could be seen in Figure 6.3.

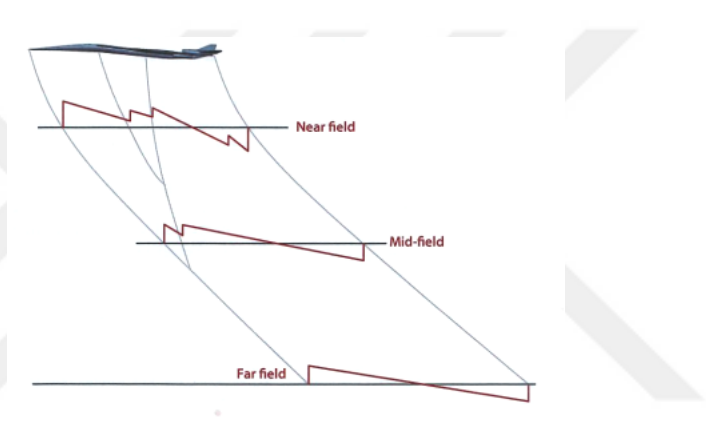


Figure 6.3 Pressure signature of a supersonic plane [69].

The shape of the shock wave in the far field is called as pressure signature, and the ground scanned by the sonic boom is called as boom carpet. To derive an optimal solution to this problem the following PDE constraint minimization problem, accompanied with Dirichlet boundary conditions, is considered [68]:

$$\mathbb{J}(u_0) = \frac{1}{2} \int_{\mathbb{R}} (u^*(x) - u(x, T))^2 dx$$
 (6.15)

subject to
$$u_t + \alpha u u_x - \epsilon u_{xx} = 0$$
 (6.16)

$$u(x,0) = u_0. (6.17)$$

Now, let us consider the sonic boom governed by the Burgers process with the following target function

$$u^*(x) = \frac{3}{2000} \sqrt{\pi} x \left(\text{erf} \left(5\sqrt{20} - x \right) + \text{erf} \left(x + 2\sqrt{20} \right) \right)$$
$$+ e^{-\left(x + 2\sqrt{20} \right)^2} - e^{-\left(x + 5\sqrt{20} \right)^2}$$

where $|x| \le 25$, and $u^*(x) = 0$ elsewhere [68]. Note that the diffusion coefficient and the advection coefficient are taken to be $\epsilon = 10^{-4}$ and $\alpha = 1$ throughout the computations. The results in Figure 6.5 is obtained with the use of the RFPIM, and

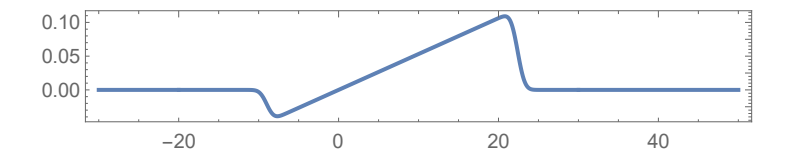


Figure 6.4 Pressure signature $u^*(x)$ for the model.

the produced results are in good agreement with the literature [68, 69]. In the figure, the black line stands for the target function u^* and the red dashed line represents the optimal solution u_0 of the problem. The green line stands for the recovered final data u_T , and it is obtained by solving the corresponding forward problem via numerical PDE solver of MATHEMATICA. Note that, instead of either the conventional or the reversed FPIM, a different PDE solver has been used intentionally to derive the solution to the corresponding forward problem. The values of the functional $\mathbb J$ for various Δx and Δt values could be observed in Table 6.4.

Table 6.4 Values of the functional \mathbb{J} for T = 50s and various values of spatial and temporal increments.

			Δt	
		0.01	0.1	1
	0.8	2.41×10^{-4}	2.42×10^{-4}	2.48×10^{-4}
Δx	0.4	1.96×10^{-4}	1.97×10^{-4}	2.02×10^{-4}
	0.2	1.76×10^{-4}	1.76×10^{-4}	1.78×10^{-4}
	0.1	1.71×10^{-4}	1.71×10^{-4}	1.72×10^{-4}

Both the quantitative and qualitative results seem to be quite acceptable. So, the RFPIM seems to be preferable for PDE-constrained optimization problems or the inverse problems as in this example.

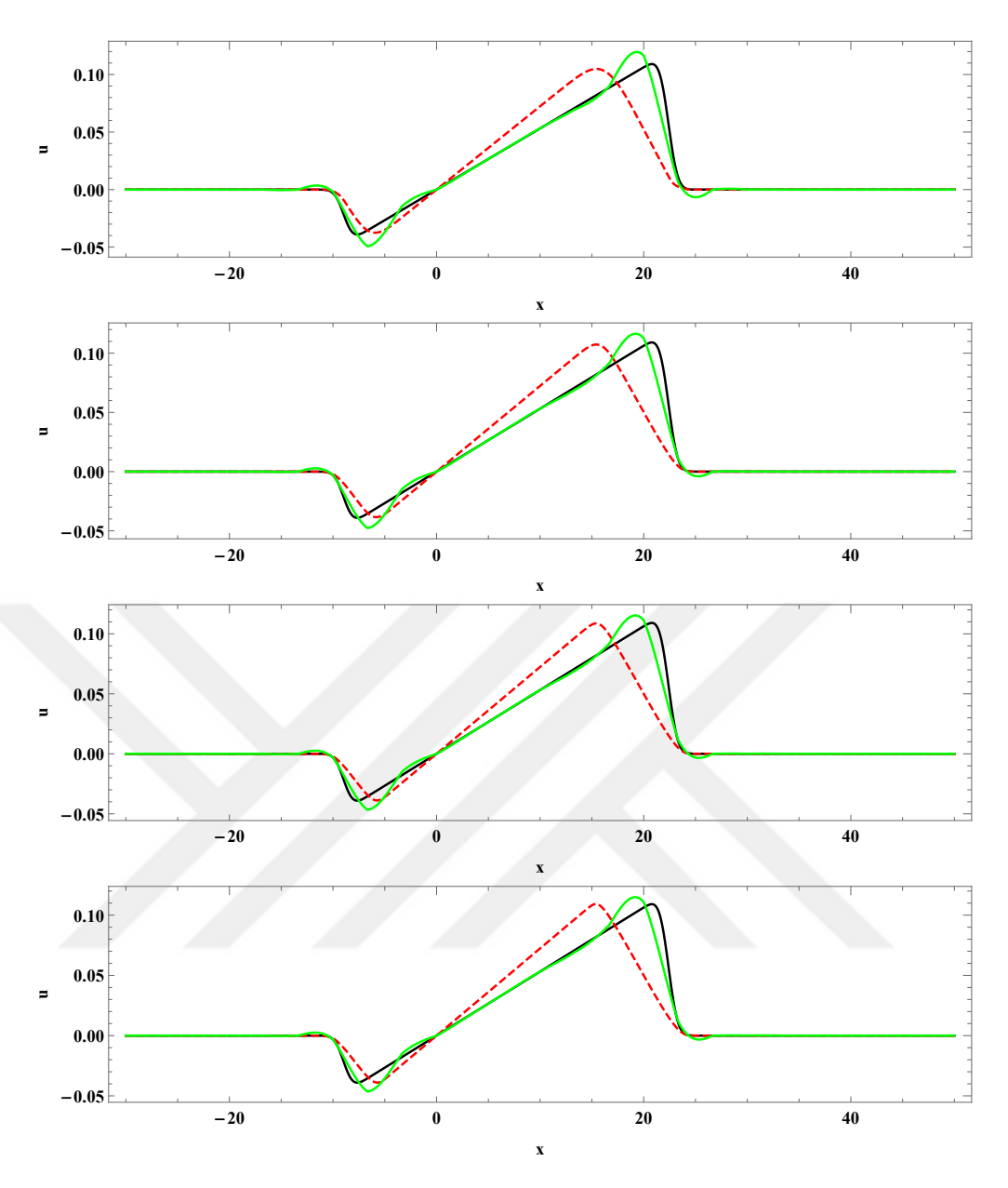


Figure 6.5 Behaviour of the target function u^* (black), the optimal solution u_0 (red) and the recovered final data u_T (green) for T=50 seconds with $\Delta x=0.8$ (first), $\Delta x=0.4$ (second), $\Delta x=0.2$ (third), and $\Delta x=0.1$ (fourth).

7

SINGULARLY PERTURBED CASES IN NONLINEAR ADVECTION DIFFUSION REACTION PROCESSES

In this chapter, as a continuation of the previous chapter, different travelling wave solutions of the kink type are derived for significant advection-diffusion-reaction mechanisms such as the singularly perturbed generalized Burgers Huxley and Burgers Fisher equations. To achieve this, a nonlinear transformation and an ansatz method have been utilized. Stability analysis is performed on different types of equations to detect the effects of the coefficients on the stability of the obtained solutions. Subsequently, the performance of the RFPIM has been examined concerning the solution procedures of inverse problems in the singularly perturbed advection diffusion reaction mechanisms.

Most of the physical mechanisms including convection, reaction, dispersion, etc. are governed by nonlinear partial differential equations (PDEs) [16, 91]. Such physical systems represented by nonlinear PDEs may possess traveling wave solutions. Since their shapes have been conserved through the process, traveling waves are important phenomena in nonlinear wave theory. In this chapter, firstly, traveling wave solutions of the following model equations

$$u_t + \alpha u^{\delta} u_x - \epsilon u_{xx} = \beta u (1 - u^{\delta}) (u^{\delta} - \gamma)$$
 (7.1)

and

$$u_t + \alpha u^{\delta} u_x - \epsilon u_{xx} = \beta u (1 - u^{\delta}) \tag{7.2}$$

where α , β , ϵ , δ and γ are parameters such that $0 < \epsilon$, $0 < \alpha$, $0 \le \beta$, $0 < \delta$, $\gamma \in (0,1)$ have been derived. Then, the RFPIM is employed to observe numerical behaviour of the mentioned problems in the following sections. So, the formerly obtained analytical solutions could be utilized to test the efficiency of the RFPIM.

In the literature, Equation 7.1 is called as the singularly perturbed generalized Burgers-Huxley equation (SPGBHE), and Equation 7.2 is called as the singularly

perturbed generalized Burgers Fisher equation (SPGBFE). In the model equations, the term uu_x represents the movement of a fluid material usually by means of a heat transfer or represents the bulk motion of a suspended or dissolved material in a fluid. The former one is called convection and the latter one is called advection. Moreover, the term u_{xx} represents the diffusion process. In the model equations, the parameter ϵ stands for the diffusion coefficient or kinematic viscosity. Besides, the parameter δ has been put to control the degree of the nonlinearity, and the parameters β and γ represent the coefficients of reaction terms.

According to previous studies when the kinematic viscosity is too small, in other words, the coefficient of diffusion ϵ is too small, any exact solution of these equations has not been known yet. From the viewpoint of characteristics of a PDE, in the situation of zero kinematic viscosity, $\epsilon=0$, the parabolic behaviour of the mentioned equations evolve to hyperbolic behaviour. Parabolic and hyperbolic PDEs have significantly different solution procedures. In this respect, the aim of this study is to develop some traveling wave solutions for the SPGBHE and the SPGBFE. To achieve this, the method introduced by Wang et al. [92] and Abdelkader [88] is followed. In addition, the stability behaviour of the solutions obtained is analyzed in detail.

It is a noticable fact that Equations 7.1 and 7.2 represent a wide variety of nonlinear evolution equations. From an application point of view, these equations include many different and important mechanisms such as advection, diffusion and reaction. Particularly, if $\epsilon=0$, then Equation 7.2 represents an advection-reaction mechanism. If $\epsilon=\beta=0$ and $\alpha=\delta=1$, both Equations 7.1 and 7.2, independently, turns to be the inviscid Burgers equation.

In this chapter, traveling wave solutions of the kink shape have been obtained. Kinks possess a time-independent behaviour i.e. permanent profile. Another interesting property of kinks is that there are also anti-kinks like anti-particles. Kink and anti-kink forms can be seen in Figures 7.1 and 7.2.

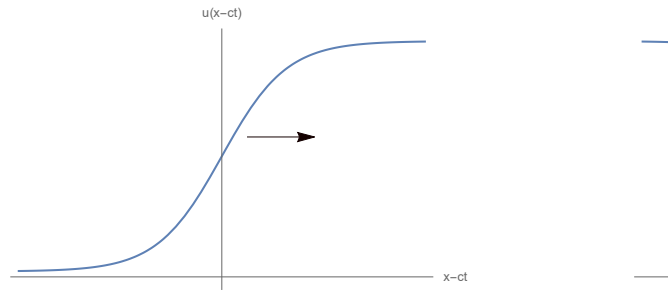


Figure 7.1 Profile of a kink

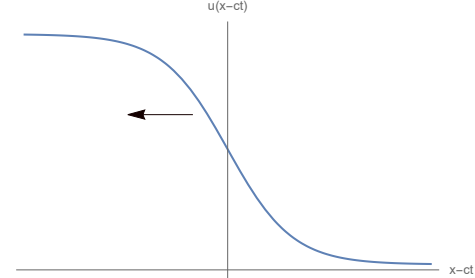


Figure 7.2 Profile of an anti-kink

There are many books and research articles published in the literature to discover the

behaviour of advection-diffusion-reaction mechanisms using continuous or discrete methods [74–87, 93, 94]. The main reason that led us to this consideration is the desire to observe the effects of the parameters in Equations 7.1 and 7.2 on the behaviour of solutions, especially in terms of stability. In this respect, to capture the stability behaviour of the equilibrium points, a linear stability analysis has been performed. The stability behaviour of the obtained solutions has been examined even for the limiting case $\epsilon \to 0$.

7.1 Analytical Solution of the Singularly Perturbed Generalized Burgers-Huxley Equation

The following useful nonlinear transformation

$$u = v^{1/\delta} \tag{7.3}$$

can be utilized to ease the nonlinearity in Equation 7.1. Use of Equation 7.3 in Equation 7.1 leads to

$$v_t + \alpha v v_x - \epsilon v_{xx} - \epsilon \left(\frac{1}{\delta} - 1\right) \frac{1}{v} (v_x)^2 = \delta \beta v (1 - v)(v - \gamma). \tag{7.4}$$

Equation 7.4 becomes an ordinary differential equation by letting $v(x, t) = v(x-ct) = v(\xi)$ as

$$-c\frac{dv}{d\xi} + \alpha v \frac{dv}{d\xi} - \epsilon \frac{d^2v}{d\xi^2} - \epsilon \left(\frac{1}{\delta} - 1\right) \frac{1}{v} \left(\frac{dv}{d\xi}\right)^2 =$$

$$= \delta \beta v (1 - v)(v - \gamma). \tag{7.5}$$

Any solution of Equation 7.5 is necessarily a traveling wave solution of the SPGBHE. In the following section, traveling wave solutions to the SPGBHE are found by assuming a relation between $dv/d\xi$ and v.

7.1.1 Solution Procedure of the SPGBHE

Firstly the ansatz $dv/d\xi = av(1-v)$ and secondly the ansatz $dv/d\xi = av(v-\gamma)$ are considered where a is a real scalar to be determined later.

7.1.1.1 First Ansatz

The assumption

$$\frac{dv}{d\xi} = av(1-v) \tag{7.6}$$

gives rise to

$$\frac{d^2v}{d\xi^2} = a^2v(1-v)(1-2v). \tag{7.7}$$

By plugging Equations 7.6 and 7.7 into Equation 7.5, the following polynomial equality

$$0 = -\frac{a^2 v^3 \epsilon}{\delta} - a^2 v^3 \epsilon + \frac{2a^2 v^2 \epsilon}{\delta} + a^2 v^2 \epsilon - \frac{a^2 v \epsilon}{\delta} + acv^2$$
$$-acv - a\alpha v^3 + a\alpha v^2 + \beta \delta v^3 - \beta \gamma \delta v^2 - \beta \delta v^2 + \beta \gamma \delta v$$

can be obtained. By expanding the last equation and organizing it in terms of the powers of v, the following system of equations

$$-\frac{a^2\epsilon}{\delta} - ac + \beta\gamma\delta = 0, (7.8)$$

$$-\frac{a^2\epsilon}{\delta} - a^2\epsilon - a\alpha + \beta\delta = 0, \tag{7.9}$$

$$\frac{2a^{2}\epsilon}{\delta} + a^{2}\epsilon + \alpha a + ac - \beta\gamma\delta - \beta\delta = 0$$
 (7.10)

can be found. Lastly, solving Equations 7.8-7.10 for a and c, it has been obtained that

$$a_{1,2} = \frac{\delta\left(-\alpha \pm \sqrt{\alpha^2 + 4\beta(\delta + 1)\epsilon}\right)}{2(\delta + 1)\epsilon}$$
(7.11)

and

$$c_{1,2} = \frac{\alpha(\gamma\delta + \gamma + 1) \pm (\gamma\delta + \gamma - 1)\sqrt{\alpha^2 + 4\beta(\delta + 1)\epsilon}}{2(\delta + 1)}.$$
 (7.12)

Now, integrating Equation 7.6, it can be found that

$$\nu(\xi) = \frac{1}{1 + e^{-a\xi - b}} \tag{7.13}$$

where b is an integration constant, and is taken to be 0 in the following computations. Hence, by using Equations 7.3, 7.11 and 7.12, two distinct traveling wave solutions of the SPGBHE can be found as

$$u_{1,2}(x,t) = \left(\frac{1}{1 + e^{-a(x - ct)}}\right)^{1/\delta} \tag{7.14}$$

where a and c are as in Equations 7.11 and 7.12.

Remark 7.1. Note that, by assuming just Equation 7.13 and, by plugging it in Equation 7.5 to find out possible values of a, the equation

$$\frac{e^{a\xi}\left(a^{2}\epsilon\left(\delta e^{a\xi}-1\right)+\beta\delta^{2}\left((\gamma-1)e^{a\xi}+\gamma\right)-a\delta\left(-\alpha e^{a\xi}+ce^{a\xi}+c\right)\right)}{\delta\left(e^{a\xi}+1\right)^{3}}=0 \qquad (7.15)$$

must be solved for both *a* and *c* simultaneously. Since it is almost impossible to solve such non-polynomial equations, in this study, it is not preferred to use the mentioned assumption.

7.1.1.2 Second Ansatz

In a similar manner, assuming

$$\frac{dv}{d\xi} = av(v - \gamma) \tag{7.16}$$

a and c can be computed as

$$a_{3,4} = \frac{\delta \left(\alpha \mp \sqrt{\alpha^2 + 4\beta(\delta + 1)\epsilon}\right)}{2(\delta + 1)\epsilon}$$
(7.17)

and

$$c_{3,4} = \frac{\alpha(\gamma + \delta + 1) \pm (-\gamma + \delta + 1)\sqrt{\alpha^2 + 4\beta(\delta + 1)\epsilon}}{2(\delta + 1)}.$$
 (7.18)

Thus, the corresponding traveling waves can be found as

$$u_{3,4}(x,t) = \left(\frac{\gamma}{1 - e^{a\gamma(x - ct)}}\right)^{1/\delta}$$
 (7.19)

where a and c are as in Equations 7.17 and 7.18.

7.1.2 Stability Analysis for the SPGBHE

For a deeper analysis from the point of view of stability, let us reconsider Equation 7.5 by letting

$$\frac{dv}{d\xi} = w \tag{7.20}$$

and

$$\frac{dw}{d\xi} = \frac{1}{\epsilon} \left[-cw + \alpha vw - \epsilon \left(\frac{1}{\delta} - 1 \right) \frac{w^2}{v} - \delta \beta v (1 - v) (v - \gamma) \right]. \tag{7.21}$$

Hence, Equation 7.5 has been converted to a first order ODE system, and a stability analysis can be given in the Poincaré phase plane. First of all, the zero-growth isoclines should be found by solving equations

$$\frac{dv}{d\xi} = 0 \text{ and } \frac{dw}{d\xi} = 0. \tag{7.22}$$

Solutions of system 7.22 are (0,0), (1,0) and $(\gamma,0)$. These values of (ν,w) can be interpreted as steady-state solutions of the system. Now, let us define $p(\nu,w)$ and

$$q(v, w)$$
 as

$$p(v,w) := \frac{dv}{d\xi} = w$$

and

$$q(v,w) := \frac{dw}{d\xi} = \frac{1}{\epsilon} \left[-cw + \alpha vw - \epsilon \left(\frac{1}{\delta} - 1 \right) \frac{w^2}{v} - \delta \beta v (1 - v)(v - \gamma) \right].$$

The Jacobian matrix of the system p = 0 and q = 0 can be computed as

$$\begin{pmatrix} p_v & p_w \\ q_v & q_w \end{pmatrix} = \begin{pmatrix} 0 & 1 \\ \frac{(1-\delta)w^2}{\delta v^2} + \frac{\alpha w - (1-v)v\beta\delta - (1-v)\beta(v-\gamma)\delta + v\beta(v-\gamma)\delta}{\epsilon} & -\frac{c}{\epsilon} - \frac{2w(1-\delta)}{\delta v} + \frac{v\alpha}{\epsilon} \end{pmatrix}.$$

The eigenvalues of the Jacobian matrix are obtained as follows:

$$\lambda_{1} = \frac{-c - \sqrt{c^{2} - 4\beta\gamma\delta\epsilon}}{2\epsilon}$$
$$\lambda_{2} = \frac{-c + \sqrt{c^{2} - 4\beta\gamma\delta\epsilon}}{2\epsilon}$$

for the equilibrium point (v, w) = (0, 0) and

$$\lambda_{3} = \frac{(\alpha - c) - \sqrt{(\alpha - c)^{2} - 4\beta(1 - \gamma)\delta\epsilon}}{2\epsilon}$$
$$\lambda_{4} = \frac{(\alpha - c) + \sqrt{(\alpha - c)^{2} - 4\beta(1 - \gamma)\delta\epsilon}}{2\epsilon}$$

for the equilibrium point (v, w) = (1, 0) and

$$\lambda_{5} = \frac{(\alpha \gamma - c) - \sqrt{(\alpha \gamma - c)^{2} + 4\beta \gamma (1 - \gamma)\delta \epsilon}}{2\epsilon}$$

$$\lambda_{6} = \frac{(\alpha \gamma - c) + \sqrt{(\alpha \gamma - c)^{2} + 4\beta \gamma (1 - \gamma)\delta \epsilon}}{2\epsilon}$$

for the equilibrium point $(v, w) = (\gamma, 0)$. Now, the real parts of the eigenvalue pairs are considered for each equilibrium point separately. Whenever both eigenvalues have negative real parts, then it is concluded that the equilibrium point is stable. If both of the real parts are positive then the equilibrium point is said to be unstable. Otherwise, the equilibrium point is a saddle point.

Remark 7.2. Since the inequality $|c| > \sqrt{c^2 - 4\beta\gamma\delta\epsilon}$ is always true, the inequalities $Re\{\lambda_1\} < 0$ and $Re\{\lambda_2\} < 0$ hold when c > 0. Therefore, (v, w) = (0, 0) is a stable point when c > 0. Besides, if c < 0 then the inequalities $Re\{\lambda_1\} > 0$ and $Re\{\lambda_1\} > 0$ necessarily hold, and hence (v, w) = (0, 0) is an unstable point when c < 0.

Remark 7.3. Since $|\alpha - c| > \sqrt{(\alpha - c)^2 - 4\beta(1 - \gamma)\delta\epsilon}$, the inequalities $Re\{\lambda_3\} < 0$ and

 $Re\{\lambda_4\}$ < 0 necessarily hold when $\alpha - c > 0$. Thus, $(\nu, w) = (1, 0)$ is seen to be a stable point when $\alpha - c > 0$. Besides, if $\alpha - c < 0$ then both $Re\{\lambda_3\} > 0$ and $Re\{\lambda_4\} > 0$ absolutely hold, and hence $(\nu, w) = (1, 0)$ is an unstable point if $\alpha - c < 0$.

Remark 7.4. Whether the term $(\alpha \gamma - c)$ is positive or negative, since $(\alpha \gamma - c)$ is always less than $\sqrt{(\alpha \gamma - c)^2 + 4\beta \gamma (1 - \gamma)\delta \epsilon}$, both $Re\{\lambda_5\} < 0$ and $Re\{\lambda_6\} > 0$ always hold. Therefore, the equilibrium point $(\nu, w) = (\gamma, 0)$ corresponds to a saddle point.

Hence, to obtain stable traveling wave solutions to the SPGBHE at least one of the conditions c > 0 and $\alpha - c > 0$ is required. In this respect, the following lemmas can be given without proof.

Lemma 7.1. The following conditions hold for the traveling wave speed c_k 's where k = 1, 2, 3, 4:

(i)
$$c_1 > 0$$
 if $\gamma < 1/(1 + \delta)$,

(ii)
$$c_2 > 0$$
 if $1/(1+\delta) \le \gamma \le 1$,

(iii) $c_3 > 0$ always true,

(iv)
$$c_4 > 0$$
 if $\delta < \alpha / \sqrt{\beta \epsilon}$.

Lemma 7.2. The following conditions hold for the traveling wave speed c_k 's where k = 1, 2, 3, 4:

(i)
$$\alpha - c_1 > 0$$
 if $\delta \alpha^2 > \beta \epsilon$,

(ii)
$$\alpha - c_2 > 0$$
 if $\gamma < 1/(1 + \delta)$,

- (iii) $\alpha c_3 > 0$ always false,
- (iv) $\alpha c_4 > 0$ always true.

Theorem 7.1. The equilibrium point (v, w) = (0, 0) is stable for the traveling wave speeds c_1 , c_2 , and c_4 whenever the conditions $\gamma < 1/(1 + \delta)$, $1/(1 + \delta) \le \gamma \le 1$, and $\delta < \alpha/\sqrt{\beta \epsilon}$ are satisfied, respectively. Besides, the equilibrium point (v, w) = (0, 0) is always stable for wave speed c_3 .

Proof. See Remark 7.2 and Lemma 7.1.

Theorem 7.2. The equilibrium point (v, w) = (1, 0) is stable for the traveling wave speeds c_1 , and c_2 whenever the conditions $\delta \alpha^2 > \beta \epsilon$, and $\gamma < 1/(1 + \delta)$ are satisfied, respectively. Besides, the equilibrium point (v, w) = (1, 0) is always stable for the wave speed c_4 while it is always unstable for the wave speed c_3 .

Proof. See Remark 7.3 and Lemma 7.2.

Theorem 7.3. The equilibrium point $(v, w) = (\gamma, 0)$ is a saddle point for any wave speed c_k , k = 1, 2, 3, 4.

Proof. See Remark 7.4.

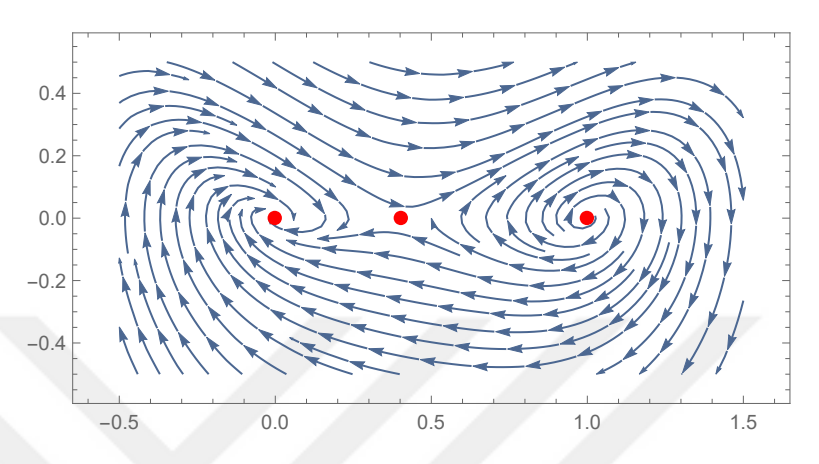


Figure 7.3 2D graph of the vector field (p(v, w), q(v, w)) for c_1 with $\alpha = 1$, $\beta = 1$, $\epsilon = 1$, and $\gamma = 0.4$.

For instance, if the parameters are chosen as $\alpha = 1$, $\beta = 1$, $\epsilon = 1$, and $\gamma = 0.4$ for the wave speed c_1 then it is inevitably seen that the condition in Theorem 7.1 is satisfied but the criterion in Theorem 7.2 is not fulfilled. Therefore, (0,0) is a stable equilibrium point while (1,0) is an unstable equilibrium point. Notice also that $(\gamma,0)$ is a saddle point (see Figure 7.3). The equilibrium points are shown by the red dots in Figure 7.3.

7.1.3 Stability Analysis under Advection Dominant Case

Secondly, the stability behaviour must be considered carefully when Equation 7.1 is forced to be advection dominant ($\epsilon \to 0$). Firstly, let us define the eigenvalues under advection dominant case as follows:

$$\lim_{\epsilon \to 0} \lambda_k = \lambda_k^0 \tag{7.23}$$

for k = 1, 2, 3, 4, 5, 6.

Corollary 7.1. Under advection dominance; for the wave speed c_1 , the equilibrium point (v, w) = (0, 0) is stable whenever the condition

$$\gamma < \frac{1}{(1+\delta)^2} \tag{7.24}$$

Table 7.1 Eigenvalues in the limiting case, $\epsilon \to 0$, for the wave speeds c_1 and c_2 .

Eigenvalues	For the wave speed c_1	For the wave speed c_2
λ_1^0	$\beta \left(\gamma (1+\delta)^2 - 1 \right) / \alpha$	$\beta(1-\gamma)(1+\delta)/\alpha$
λ_2^0	$-\beta\gamma\delta(1+\delta)/\alpha$	$-\beta \delta/\alpha$
2.0	0(1)(1 5) /	0.5/
$\lambda^0_3 \ \lambda^0_4$	$\beta(1-\gamma)(1+\delta)/\alpha$	$\beta\delta/\alpha$
λ_4^0	$-\beta \left(2+\delta-2\gamma-2\gamma\delta\right)/\alpha$	$-\beta \left(-1+\gamma+\delta+\delta\gamma\right)/\alpha$
2.0	$a \left(\begin{array}{cccccccccccccccccccccccccccccccccccc$	0 (1 , , , 5) /0
λ_5^0	$\beta \left(-1 + \gamma + \gamma o + \frac{\gamma \gamma}{ -1 + \gamma + \gamma \delta }\right) / 2\alpha$	$-\beta \left(-1+\gamma+\gamma\delta\right)/2\alpha$
λ_6^0	$\beta \left(-1 + \gamma + \gamma \delta + \frac{-1 + (-2 + \gamma)\gamma(-1 + \delta^2)}{ -1 + \gamma + \gamma \delta } \right) / 2\alpha$ $\beta \left(-1 + \gamma + \gamma \delta - \frac{-1 + (-2 + \gamma)\gamma(-1 + \delta^2)}{ -1 + \gamma + \gamma \delta } \right) / 2\alpha$	$-\beta \left(-1+\gamma+\gamma\delta\right)/2\alpha$

Table 7.2 Eigenvalues in the limiting case, $\epsilon \to 0$, for the wave speeds c_3 and c_4 .

Eigenvalues	For the wave speed c_3	For the wave speed c_4
$\lambda_1^0 \ \lambda_2^0$	$-\beta(1-\gamma)(1+\delta)/\alpha$	$\beta \left((1+\delta)^2 - \gamma \right) / \alpha$
λ_2^0	$-eta\gamma\delta/lpha$	$-\beta\delta(1+\delta)/\alpha$
- 0		
λ_3^0	$-\beta(1+\delta-\gamma)/2\alpha$	$\beta(1-\gamma)\delta(1+\delta)/\alpha(1+\delta-\gamma)$
λ_4^0	$-\beta(1+\delta-\gamma)/2\alpha$	$\beta (1 + \gamma^2 + \delta + \gamma(-2 + \delta)(1 + \delta)) / \alpha(1 + \delta - \gamma)$
2.0	0.(1 . 5 . 5) /	0(1)(1 ; 5) /
$\lambda_5^0 \ \lambda_6^0$	$-\beta (1-\gamma+\delta+\gamma\delta)/\alpha$	$-\beta(1-\gamma)(1+\delta)/\alpha$
λ_6^0	$\beta\gamma\delta/\alpha$	$\beta (2+2\delta-2\gamma-\gamma\delta)/\alpha$

is satisfied, otherwise, it is a saddle point. Moreover, the equilibrium point (0,0) is unconditionally stable for the traveling wave speed c_3 , while it is a saddle point for the wave speeds c_2 and c_4 .

Corollary 7.2. Under advection dominance; the equilibrium point (v, w) = (1, 0) is stable for the traveling wave speed c_3 , is unstable for the wave speed c_4 , and is a saddle point for the wave speed c_2 . The equilibrium point (1,0) is a saddle point for the wave speed c_1 whenever the condition

$$\gamma < \frac{1}{2} + \frac{1}{2(1+\delta)} \tag{7.25}$$

is satisfied, otherwise, it is unstable.

Corollary 7.3. Under advection dominance; the equilibrium point $(v, w) = (\gamma, 0)$ is unconditionally stable for the traveling wave speed c_1 , while it is a saddle point for the wave speeds c_3 and c_4 . For the wave speed c_2 , the equilibrium point $(\gamma, 0)$ is stable if the condition

$$\frac{1}{1+\delta} < \gamma \tag{7.26}$$

is satisfied, otherwise, it is unstable.

7.2 Analytical Solution of the Singularly Perturbed Generalized Burgers Fisher Equation

To obtain a traveling wave solution to the generalized form of the singularly perturbed Burgers Fisher equation, if the nonlinear transformation $v = u^{\delta}$ is utilized and the equality $v(x,t) = v(x-ct) = v(\xi)$ is assumed, then the following ordinary differential equation

$$-c\frac{dv}{d\xi} + \alpha v \frac{dv}{d\xi} - \epsilon \frac{d^2v}{d\xi^2} - \epsilon \left(\frac{1}{\delta} - 1\right) \frac{1}{v} \left(\frac{dv}{d\xi}\right)^2 = \delta \beta v (1 - v)$$
 (7.27)

is obtained. Now, taking the ansatz $\frac{dv}{d\xi} = av(1-v)$ for some scalar a, following the method in the previous section, the traveling wave solution

$$u_5(x,t) = \left(\frac{1}{1 + e^{-a_5(x - c_5 t)}}\right)^{1/\delta}$$
 (7.28)

to Equation 7.2 can be obtained, where

$$a_5 = -\frac{\alpha \delta}{(1+\delta)\epsilon},$$

$$c_5 = \frac{\alpha}{1+\delta} + \frac{\beta(1+\delta)\epsilon}{\alpha}.$$

7.2.1 Stability Analysis for the SPGBFE

As is the case for the SPGBHE, by defining

$$p(v,w) := \frac{dv}{d\xi} = w$$

and

$$q(v,w) := \frac{dw}{d\xi} = \frac{1}{\epsilon} \left[-cw + \alpha vw - \epsilon \left(\frac{1}{\delta} - 1 \right) \frac{w^2}{v} - \delta \beta v (1 - v) \right],$$

the zero-growth isoclines of the system are obtained as (v, w) = (0, 0) and (v, w) = (1, 0). The Jacobian matrix of the first order ODE system is found to be

$$\begin{pmatrix} p_{v} & p_{w} \\ q_{v} & q_{w} \end{pmatrix} = \begin{pmatrix} 0 & 1 \\ \frac{(1-\delta)w^{2}}{\delta v^{2}} + \frac{\beta\delta(2u-1)+\alpha v}{\epsilon} & \frac{v\alpha-c}{\epsilon} + \frac{2w(\delta-1)}{\delta v} \end{pmatrix}.$$

Eigenvalues of the Jacobian matrix can be computed as

$$\lambda_{1} = \frac{-c - \sqrt{c^{2} - 4\beta \delta \epsilon}}{2\epsilon}$$
$$\lambda_{2} = \frac{-c + \sqrt{c^{2} - 4\beta \delta \epsilon}}{2\epsilon}$$

for the equilibrium point (v, w) = (0, 0), and

$$\lambda_{3} = \frac{\alpha - c - \sqrt{(\alpha - c)^{2} + 4\beta\delta\epsilon}}{2\epsilon}$$
$$\lambda_{4} = \frac{\alpha - c + \sqrt{(\alpha - c)^{2} + 4\beta\delta\epsilon}}{2\epsilon}$$

for the equilibrium point (v, w) = (1, 0).

Remark 7.5. (v, w) = (0, 0) corresponds to an asymptotically stable equilibrium point while (v, w) = (1, 0) represents a saddle point.

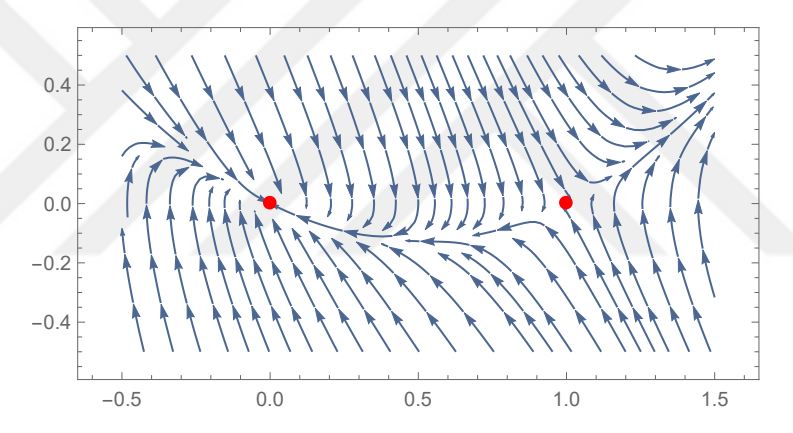


Figure 7.4 2D graph of the vector field (p(v, w), q(v, w)) for c_5 with $\alpha = 1$, $\beta = 1$, $\epsilon = 1$, and $\delta = 1$

For instance, if the parameters of the system are chosen as $\alpha = 1$, $\beta = 1$, $\epsilon = 1$, and $\delta = 1$ for the wave speed c_5 then it is found that $\lambda_1 = -2$, $\lambda_2 = -0.5$, $\lambda_3 = -2$, and $\lambda_4 = +0.5$. Hence, it can be concluded that the equilibrium point (0,0) is stable while the equilibrium point (1,0) is a saddle point. This can be observed pictorially in Figure 7.4.

Theorem 7.4. In advection dominant cases, if $0 < \delta < 1$ then the equilibrium point (v, w) = (0, 0) remains stable.

Proof. If the following limits are considered

$$\lim_{\epsilon \to 0} \lambda_1 = \frac{\beta(\delta - 1)(\delta + 1)}{\alpha} \tag{7.29}$$

$$\lim_{\epsilon \to 0} \lambda_2 = -\frac{\beta \delta(\delta + 1)}{\alpha} \tag{7.30}$$

and the presumed inequality $0 < \delta < 1$ is taken into account then we can deduce that both eigenvalues λ_1^0 and λ_2^0 have negative real parts.

Corollary 7.4. In advection dominant cases, the equilibrium point (v, w) = (1, 0) is a non-hyperbolic equilibrium.

Proof. The following limits

$$\lim_{\epsilon \to 0} \lambda_3 = -\frac{\beta(\delta + 1)}{\alpha} \tag{7.31}$$

$$\lim_{\epsilon \to 0} \lambda_4 = 0 \tag{7.32}$$

are taken into consideration. Since λ_3^0 remains in the left half of the complex plane and $\lambda_4^0 = 0$, the equilibrium point (1,0) is a non-hyperbolic equilibrium.

In the case of having one zero eigenvalue, we have more than one equilibrium point. Indeed, we have a line of equilibrium points which is pointing towards the eigenvector corresponding to this eigenvalue.

7.3 Numerical Solutions via the RFPIM

One of the important tools that can be applied in testing a newly proposed method is the singularly perturbed nonlinear partial differential equations. In this section, then, some numerical examples are implemented to show the effectiveness of the reversed fixed point iteration method to capture the physical nature governed by a class of singularly perturbed nonlinear partial differential equations. In this respect, in the following examples the singularly perturbed generalized Burgers Huxley and Burgers Fisher equations are considered. In the solution procedure, a semi discretization approach has been adopted. Both Equation 7.1 and Equation 7.2 could be considered as

$$u_t = F(u, u_x, u_{xx}).$$
 (7.33)

If the last equation is temporally discretized via the reversed forward in time scheme, the following semi discrete equation is obtained:

$$\frac{u_n - u_{n+1}}{\Delta t} = F(u, u_x, u_{xx})|_{t = t_{n+1}}. (7.34)$$

Hence, the scheme

$$u_n = u_{n+1} + \Delta t F(u, u_x, u_{xx})|_{t=t_{n+1}}$$
(7.35)

is obtained. In the solution procedures of the following examples Δt is taken to be the final time T. Then the approximate initial data $\tilde{u}(x,0)$ is recovered by using the final data u(x,T) via the RFPIM.

Example 1. In this example, an inverse problem in the SPGBHE is considered. Notice that

$$F(u, u_x, u_{xx}) = -\alpha u^{\delta} u_x + \epsilon u_{xx} + \beta u (1 - u^{\delta}) (u^{\delta} - \gamma)$$

$$(7.36)$$

for this case. To begin with, a final data or final condition u(x,T) is produced via analytical solution 7.14 to Equation 7.1. The derived results, the recovered initial data $\tilde{u}(x,0)$, by using the RFPIM have been compared with the initial condition obtained via the exact solution in Equation 7.14.

The results indicate that the present method is much more accurate for the smaller values of the parameter of nonlinearity as indicated in Table 7.3. Besides, for the critical values of the diffusion coefficient, $\epsilon \ll 1$, any change in the diffusion coefficient does not matter a significant difference in the accuracy (see Table 7.4).

Table 7.3 $L^2(-\infty, \infty)$ errors for Example 1 for various values of δ with $\alpha = 1$, $\beta = 1$, $\epsilon = 10^{-5}$, and $\gamma = 0.5$ with $\Delta t = T$.

T	$\delta = 1/2$	$\delta = 1$	$\delta = 2$	$\delta = 5$
0.1	0.000106	0.000228	0.000441	0.000904
0.2	0.000422	0.000912	0.001765	0.003612
0.3	0.000950	0.002052	0.003970	0.008107
0.4	0.001689	0.003647	0.007052	0.014356
0.5	0.002639	0.005696	0.011007	0.022321
0.6	0.003800	0.008199	0.015826	0.031948
0.7	0.005171	0.011153	0.021504	0.043179
0.8	0.006752	0.014556	0.028030	0.055949
0.9	0.008543	0.018408	0.035394	0.070184
1.0	0.010544	0.022705	0.043584	0.085811

According to the results in Table 7.5, an increase in the reaction coefficient could lead to a decrease in the accuracy of the current method. A similar result can be observed in Table 7.6 for the reaction parameter β . Notice also that these results are valid for a challenging condition as $\epsilon = 10^{-5}$.

In Table 7.7, despite the very striking choice of kinematic viscosity, it can be observed that an increase in the advection coefficient slightly reduces the effectiveness of the proposed method. Recovery of the initial condition and the corresponding absolute error for the inverse problem in the SPGBHE with $\alpha = 1$, $\beta = 1$, $\delta = 1$, $\epsilon = 10^{-10}$,

Table 7.4 $L^2(-\infty, \infty)$ errors for Example 1 for various values of ϵ with $\alpha = 1$, $\beta = 1$, $\gamma = 0.5$, and $\delta = 1$ with $\Delta t = T$.

T	$\epsilon = 10^{-15}$	$\epsilon = 10^{-10}$	$\epsilon = 10^{-5}$	$\epsilon = 10^{-3}$	$\epsilon = 1.0$
0.1	0.000221	0.000228	0.000228	0.000191	0.0128293
0.2	0.000897	0.000913	0.000912	0.000837	0.0254972
0.3	0.002029	0.002053	0.002052	0.001938	0.0380039
0.4	0.003615	0.003649	0.003647	0.003492	0.0503496
0.5	0.005655	0.005698	0.005696	0.005500	0.0625345
0.6	0.008148	0.008201	0.008199	0.007959	0.0745589
0.7	0.011091	0.011156	0.011153	0.010869	0.0864234
0.8	0.014484	0.014560	0.014556	0.014227	0.0981283
0.9	0.018325	0.018412	0.018408	0.018032	0.1096740
1.0	0.022610	0.022709	0.022705	0.022282	0.1210620

Table 7.5 $L^2(-\infty,\infty)$ errors for Example 1 for various values of γ with $\alpha=1$, $\beta=1$, $\delta=1$, and $\epsilon=10^{-5}$ with $\Delta t=T$.

T	$\gamma = 0.01$	$\gamma = 0.3$	$\gamma = 0.5$	$\gamma = 0.7$	$\gamma = 0.99$
0.1	2.74×10^{-7}	0.000082	0.000228	0.000447	0.000894
0.2	3.66×10^{-7}	0.000328	0.000912	0.001788	0.003575
0.3	2.76×10^{-7}	0.000738	0.002052	0.004021	0.008037
0.4	3.30×10^{-9}	0.001313	0.003647	0.007144	0.014269
0.5	4.52×10^{-7}	0.002051	0.005696	0.011154	0.022258
0.6	1.09×10^{-6}	0.002954	0.008199	0.016045	0.031983
0.7	1.91×10^{-6}	0.004020	0.011153	0.021811	0.043425
0.8	2.91×10^{-6}	0.005249	0.014556	0.028448	0.056556
0.9	4.09×10^{-6}	0.006642	0.018408	0.035945	0.071348
1.0	5.46×10^{-6}	0.008197	0.022705	0.044297	0.087768

and $\gamma = 0.01$ with $\Delta t = T = 1.0$ can be observed in Figure 7.5. In the figure, and also in the following figures in this example, the red curve stands for the approximate solution while the dashed blue curve represents the exact solution. The absolute errors are shown by the green dashed curve in the figures.

Example 2. In this example, an inverse problem in the SPGBFE is considered. To begin with, a final data or final condition is produced via analytical solution 7.28 to the accompanying problem with the IBCs derived from the analytical solution of Equation 7.2. The derived results by using the RFPIM have been compared with the initial condition obtained via Equation 7.28. According to the results in Tables 7.8, the current method is seen to produce more accurate results for relatively smaller values of δ . Again, the errors in $L^2(-\infty, \infty)$ sense could be observed for various values of ϵ .

Table 7.6 $L^2(-\infty, \infty)$ errors for Example 1 for various values of β with $\alpha = 1$, $\delta = 1$, $\gamma = 0.5$, and $\epsilon = 10^{-5}$ with $\Delta t = T$.

T	$\beta = 0.1$	$\beta = 0.3$	$\beta = 0.5$	$\beta = 0.7$	$\beta = 0.9$
0.1	7.20×10^{-6}	0.000037	0.000081	0.000133	0.000195
0.2	0.000029	0.000150	0.000323	0.000534	0.000779
0.3	0.000065	0.000337	0.000726	0.001202	0.001752
0.4	0.000115	0.000600	0.001290	0.002137	0.003114
0.5	0.000180	0.000937	0.002016	0.003338	0.004865
0.6	0.000260	0.001349	0.002903	0.004806	0.007003
0.7	0.000353	0.001837	0.003950	0.006540	0.009527
0.8	0.000462	0.002399	0.005159	0.008539	0.012436
0.9	0.000584	0.003036	0.006528	0.010803	0.015729
1.0	0.000721	0.003748	0.008057	0.013331	0.019404

Table 7.7 $L^2(-\infty, \infty)$ errors for Example 1 for various values of α with $\beta = 1$, $\delta = 1$, $\gamma = 0.5$, and $\epsilon = 10^{-5}$ with $\Delta t = T$.

	T	$\alpha = 0.1$	$\alpha = 0.3$	$\alpha = 0.5$	$\alpha = 0.7$	$\alpha = 0.9$
•	0.1	0.000060	0.000123	0.000160	0.000190	0.000216
	0.2	0.000265	0.000495	0.000643	0.000762	0.000865
	0.3	0.000613	0.001118	0.001449	0.001716	0.001946
	0.4	0.001104	0.001989	0.002576	0.003050	0.003460
	0.5	0.001739	0.003109	0.004024	0.004764	0.005404
	0.6	0.002517	0.004477	0.005792	0.006858	0.007778
	0.7	0.003437	0.006093	0.007880	0.009329	0.010580
	0.8	0.004499	0.007954	0.010286	0.012176	0.013809
	0.9	0.005702	0.010061	0.013008	0.015398	0.017462
	1.0	0.007046	0.012412	0.016046	0.018993	0.021539

The results seem quite acceptable and this situation is of great importance especially for smaller values of the diffusion coefficient.

As the values of the reaction coefficient move from -1 to 0, a decrease in the L^2 error is observed in Table 7.10. Similarly, an increase in the advection coefficient causes a relative increase in the accuracy of the present method as depicted in Table 7.11, in most cases. In Figure 7.6, the recovery of the initial data from the final data and the picture of the absolute error could be observed for the almost optimal values of the parameters towards the success of the proposed technique.

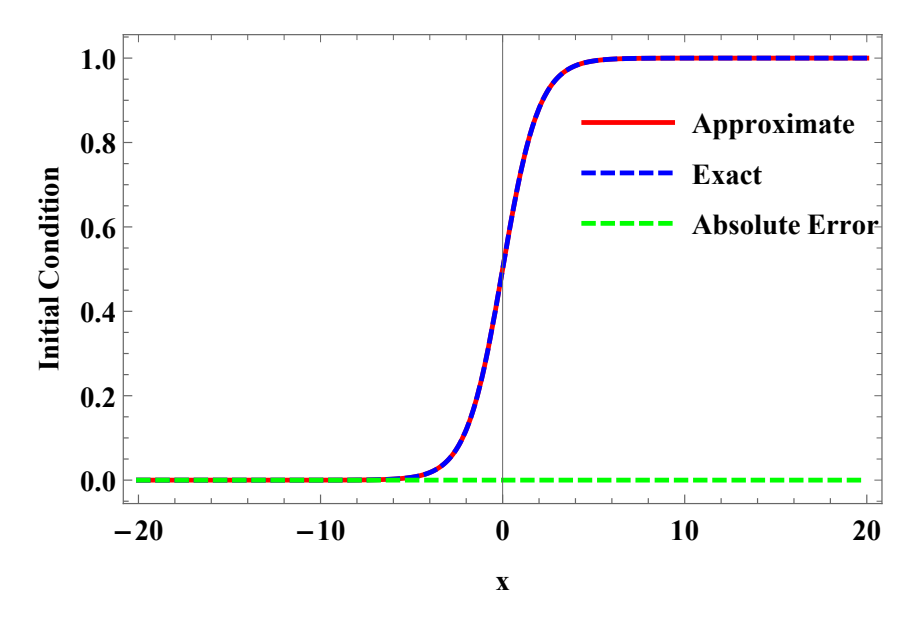


Figure 7.5 Recovery of the initial condition and the absolute error for the inverse problem in the SPGBHE at T=1.0 with $\alpha=1,~\beta=1,~\delta=1,~\epsilon=10^{-10}$, and $\gamma=0.01$ with $\Delta t=T$.

Table 7.8 $L^2(-\infty,\infty)$ errors for Example 2 for various values of δ with $\alpha=1$, $\beta=-1$, and $\epsilon=1$ with $\Delta t=T$.

\overline{T}	$\delta = 0.1$	$\delta = 0.3$	$\delta = 0.5$	$\delta = 0.7$	$\delta = 0.9$
0.1	0.001727	0.006028	0.009041	0.010884	0.011899
0.2	0.003450	0.011970	0.017763	0.021075	0.022623
0.3	0.005170	0.017827	0.026166	0.030574	0.032177
0.4	0.006886	0.023598	0.034251	0.039386	0.040573
0.5	0.008599	0.029284	0.042018	0.047515	0.047830
0.6	0.010309	0.034884	0.049469	0.054969	0.053975
0.7	0.012015	0.040400	0.056606	0.061758	0.059043
0.8	0.013719	0.045830	0.063430	0.067893	0.063084
0.9	0.015418	0.051175	0.069945	0.073390	0.066164
1.0	0.017115	0.056436	0.076151	0.078267	0.068372

Table 7.9 $L^2(-\infty, \infty)$ errors for Example 2 for various values of ϵ with $\alpha = 1$, $\beta = -1$, and $\delta = 1$ with $\Delta t = T$.

T	$\epsilon = 0.25$	$\epsilon = 0.50$	$\epsilon = 0.75$	$\epsilon = 1.00$	$\epsilon = 2.0$
0.1	0.025820	0.018029	0.014410	0.012184	0.007726
0.2	0.051640	0.035603	0.027829	0.022919	0.012670
0.3	0.077460	0.052721	0.040261	0.032217	0.014874
0.4	0.103280	0.069387	0.051715	0.040095	0.014465
0.5	0.129099	0.085604	0.062206	0.046585	0.011870
0.6	0.154919	0.101375	0.071751	0.051733	0.009022
0.7	0.180739	0.116705	0.080376	0.055606	0.012003
0.8	0.206559	0.131602	0.088113	0.058297	0.022120
0.9	0.232379	0.146070	0.094999	0.059938	0.036372
1.0	0.258199	0.160120	0.101082	0.060715	0.053800

Table 7.10 $L^2(-\infty, \infty)$ errors for Example 2 for various values of β with $\alpha = 1$, $\delta = 1$, and $\epsilon = 1$ with $\Delta t = T$.

•	T	$\beta = -0.9$	$\beta = -0.7$	$\beta = -0.5$	$\beta = -0.3$	$\beta = -0.1$
	0.1	0.012365	0.012649	0.012829	0.012907	0.012881
	0.2	0.023640	0.024775	0.025497	0.025807	0.025704
	0.3	0.033833	0.036380	0.038004	0.038701	0.038468
	0.4	0.042952	0.047466	0.050350	0.051588	0.051175
	0.5	0.051014	0.058035	0.062535	0.064469	0.063824
	0.6	0.058040	0.068093	0.074559	0.077344	0.076415
	0.7	0.064059	0.077643	0.086423	0.090212	0.088947
	0.8	0.069111	0.086693	0.098128	0.103073	0.101422
	0.9	0.073245	0.095249	0.109674	0.115928	0.113839
	1.0	0.076528	0.103321	0.121062	0.128777	0.126199

Table 7.11 $L^2(-\infty,\infty)$ errors for Example 2 for various values of α with $\beta=-1$, $\delta=1$, and $\epsilon=0.1$ with $\Delta t=T$.

T	$\alpha = 0.1$	$\alpha = 0.3$	$\alpha = 0.5$	$\alpha = 0.7$	$\alpha = 0.9$
0.1	0.001697	0.000140	0.002959	0.006373	0.010158
0.2	0.007199	0.004632	0.002742	0.010380	0.018589
0.3	0.016602	0.013484	0.001327	0.012059	0.025311
0.4	0.030067	0.026645	0.007687	0.011524	0.030352
0.5	0.047802	0.044052	0.017564	0.009188	0.033766
0.6	0.070056	0.065619	0.030644	0.007071	0.035641
0.7	0.097097	0.091239	0.046880	0.010674	0.036128
0.8	0.129195	0.120783	0.066233	0.019863	0.035477
0.9	0.166599	0.154096	0.088661	0.032294	0.034126
1.0	0.209518	0.191003	0.114116	0.047345	0.032820

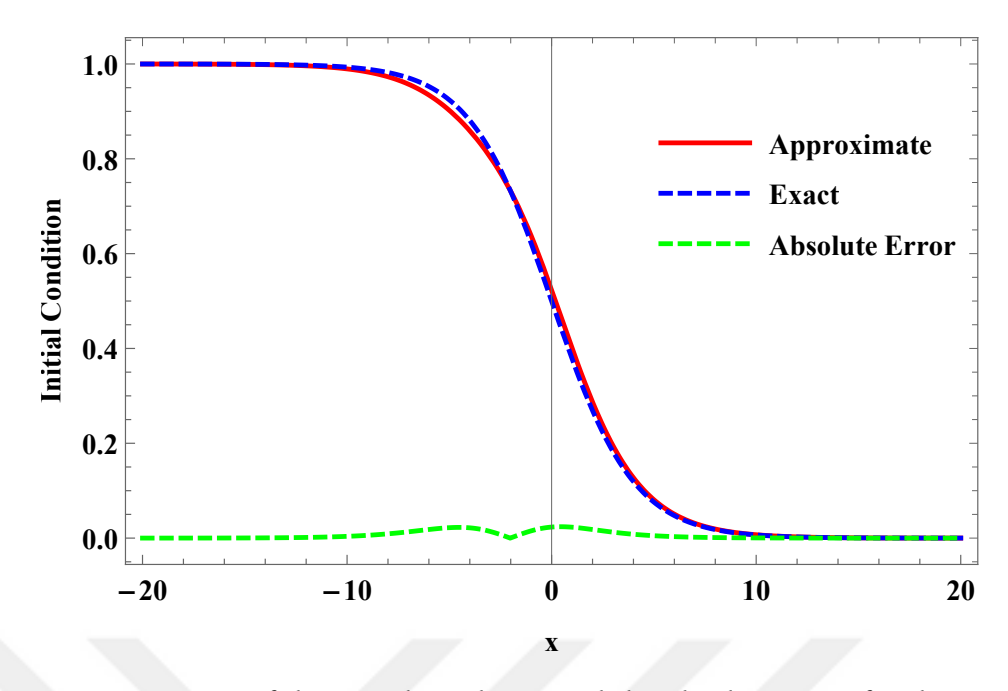


Figure 7.6 Recovery of the initial condition and the absolute error for the inverse problem in the SPGBFE at T=1.0 with $\alpha=1.0$, $\beta=-1.0$, $\delta=1.0$, and $\epsilon=1.0$ with $\Delta t=T$.

8 TWO DIMENSIONAL ADVECTION DIFFUSION PROCESSES

The RFPIM has been employed to obtain numerical solutions to various one-dimensional, even if they are challenging, problems represented by PDEs thus far. In this chapter, the two dimensional coupled Burgers equations

$$u_t + uu_x + vu_y = \epsilon(u_{xx} + u_{yy}) \tag{8.1}$$

$$v_t + uv_x + vv_y = \epsilon(v_{xx} + v_{yy}) \tag{8.2}$$

will be discussed where the common term ϵ stands for the kinematic viscosity. The exact solution of this system of equations derived via Hopf Cole transformation in [95] as follows

$$u(x,y,t) = \frac{3}{4} - \frac{1}{4(1 + e^{(-4x + 4y - t)/(32\epsilon)})},$$
(8.3)

$$v(x,y,t) = \frac{3}{4} + \frac{1}{4(1 + e^{(-4x + 4y - t)/(32\epsilon)})}.$$
 (8.4)

Here, the RFPIM will be implemented to identify the initial conditions u(x, y, 0) and v(x, y, 0) based on the final conditions u(x, y, T) and v(x, y, T) for a given final time T. Note that, the initial and final conditions are taken from the exact solutions. Then, the approximate initial conditions $\tilde{u}(x, y, 0)$ and $\tilde{v}(x, y, 0)$ are derived via the RFPIM.

8.1 Implementation of the RFPIM and Numerical Observations

A semi-discrete scheme is utilized in this section to reach continuous approximate initial conditions $\tilde{u}(x,y,0)$ and $\tilde{v}(x,y,0)$ for the coupled Burgers equation. To obtain the semi-discrete scheme, the terms u_t and v_t in Equation 8.1 and Equation 8.2 are need to be replaced with a forward finite difference scheme first. Thus, the RFPIM could be employed to get the needed scheme as follows:

$$\frac{u(x, y, (n+1)\Delta t) - u(x, y, n\Delta t)}{\Delta t} + u(x, y, n\Delta t)u_x(x, y, n\Delta t) +$$

$$+ v(x, y, n\Delta t)u_y(x, y, n\Delta t) = \epsilon(u_{xx}(x, y, n\Delta t) + u_{yy}(x, y, n\Delta t))$$

$$\frac{v(x, y, (n+1)\Delta t) - v(x, y, n\Delta t)}{\Delta t} + u(x, y, n\Delta t)v_x(x, y, n\Delta t) +$$

$$+ v(x, y, n\Delta t)v_y(x, y, n\Delta t) = \epsilon(v_{xx}(x, y, n\Delta t) + v_{yy}(x, y, n\Delta t))$$

and by reversing the iterations the last equations yield

$$\frac{u(x,y,n\Delta t)-u(x,y,(n+1)\Delta t)}{\Delta t}-u(x,y,(n+1)\Delta t)u_x(x,y,(n+1)\Delta t)-\\ -v(x,y,(n+1)\Delta t)u_y(x,y,(n+1)\Delta t)=\epsilon(u_{xx}(x,y,(n+1)\Delta t)+u_{yy}(x,y,(n+1)\Delta t))\\ \frac{v(x,y,n\Delta t)-v(x,y,(n+1)\Delta t)}{\Delta t}-u(x,y,(n+1)\Delta t)v_x(x,y,(n+1)\Delta t)-\\ -v(x,y,(n+1)\Delta t)v_y(x,y,(n+1)\Delta t)=\epsilon(v_{xx}(x,y,(n+1)\Delta t)+v_{yy}(x,y,(n+1)\Delta t)).$$

Thus, the last equation produces an explicit semi-discrete scheme for $u(x, y, n\Delta t)$ and $v(x, y, n\Delta t)$. To observe the numerical efficiency of the current method, the coupled Burgers equations are considered in the domain $\Omega = \{(x, y) \in [0, 1] \times [0, 1]\}$, and then, $\tilde{u}(x, y, 0)$ and $\tilde{v}(x, y, 0)$ have been computed via the RFPIM. The obtained initial conditions have been compared with the exact ones for various values of the diffusion coefficient ϵ , the time increment Δt , and the final time T. The quantitative results in Tables 8.1-8.4 reveal that the RFPIM has an outstanding numerical performance to identify the exact initial conditions. Note that the results provided in the tables represent the error in the $L^2(0,1)$ sense. In most cases, the performance of the RFPIM has been seen to be its maximum when $\Delta t = T$.

Table 8.1 $L^2(0,1)$ errors for various values of Δt with $\epsilon = 0.01$ and T = 0.5.

Δt	и	ν
0.100	3.17×10^{-2}	3.17×10^{-2}
0.125	2.92×10^{-2}	2.92×10^{-2}
0.167	2.52×10^{-2}	2.52×10^{-2}
0.250	2.78×10^{-2}	2.78×10^{-2}
0.500	2.51×10^{-2}	2.51×10^{-2}

Table 8.2 $L^2(0,1)$ errors for various values of Δt with $\epsilon = 0.01$ and T = 1.0.

Δt	и	ν
0.200	5.83×10^{-2}	5.83×10^{-2}
0.250	5.36×10^{-2}	5.36×10^{-2}
0.333	4.63×10^{-2}	4.63×10^{-2}
0.500	3.46×10^{-2}	3.46×10^{-2}
1.000	4.93×10^{-2}	4.93×10^{-2}

Table 8.3 $L^2(0,1)$ errors for various values of Δt with $\epsilon = 0.001$ and T = 0.1.

Δt	и	ν
0.020	1.97×10^{-2}	1.97×10^{-2}
0.025	1.82×10^{-2}	1.82×10^{-2}
0.033	1.57×10^{-2}	1.57×10^{-2}
0.050	1.19×10^{-2}	1.19×10^{-2}
0.100	1.76×10^{-2}	1.76×10^{-2}

Table 8.4 $L^2(0,1)$ errors for various values of ϵ and T with $\Delta t = T$.

	T = 0.1	T = 0.5	T = 1.0	T = 5.0	T = 10.0
$\epsilon = 0.01$	6.94×10^{-3}	2.52×10^{-2}	4.93×10^{-2}	1.60×10^{-1}	1.64×10^{-1}
$\epsilon = 0.1$	8.20×10^{-4}	4.07×10^{-3}	8.38×10^{-3}	4.54×10^{-2}	2.46×10^{-2}
$\epsilon = 0.5$	3.96×10^{-5}	2.05×10^{-4}	4.55×10^{-4}	5.78×10^{-3}	1.91×10^{-2}
$\epsilon = 1.0$	9.96×10^{-6}	5.17×10^{-5}	1.16×10^{-4}	1.54×10^{-3}	5.64×10^{-3}
$\epsilon = 2.0$	2.49×10^{-6}	1.30×10^{-5}	2.91×10^{-5}	3.95×10^{-4}	1.49×10^{-3}

9 RESULTS AND DISCUSSION

A novel approach to finding unstable equilibria of a dynamical system, the reversed fixed-point iteration method, has been presented in this thesis. The method can be seen to be a significant contribution when unstable equilibrium solutions of a nonlinear system are investigated. This discovery has been underpinned via the following results observed in the remarkable implementations:

Classification of the relatively homogeneously distributed roots of a polynomial and determination of unstable equilibria have been carried out. Also, the numerical illustrations of the present method have been carried out in \mathbb{R}^2 or \mathbb{R}^3 .

In population dynamical models, unstable thresholds have been found via the RFPIM. It has been observed that the use of relatively larger step sizes increases the accuracy of the method.

Unstable solutions of the nonlinear Fredholm integral equations of the second kind have been successfully computed via the current method.

Unstable equilibrium position comes out in the nonlinear control theory, such as in the pendulum problem, which is one of the most fundamental examples, has been determined.

The behaviour of unstable equilibria in chaos has been strikingly discovered in a particular example. The fixed points, of repelling nature, behaving like a resonator, have been localized properly.

Unstable steady-states of an ordinary differential operator have been successfully determined by using the present method. It has been found that the use of relatively larger step sizes significantly increases the efficiency of the present method. Hence, the need for storage space and the time required for computations have been meaningfully decreased.

The RFPIM has been implemented to generate numerical solutions of the significant forms of advection-diffusion-reaction equations. The derived results have been seen to be in good agreement with the corresponding ones in the literature and/or ones of the exact solutions. Absolute and relative errors, the RMSE, and the L^2 errors have been seen to be remarkably low, and the present method has been seen to be highly capable of capturing the sharp behaviour of the physical models even under advection dominant cases, $\epsilon \to 0$.

Throughout this thesis, the RFPIM has been seen to capture the behaviour of a nonlinear system successfully near unstable equilibria without facing any conventional drawbacks. In future studies, attention may be focused on the implementation of the RFPIM to solve high-dimensional or various nonlinear PDEs representing more realistic processes. Furthermore, the present method can be utilized to understand the unstable equilibria of various dynamical systems or unstable equilibrium solutions of different mathematical models arising in a wide range of spectrums including stochastic or chaotic processes, control problems, and so on.

- [1] L. E. J. Brouwer, "Über abbildung von mannigfaltigkeiten," *Mathematische Annalen*, vol. 71, pp. 97–115, 1911.
- [2] J. Schauder, "Der fixpunktsatz in funktional-raumen," *Studia math.*, vol. 2, pp. 171–180, 1930.
- [3] A. Tychonoff, "Ein fixpunktsatz," *Mathematische Annalen*, vol. 111, no. 1, pp. 767–776, 1935.
- [4] K. Fan, "A generalization of tychonoff's fixed point theorem," *Mathematische Annalen*, vol. 142, no. 3, pp. 305–310, 1961.
- [5] S. Banach, "Sur les opérations dans les ensembles abstraits et leur application aux équations intégrales," *Fund. math*, vol. 3, no. 1, pp. 133–181, 1922.
- [6] W. A. Kirk, "A fixed point theorem for mappings which do not increase distances," *The American mathematical monthly*, vol. 72, no. 9, pp. 1004–1006, 1965.
- [7] F. E. Browder, "Nonexpansive nonlinear operators in a banach space," *Proceedings of the National Academy of Sciences of the United States of America*, vol. 54, no. 4, p. 1041, 1965.
- [8] F. E. Browder, W. Petryshyn, "The solution by iteration of nonlinear functional equations in banach spaces," *Bulletin of the American mathematical society*, vol. 72, no. 3, pp. 571–575, 1966.
- [9] R. Bing, "The elusive fixed point property," *The American Mathematical Monthly*, vol. 76, no. 2, pp. 119–132, 1969.
- [10] M. A. Krasnosel'skii, G. M. Vainikko, R. Zabreyko, Y. B. Ruticki, V. V. Stet'senko, *Approximate solution of operator equations*. Springer Science & Business Media, 2012.
- [11] M. R. Taskovic, "Some results in the fixed point theory ii," *Publ. Inst. Math*, vol. 41, pp. 249–258, 1980.
- [12] M. Krasnoselsky, "Two remarks on the method of successive approximation," *Usp. Mat. Nauk*, vol. 10, pp. 123–127, 1955.
- [13] S. Kakutani, "A generalization of brouwer's fixed point theorem," *Duke mathematical journal*, vol. 8, no. 3, pp. 457–459, 1941.
- [14] R. S. Stepleman, "A characterization of local convergence for fixed point iterations in r¹," *SIAM Journal on Numerical Analysis*, vol. 12, no. 6, pp. 887–894, 1975.
- [15] A. M. Ostrowski, Solution of equations in Euclidean and Banach spaces. Academic Press, 1973.

- [16] S. Strogatz, Nonlinear dynamics and chaos: with applications to physics, biology, chemistry, and engineering. 2015.
- [17] G. Adomian, R. Rach, "On the solution of algebraic equations by the decomposition method," *Journal of mathematical analysis and applications*, vol. 105, no. 1, pp. 141–166, 1985.
- [18] J. H. Mathews, K. D. Fink, *Numerical methods using MATLAB*. Pearson prentice hall Upper Saddle River, NJ, 2004, vol. 4.
- [19] E. W. Cheney, D. R. Kincaid, *Numerical Mathematics and Computing*. Cengage Learning, 2008.
- [20] R. L. Devaney, *An introduction to chaotic dynamical systems*. Chapman and Hall/CRC, 1989.
- [21] G. C. Layek, An introduction to dynamical systems and chaos. Springer, 2015.
- [22] W. E. Boyce, R. C. DiPrima, H. Villagómez Velázquez, et al., Elementary differential equations and boundary value problems. Ecuaciones diferenciales y problemas con valores en la frontera. 2004.
- [23] A. M. Wazwaz, Linear and nonlinear integral equations. Springer, 2011, vol. 639.
- [24] A. Alturk, T. Cosgun, "The use of lavrentiev regularization method in fredholm integral equations of the first kind," *International Journal of Advances in Applied Mathematics and Mechanics*, vol. 7, no. 2, pp. 70–79, 2019.
- [25] S. M. Zemyan, *The classical theory of integral equations: a concise treatment*. Springer Science & Business Media, 2012.
- [26] G. Tigan, "Controlling chaos of a dynamical system with feedback control," *Carpathian Journal of Mathematics*, pp. 153–161, 2006.
- [27] N. Kumar, "Unsteady flow against dispersion in finite porous media," *Journal of Hydrology*, vol. 63, no. 3-4, pp. 345–358, 1983.
- [28] M. H. Chaudhry, D. E. Cass, J. E. Edinger, "Modeling of unsteady-flow water temperatures," *Journal of Hydraulic Engineering*, vol. 109, no. 5, pp. 657–669, 1983.
- [29] Z. Zlatev, R. Berkowicz, L. P. Prahm, "Implementation of a variable stepsize variable formula method in the time-integration part of a code for treatment of long-range transport of air pollutants," *Journal of Computational Physics*, vol. 55, no. 2, pp. 278–301, 1984.
- [30] H. Karahan, "An iterative method for the solution of dispersion equation in shallow water," *WIT Transactions on Ecology and the Environment*, vol. 49, 2001.
- [31] F. M. Holly Jr, J.-M. Usseglio-Polatera, "Dispersion simulation in two-dimensional tidal flow," *Journal of hydraulic engineering*, vol. 110, no. 7, pp. 905–926, 1984.
- [32] J. R. Salmon, J. A. Liggett, R. H. Gallagher, "Dispersion analysis in homogeneous lakes," *International Journal for Numerical Methods in Engineering*, vol. 15, no. 11, pp. 1627–1642, 1980.
- [33] P. Chatwin, C. Allen, "Mathematical models of dispersion in rivers and estuaries," *Annual Review of Fluid Mechanics*, vol. 17, no. 1, pp. 119–149, 1985.

- [34] Q. N. Fattah, J. A. Hoopes, "Dispersion in anisotropic, homogeneous, porous media," *Journal of Hydraulic Engineering*, vol. 111, no. 5, pp. 810–827, 1985.
- [35] J. Makmul, "A cellular automaton model for pedestrians' movements influenced by gaseous hazardous material spreading," *Modelling and Simulation in Engineering*, vol. 2020, 2020.
- [36] Y. Sakumoto, I. Taniguchi, "Fast directional energy interchange used in mcmc-based autonomous decentralized mechanism toward a resilient microgrid," *Journal of Information Processing*, vol. 28, pp. 75–85, 2020.
- [37] E. Sousa, "Finite differences for the convection-diffusion equation: On stability and boundary conditions," Ph.D. dissertation, University of Oxford, 2001.
- [38] J. Douglas Jr, T. F. Russell, "Numerical methods for convection-dominated diffusion problems based on combining the method of characteristics with finite element or finite difference procedures," *SIAM Journal on Numerical Analysis*, vol. 19, no. 5, pp. 871–885, 1982.
- [39] Y. Cheng, C.-W. Shu, "Superconvergence of discontinuous galerkin and local discontinuous galerkin schemes for linear hyperbolic and convection-diffusion equations in one space dimension," *SIAM Journal on Numerical Analysis*, vol. 47, no. 6, pp. 4044–4072, 2010.
- [40] K. Yon-chol, Y. Nam, C. Dong-ho, "A nearly analytic discrete method for one-dimensional unsteady convection-dominated diffusion equations," *Communications*, vol. 3, 2019.
- [41] H. Ding, Y. Zhang, "A new difference scheme with high accuracy and absolute stability for solving convection–diffusion equations," *Journal of Computational and Applied Mathematics*, vol. 230, no. 2, pp. 600–606, 2009.
- [42] J. Watkins, K. Asthana, A. Jameson, "A numerical analysis of the nodal discontinuous galerkin scheme via flux reconstruction for the advection-diffusion equation," *Computers & Fluids*, vol. 139, pp. 233–247, 2016.
- [43] C. H. Bruneau, P. Fabrie, P. Rasetarinera, "An accurate finite difference scheme for solving convection-dominated diffusion equations," *International journal for numerical methods in fluids*, vol. 24, no. 2, pp. 169–183, 1997.
- [44] H. Wang, Q. Zhang, "Error estimate on a fully discrete local discontinuous galerkin method for linear convection-diffusion problem," *Journal of Computational Mathematics*, pp. 283–307, 2013.
- [45] N. Tanaka, Y. Motoyama, "Error estimation of numerical solutions of linear convection–diffusion problem," *International Journal of Computational Fluid Dynamics*, vol. 19, no. 1, pp. 61–66, 2005.
- [46] G. Gurarslan, M. Sari, "Numerical solutions of linear and nonlinear diffusion equations by a differential quadrature method (dqm)," *International Journal for Numerical Methods in Biomedical Engineering*, vol. 27, no. 1, pp. 69–77, 2011.
- [47] G. Gurarslan, H. Karahan, D. Alkaya, M. Sari, M. Yasar, "Numerical solution of advection-diffusion equation using a sixth-order compact finite difference method," *Mathematical Problems in Engineering*, vol. 2013, 2013.

- [48] M. Sari, G. Gurarslan, A. Zeytinoglu, "High-order finite difference schemes for solving the advection-diffusion equation," *Mathematical and Computational Applications*, vol. 15, no. 3, pp. 449–460, 2010.
- [49] N. Liron, J. Rubinstein, "Calculating the fundamental solution to linear convection-diffusion problems," *SIAM Journal on Applied Mathematics*, vol. 44, no. 3, pp. 493–511, 1984.
- [50] S. Purkayastha, B. Kumar, "Analytical solution of the one-dimensional contaminant transport equation in groundwater with time-varying boundary conditions," *Ish Journal of Hydraulic Engineering*, vol. 26, no. 1, pp. 78–83, 2020.
- [51] S. Ortleb, "L2-stability analysis of imex- (σ, μ) dg schemes for linear advection-diffusion equations," *Applied Numerical Mathematics*, vol. 147, pp. 43–65, 2020.
- [52] V. Suman, T. K. Sengupta, C. J. D. Prasad, K. S. Mohan, D. Sanwalia, "Spectral analysis of finite difference schemes for convection diffusion equation," *Computers & Fluids*, vol. 150, pp. 95–114, 2017.
- [53] L. Campbell, B. Yin, "On the stability of alternating-direction explicit methods for advection-diffusion equations," *Numerical Methods for Partial Differential Equations: An International Journal*, vol. 23, no. 6, pp. 1429–1444, 2007.
- [54] T. F. Chan, "Stability analysis of finite difference schemes for the advection-diffusion equation," *SIAM journal on numerical analysis*, vol. 21, no. 2, pp. 272–284, 1984.
- [55] E. Sousa, "The controversial stability analysis," *Applied Mathematics and Computation*, vol. 145, no. 2-3, pp. 777–794, 2003.
- [56] T. Cosgun, M. Sari, "A novel approach regarding the fixed points of repelling nature," *Chaos, Solitons & Fractals*, vol. 153P1, p. 111573, 2021.
- [57] W. Research, *Mathematica software*, Version 12.0, 2019. [Online]. Available: http://www.wolfram.com.
- [58] M. Sari, S. Mussa, H. Tunc, "A higher order compact scheme for the nonlinear advection diffusion process," *Proceedings of the Institute of Mathematics and Mechanics*, vol. 45, no. 2, pp. 295–310, 2019. DOI: 10.29228/proc.10.
- [59] M. Sari, H. Tunc, "An optimization technique in analyzing the burgers equation," *Sigma Journal of Engineering and Natural Sciences*, vol. 35, no. 3, pp. 369–386, 2017.
- [60] H. Lu, D.M.Tartakovsky, "Lagrangian dynamic mode decomposition for construction of reduced-order models of advection-dominated phenomena," *Journal of Computational Physics*, vol. 407, no. Article number: 109229, 2020. DOI: 10.1016/j.jcp.2020.109229.
- [61] W. Wood, "An exact solution for burger's equation," *Communications in Numerical Methods in Engineering*, vol. 22, pp. 797–798, 2006. DOI: 10.1002/cnm. 850.

- [62] B. Hosseini, R. Hashemi, "Solution of burgers' equation using a local-rbf meshless method," *International Journal for Computational Methods in Engineering Science and Mechanics*, vol. 12, no. 1, pp. 44–58, 2011. DOI: 10.1080/15502287.2010.540303.
- [63] J. Caldwell, P. Wanless, A. Cook, "Solution of burgers' equation for large reynolds number using finite elements with moving nodes," *Applied Mathematical Modelling*, vol. 11, no. 3, pp. 211–214, 1987. DOI: 10.1016/0307-904X(87)90005-9.
- [64] Y. Hon, X. Mao, "An efficient numerical scheme for burgers' equation," *Applied Mathematics and Computation*, vol. 95, no. 1, pp. 37–50, 1998. DOI: 10.1016/S0096-3003(97)10060-1.
- [65] L. Iskandar, A. Mohsen, "Some numerical experiments on the splitting of burgers' equation," *Numerical Methods for Partial Differential Equations*, vol. 8, no. 3, pp. 267–276, 1992. DOI: 10.1002/num.1690080303.
- [66] I. Hassanien, A. Salama, H. Hosham, "Fourth-order finite difference method for solving burgers' equation," *Applied Mathematics and Computation*, vol. 170, no. 2, pp. 781–800, 2005. DOI: 10.1016/j.amc.2004.12.052.
- [67] A. Hashemian, H. Shodja, "A meshless approach for solution of burgers' equation," *Journal of Computational and Applied Mathematics*, vol. 220, no. 1, pp. 226–239, 2008. DOI: 10.1016/j.cam.2007.08.014.
- [68] N. Allahverdi, A. Pozo, E. Zuazua, "Numerical aspects of large-time optimal control of burgers equation," *ESAIM: Mathematical Modelling and Numerical Analysis*, vol. 50, pp. 1371–1401, 2016. DOI: 10.1051/m2an/2015076.
- [69] J. J. Alonso, M. R. Colonno, "Multidisciplinary optimization with applications to sonic-boom minimization," *Annual Review of Fluid Mechanics*, vol. 44, no. 1, pp. 505–526, 2012. DOI: 10.1146/annurev-fluid-120710-101133.
- [70] H. Bateman, "Some recent researches on the motion of fluids," *Monthly Weather Review*, vol. 43, pp. 163–170, 1915. DOI: 10.1175/1520-0493(1915) 43<163: SRROTM>2.0.CO; 2.
- [71] J. Burgers, "A mathematical model illustrating the theory of turbulence," *Advances in Applied Mechanics*, vol. 1, pp. 171–199, 1948. DOI: 10.1016/S0065–2156(08)70100–5.
- [72] J. Cole, "On a quasilinear parabolic equation occurring in aerodynamics," *Quarterly of Applied Mathematics*, vol. 9, no. 3, pp. 225–236, 1951.
- [73] E. Hopf, "The partial differential equation $u_t + uu_x = vu_{xx}$," Communications on Pure and Applied Mathematics, vol. 3, no. 3, pp. 201–230, 1950. DOI: 10. 1002/cpa.3160030302.
- [74] M. K. Kadalbajoo, K. C. Patidar, "Singularly perturbed problems in partial differential equations: A survey," *Applied Mathematics and Computation*, vol. 134, no. 2-3, pp. 371–429, 2003.
- [75] C. G. Lange, R. M. Miura, "Singular perturbation analysis of boundary value problems for differential-difference equations iii. turning point problems," *SIAM Journal on Applied Mathematics*, vol. 45, no. 5, pp. 708–734, 1985.

- [76] A. J. Khattak, "A computational meshless method for the generalized burger's-huxley equation," *Applied Mathematical Modelling*, vol. 33, no. 9, pp. 3718–3729, 2009.
- [77] M. Javidi, "A modified chebyshev pseudospectral dd algorithm for the gbh equation," *Computers & Mathematics with Applications*, vol. 62, no. 9, pp. 3366–3377, 2011.
- [78] I. Celik, "Haar wavelet method for solving generalized burgers-huxley equation," *Arab Journal of Mathematical Sciences*, vol. 18, no. 1, pp. 25–37, 2012.
- [79] D. Kamboj, M. Sharma, "Singularly perturbed burger-huxley equation: Analytical solution through iteration," *International Journal of Engineering, Science and Technology*, vol. 5, no. 3, pp. 45–57, 2013.
- [80] Y. Duan, L. Kong, R. Zhang, "A lattice boltzmann model for the generalized burgers–huxley equation," *Physica A: Statistical Mechanics and its Applications*, vol. 391, no. 3, pp. 625–632, 2012.
- [81] D. Hammad, M. El-Azab, "2n order compact finite difference scheme with collocation method for solving the generalized burger's-huxley and burger's-fisher equations," *Applied Mathematics and Computation*, vol. 258, pp. 296–311, 2015.
- [82] X. Deng, "Travelling wave solutions for the generalized burgers–huxley equation," *Applied Mathematics and Computation*, vol. 204, no. 2, pp. 733–737, 2008.
- [83] M. Hassan, M. Abdel-Razek, A.-H. Shoreh, "Explicit exact solutions of some nonlinear evolution equations with their geometric interpretations," *Applied Mathematics and Computation*, vol. 251, pp. 243–252, 2015.
- [84] S. S. Nourazar, M. Soori, A. Nazari-Golshan, "On the exact solution of burgers-huxley equation using the homotopy perturbation method," *arXiv* preprint arXiv:1503.07850, 2015.
- [85] Y. Cicek, G. Tanoglu, "Strang splitting method for burgers–huxley equation," *Applied Mathematics and Computation*, vol. 276, pp. 454–467, 2016.
- [86] A. Molabahrami, F. Khani, "The homotopy analysis method to solve the burgers–huxley equation," *Nonlinear Analysis: Real World Applications*, vol. 10, no. 2, pp. 589–600, 2009.
- [87] A. Kaushik, M. Sharma, "A uniformly convergent numerical method on non-uniform mesh for singularly perturbed unsteady burger–huxley equation," *Applied mathematics and computation*, vol. 195, no. 2, pp. 688–706, 2008.
- [88] M. A. Abdelkader, "Travelling wave solutions for a generalized fisher equation," *Journal of Mathematical Analysis and Applications*, vol. 85, no. 2, pp. 287–290, 1982.
- [89] A. Monge, E. Zuazua, "Sparse source identification of linear diffusion–advection equations by adjoint methods," *Systems & Control Letters*, vol. 145, p. 104 801, 2020.

- [90] A. R. Appadu, "Numerical solution of the 1d advection-diffusion equation using standard and nonstandard finite difference schemes," *Journal of Applied Mathematics*, vol. 2013, 2013.
- [91] L. Debnath, L. Debnath, *Nonlinear partial differential equations for scientists and engineers*. Springer, 2005.
- [92] X. Wang, Z. Zhu, Y. Lu, "Solitary wave solutions of the generalised burgers-huxley equation," *Journal of Physics A: Mathematical and General*, vol. 23, no. 3, p. 271, 1990.
- [93] M. Sari, G. Gurarslan, "Numerical solutions of the generalized burgers-huxley equation by a differential quadrature method," *Mathematical Problems in Engineering*, vol. 2009, 2009.
- [94] B. R. Kumar, V. Sangwan, S. Murthy, M. Nigam, "A numerical study of singularly perturbed generalized burgers—huxley equation using three-step taylor—galerkin method," *Computers & Mathematics with Applications*, vol. 62, no. 2, pp. 776–786, 2011.
- [95] C. A. J. Fletcher, "Generating exact solutions of the two-dimensional burgers' equations," *International Journal for Numerical Methods in Fluids*, vol. 3, pp. 213–216, 1983.

PUBLICATIONS FROM THE THESIS

Papers

- 1. Tahir Cosgun and Murat Sari, Traveling wave solutions and stability behaviours under advection dominance for singularly perturbed advection-diffusion-reaction processes. Chaos, Solitons & Fractals, Volume 138, September 2020, 109881.
- 2. Tahir Cosgun and Murat Sari, A novel approach regarding the fixed points of repelling nature. Chaos, Solitons & Fractals, Volume 153P1, December 2021, 111573.
- 3. Tahir Cosgun and Murat Sari, Initial data identification in advection-diffusion processes via a reversed fixed-point iteration method. (Submitted).
- 4. Tahir Cosgun and Murat Sari, A novel method to investigate nonlinear advection-diffusion processes. (Submitted).
- 5. Tahir Cosgun and Murat Sari, A new approach for inverse optimization problems in advection dominated singularly perturbed advection-diffusion-reaction processes. (In Process).
- 6. Tahir Cosgun and Murat Sari, A novel approach for inverse problems in 2D advection-diffusion processes. (In Process).

Conference Papers

1. Tahir Cosgun and Murat Sari, A Reversed Fixed-Point Iteration Method for Burgers Equation. International Conference on Applied Mathematics in Engineering (ICAME) September 1-3, 2021 - Balikesir, Turkey.